Clemson University
TigerPrints

All Dissertations | Dissertations

8-2014

On Numerical Algorithms for Fluid Flow Regularization Models

Abigail Bowers
Clemson University, albowers3@gmail.com

Follow this and additional works at: https://tigerprints.clemson.edu/all_dissertations

 Part of the Applied Mathematics Commons

Recommended Citation
Bowers, Abigail, "On Numerical Algorithms for Fluid Flow Regularization Models" (2014). *All Dissertations*. 1277.
https://tigerprints.clemson.edu/all_dissertations/1277

This Dissertation is brought to you for free and open access by the Dissertations at TigerPrints. It has been accepted for inclusion in All Dissertations by an authorized administrator of TigerPrints. For more information, please contact kokeefe@clemson.edu.

On numerical algorithms for fluid flow regularization models

A Dissertation
Presented to
the Graduate School of
Clemson University

In Partial Fulfillment
of the Requirements for the Degree
Doctor of Philosophy
Mathematical Sciences

---

by
Abigail L. Bowers
August 2014

Accepted by:
Dr. Leo Rebholz, Committee Chair
Dr. Chris Cox
Dr. Lea Jenkins
Dr. Hyesuk Lee

Abstract

This thesis studies regularization models as a way to approximate a flow simulation at a lower computational cost. The Leray model is more easily computed than the Navier-Stokes equations (NSE), and it is more computationally attractive than the NS-α regularization because it admits a natural linearization which decouples the mass/momentum system and the filter system, allowing for efficient and stable computations. A major disadvantage of the Leray model lies in its inaccuracy. Thus, we study herein several methods to improve the accuracy of the model, while still retaining many of its attractive properties.

This thesis is arranged as follows. Chapter 2 gives notation and preliminary results to be used in subsequent chapters. Chapter 3 investigates a nonlinear filtering scheme using the Vreman and Q-criteria based indicator functions. We define these indicator functions, prove stability and state convergence of the scheme to the NSE, and provide several numerical experiments which demonstrate its effectiveness over NSE and Leray calculations on coarse meshes.

Chapter 4 investigates a deconvolution-based indicator function. We prove stability and convergence of the resulting scheme, verify the predicted convergence rates, and provide numerical experiments which demonstrate this scheme's effectiveness. Chapter 5 then extends this scheme to the magnetohydrodynamic equations. We prove stability and convergence of our algorithm, and verify the predicted convergence rates.

Chapter 6 provides a study of the Leray-$\alpha\beta$ model. We prove stability and convergence for the fully nonlinear scheme, prove conditional stability for a linearized and decoupled scheme, and provide a numerical experiment which compares our scheme with the usual Leray-α model. Specifically, we show that choosing $\beta < \alpha$ does indeed improve accuracy in computations.

Chapter 7 investigates the Leray model with fine mesh filtering. We prove stability and convergence of the algorithm, then verify the increased convergence rate associated with the finer

mesh, as predicted by the analysis. Finally, we present a benchmark problem which demonstrates the effectiveness of filtering on a finer mesh.

Table of Contents

List of Tables

List of Figures

Chapter 1

Introduction

Understanding and predicting fluid flow is an integral part of science and engineering. Modeling fluids is essential to applications in climate modeling, blood flow in arteries, and nuclear reactors. Despite having practical applications in many different areas and disciplines, it has been primarily only in the last century that computational fluid dynamics (CFD) has become a field of interest, and there is still much that has yet to be learned. Central to CFD are the Navier-Stokes equations (NSE), which describe the evolution of incompressible, Newtonian flows, which include water, oil, and air at low speeds. The NSE are given by

$$u_t + u \cdot \nabla u + \nabla p - \nu \Delta u = f \tag{1.1}$$

$$\nabla \cdot u = 0, \tag{1.2}$$

where u denotes velocity, p pressure, ν kinematic viscosity, and f body forces.

These equations were derived in the nineteenth century, but despite intense study since that time, there still remain many difficulties surrounding them. Analytically, the NSE have an incomplete solution theory. It is not known whether strong solutions exist, and although we know weak solutions exist, we are still unable to prove their uniqueness. Computationally, simulating the NSE remains difficult for many flows. The Reynolds number, denoted $Re = \frac{1}{\nu}$, is a parameter that can be used to determine the smallest active length scale of a flow, which is $O(Re^{-3/4})$ from Kolmogorov's 1941 theory [31]. Hence, the number of mesh points necessary to resolve a flow is $O(Re^{9/4})$. Since Re for a car is $\approx 10^6$ and Re for a submarine is $\approx 10^8$, the mesh points needed for

a resolved simulation lead to a need to solve non-symmetric, ill-conditioned linear systems of size $10^{18} \times 10^{18}$ at each time step, which will not be computationally feasible in the foreseeable future. But even when it is, there will be bigger problems we wish to solve.

Regularization models are one way to approximate a flow simulation at a lower computational cost. In particular, we consider the Leray regularization model [39], which is given by:

$$\begin{aligned} u_t + \bar{u} \cdot \nabla u + \nabla p - \nu \Delta u &= f && (1.3) \\ \nabla \cdot u &= 0 && (1.4) \\ -\alpha^2 \Delta \bar{u} + \bar{u} + \nabla \lambda &= u && (1.5) \\ \nabla \cdot \bar{u} &= 0, && (1.6) \end{aligned}$$

where $\alpha > 0$ is considered to be the filtering radius, and λ is a Lagrange multiplier corresponding to the divergence constraint. This model is known to be well-posed for positive α, and maintains many attractive properties of the NSE. The Leray model was originally proposed by J. Leray in 1934 as a perturbation of the NSE that was well-posed [39]. In his model, the smoothing was done by convolution with the Gaussian. Here, we follow [11] and use the α-filter, which is an $O(\alpha^4)$ approximation to the Gaussian [18], but still smooths enough to provide well-posedness, and is much more attractive computationally. The Leray model conserves energy and enstrophy [25] and is more easily computed than the NSE [11]; in particular, it can be resolved with $O(Re^{7/8})$ mesh points. Moreover, it is more computationally attractive than the NS-α regularization because it admits a natural linearization which decouples the mass/momtentum system and the filter system, allowing for efficient and stable computations.

A major disadvantage of the Leray model lies in its inaccuracy. At best, the model is $O(\alpha^2)$ accurate, and it has a tendency to over smooth solutions and distort laminar flows [5]. One common fix is to add van Cittert approximate deconvolution to the regularization, to approximately unfilter the filter. This has been shown to yield more accurate computations when used with the α-filter [34, 5]. However, higher order elements are necessary to see gains in accuracy from deconvolution, and it requires additional linear solves at each time step. Part of this thesis concerns improving this model in computations by using an incompressible filter.

As an alternative to deconvolution, we also study nonlinear filtering. This is based on indicator functions, with the idea being to filter "intelligently", by leaving resolvable regions alone

(e.g. laminar areas and coherent structures), and smoothing un-resolved scales. We use the following as a filter:

$$-\alpha^2 \nabla \cdot (a(v)\nabla \overline{v}) + \overline{v} = v, \tag{1.7}$$

where $a(v)$ satisfies,

$$0 < a(v) \leq 1 \text{ for any fluid velocity } v(x,t),$$

$$a(v) \simeq 0 \text{ selects regions requiring no local filtering,}$$

$$a(v) \simeq 1 \text{ selects regions requiring } O(\alpha) \text{ local filtering.}$$

We formulate an a such that $a \simeq 0$ in smooth regions and coherent structures, and $a \simeq 1$ where unresolvable scales exist. Our approach leads to unconditionally stable numerical algorithms that lend themselves to natural linearizations, which allows us to decouple the filter operation, giving efficient computations. Unlike deconvolution, we need not use higher order elements to see gains in accuracy, and we show this through several numerical experiments.

We employ the concept of localized filtering in several ways. First, we consider an $a(u)$ based upon physical phenomenology. In particular, we adapt Vreman's criteria [52] and the Q-criteria of Hunt, Wray, and Moin [26] to fit our needs for such a function. Vreman found a gradient-based formula, which he showed vanishes for 320 different type of laminar flows, and we transform it for use as an indicator function. The Q-criteria is based upon the deformation and spin tensors, using the assumption that spin dominates deformation in a coherent structure. The criteria gives an operator which is positive where spin is dominant and filtering is not necessary. This is rescaled and shifted using the arctan function to give a suitable indicator.

Although these functions are intuitively a good fit, and turn out to be computationally promising, they present an analytical challenge. Thus, we also use the following as an indicator function:

$$a_{D_N}(u) = |u - D_N^h \tilde{u}^h|, \tag{1.8}$$

where $\tilde{u}$ is the discrete Helmholtz filter, and D_N represents N-th order discrete van Cittert deconvolution, defined by

$$D_N = \sum_{n=0}^{N} (I - F)^n, \quad N = 0, 1, 2, \ldots$$

where $Fu := \tilde{u}$. Here, the idea is that when u is smooth, we expect no regularization is necessary and $u \approx D_N^h \tilde{u}^h$. This indicator function does allow for mathematically rigorous analysis, though proving optimal convergence of the numerical method is quite challenging.

The use of an indicator function also extends to coupled systems. The magnetohydrodynamic equations (MHD) model the evolution of electrically conducting fluids. The equations are a combination of the NSE and Maxwell's equations. MHD can be regularized in a similar manner to the NSE. The Leray-MHD model, studied in [53], is given by

$$\begin{aligned} u_t + \bar{u} \cdot \nabla u - \nu \Delta u - s\bar{B} \cdot \nabla B + \nabla p &= f & (1.9) \\ B_t + Re_m^{-1} \Delta B + \bar{u} \cdot \nabla B - \bar{B} \cdot \nabla u - \nabla \lambda &= \nabla \times g & (1.10) \\ \nabla \cdot \bar{u} = \nabla \cdot \bar{B} &= 0, & (1.11) \end{aligned}$$

where $\nabla \times g$ is forcing on the magnetic field, B, Re_m is the magnetic Reynolds number, and s is the coupling number. We can use our local filtering approach to filter both u and B, and as before we can linearize and decouple the system in an unconditionally stable way to allow for more efficient computations, and the analysis which applies to the deconvolution-based indicator function can be extended to MHD.

Another approach to improving the regularization models is through dissipation scale modeling via the "β method", introduced by Fried and Gurtin [16]. The model was proposed as a way to capture the separation between the inertial range (modeled by α) and the dissipation range scales (modeled by $0 < \beta < \alpha$). In other words, the model can better predict some "lost" subgrid scales. The Leray-$\alpha\beta$-deconvolution model is given by

$$\begin{aligned} u_t + D_N \bar{u} \cdot \nabla u + \nabla p - \nu(1 - \beta^2 \Delta) \Delta \bar{u} &= f & (1.12) \\ \nabla \cdot u &= 0 & (1.13) \\ -\alpha^2 \Delta \bar{u} + \bar{u} + \nabla \lambda &= u & (1.14) \\ \nabla \cdot \bar{u} &= 0. & (1.15) \end{aligned}$$

Here, D_N represents N-th order van Cittert deconvolution, defined above. Note that when $\beta = \alpha$, this reduces to the Leray-α-deconvolution model.

At first glance this appears to be a fourth order model, which is unattractive because it

would require C^1 finite elements. However, we use the following identity to reduce the viscous term:

$$-\nu(1-\beta^2\Delta)\Delta\bar{u} = -\nu\left(1-\frac{\alpha^2-\beta^2}{\alpha^2}\right)\Delta u - \nu\left(\frac{\alpha^2-\beta^2}{\alpha^2}\right)\Delta\bar{u}. \tag{1.16}$$

We thus have a second order system that can be linearized and decoupled in a stable way with a mild timestep restriction for stability (which we prove).

Yet another method of improving the Leray model is through fine mesh filtering. Here, we will filter on a finer mesh, which will cause less damping of coherent flow structures, and provide a localized effect of the filtering. In contrast to deconvolution, our method avoids regularity issues on the boundary, and does not introduce extra computational cost. As before, the filter system is decoupled from the mass/momentum system, and even though it is solved on a finer mesh, the filter solve can be considered as equivalent to a well conditioned (shifted) Stokes problem, and moreover, we are using the same matrix at every timestep. Although our analysis shows that using (P_3, P_2) elements on the coarse mesh is necessary for optimal accuracy, we are able to filter with (P_2, P_1) elements and still achieve optimal error estimates. Our numerical method for the model is unconditionally stable and optimally convergent, with element choice and filter radius guided by the analysis.

This thesis is arranged as follows. Chapter 2 gives notation and preliminary results to be used in subsequent chapters. Chapter 3 investigates a nonlinear filtering scheme using the Vreman and Q-criteria based indicator functions. We define these indicator functions, prove stability, and state convergence of our scheme to the NSE, and provide several numerical experiments which demonstrate its effectiveness over NSE and Leray computations on the same meshes.

Chapter 4 investigates the deconvolution-based indicator function. We prove stability and convergence of our scheme, verify the predicted convergence rate, and provide numerical experiments which demonstrate this scheme's effectiveness. Chapter 5 then extends this scheme to the MHD equations. We prove stability and convergence of our algorithm, and verify the convergence rate predicted by the analysis.

Chapter 6 provides a numerical study of the Leray-$\alpha\beta$ model. We prove stability and convergence for the fully nonlinear scheme, prove conditional stability for a linearized and decoupled scheme, and provide a numerical experiment which compares our scheme with the usual Leray-α model. Specifically, we show that choosing $\beta < \alpha$ does indeed improve accuracy in computations.

Chapter 7 investigates the Leray model with fine mesh filtering. We prove stability and convergence of the algorithm, then verify the increased convergence rate associated with the finer mesh, as predicted by the analysis. We then present a benchmark problem which demonstrates the effectiveness of filtering on a finer mesh.

Finally, chapter 8 provides a summary of the work presented in this thesis.

Chapter 2

Preliminaries

We denote by $\Omega \subset \mathbb{R}^d$ (d=2 or 3) an open, simply connected domain with piecewise smooth boundary. The $L^2(\Omega)$ norm and inner product will be denoted by $\|\cdot\|$ and $(\cdot,\cdot)$. For simplicity of the presentation, we assume no-slip boundary conditions, but extension to other common boundary conditions would be done in the usual way. In this setting, the appropriate velocity and pressure spaces are defined as

$$X := (H_0^1(\Omega))^d,\ Q := L_0^2(\Omega).$$

Note that the Poincare inequality holds in X: For $v \in X$,

$$\|v\| \leq C_P \|\nabla v\|, \tag{2.1}$$

where C_P depends only on the size of the domain. We use as the norm on X , $\|v\|_X := \|\nabla v\|_{L^2}$, and denote the dual space of X by $X^\star$, with the norm $\|\cdot\|_\star$. The space of weakly divergence free functions is given by

$$V := \{v \in X :\ (\nabla \cdot v, q) = 0\ \ \forall q \in Q\}.$$

We denote conforming velocity, pressure finite element spaces based on edge to edge triangulations (tetrahedralizations) of Ω (with maximum element diameter h) by

$$X_h \subset X,\ Q_h \subset Q.$$

We assume that $X_h,\ Q_h$ satisfy the usual inf-sup stability condition [21]. The discretely divergence-free subspace of X_h, is given by

$$V_h := \{v_h \in X_h, (\nabla \cdot v_h, q_h) = 0 \ \ \forall q_h \in Q_h\}.$$

For our computations, we use Taylor-Hood (TH) and Scott-Vogelius (SV) element pairs (in the appropriate setting), both of which are known to satisfy the inf-sup condition [8, 54, 2].

On a triangular (tetrahedral) mesh τ_h, TH elements are defined to be the mixed pair $((P_k)^d, P_{k-1})$ and SV elements $((P_k)^d, P_{k-1}^{\text{disc}})$, where P_k denotes element-wise polynomials of degree k. SV elements provide $\nabla \cdot X_h \subset Q_h$, and thus V_h contains only functions which are *pointwise* divergence free (choose $q_h = \nabla \cdot v_h$). SV elements have recently been used to successfully compute approximations to the NSE and related models [9, 40, 10, 42, 29]. The LBB stability of SV elements requires some restrictions on the mesh and polynomial degree, as without any, LBB requires $k = 4$ in 2D and $k = 6$ in 3D [51, 50, 56]. If a barycenter-refined mesh is used, for example, then only $k = d$ is required [45, 54] for LBB. Requiring a mesh be a barycenter refinement of a regular mesh is only a mild restriction, and we use this mesh condition for our computations. Even lower order elements can be LBB stable, but at the expense of using more complex mesh structures [55, 57]. Both element pairs satisfy the following approximation properties [8, 19, 54]:

$$\inf_{v_h \in X_h} \|u - v_h\| \ \leq \ Ch^{k+1}|u|_{k+1}, \ \ u \in (H^{k+1}(\Omega))^d, \tag{2.2}$$

$$\inf_{v_h \in V_h} \|u - v_h\|_1 \ \leq \ Ch^{k}|u|_{k+1}, \ \ u \in (H^{k+1}(\Omega))^d, \tag{2.3}$$

$$\inf_{r_h \in Q_h} \|p - r_h\| \ \leq \ Ch^{k}|p|_{k}, \ \ p \in H^{k}(\Omega). \tag{2.4}$$

We will assume the mesh is sufficiently regular for the inverse inequality to hold with $C_i \approx O(1)$:

$$\|\nabla u_h\| \leq C_i h^{-1} \|u_h\| \ \forall u_h \in X_h.$$

It will be notationally convenient to define a discrete divergence-free Laplace operator (i.e., a discrete Stokes operator) $\Delta_h : X \to V_h$: Given $\phi_h \in V_h$, find $\Delta_h \phi \in V_h$ satisfying $(\Delta_h \phi, v_h) = -(\nabla \phi, \nabla v_h) \ \ \forall v_h \in V_h$ [22].

Lemma 2.0.1. *For $\phi \in H^2(\Omega) \cap X$,*

$$\|\Delta_h \phi\| \leq \|\Delta \phi\|. \tag{2.5}$$

Proof. We start by writing

$$\|\Delta_h \phi\|^2 = (\Delta_h \phi, \Delta_h \phi).$$

By the definition of Δ_h, Green's theorem, and Cauchy-Schwarz, we have

$$\begin{aligned} (\Delta_h \phi, \Delta_h \phi) &= -(\nabla \phi, \nabla \Delta_h \phi) \\ &= (\Delta \phi, \Delta_h \phi) \\ &\leq \|\Delta \phi\| \|\Delta_h \phi\|, \end{aligned}$$

which implies the result. □

Denote $u(t^{n+1/2}) = u((t^{n+1} + t^n)/2)$ for continuous variables and $u^{n+1/2} = (u^{n+1} + u^n)/2$ for both continuous and discrete variables.

We use the skew-symmetric trilinear form to ensure stability of the numerical method.

Definition 2.0.2 (Skew Symmetric operator b^*)**.** *Define the skew-symmetric trilinear form $b^* : X \times X \times X \to \mathbb{R}$ as*

$$b^*(u, v, w) := \frac{1}{2}(u \cdot \nabla v, w) - \frac{1}{2}(u \cdot \nabla w, v) \tag{2.6}$$

There are several important estimates for the b^* operator that we will employ in subsequent sections.

Lemma 2.0.3. *For $u, v, w \in X$, and also $v \in L^\infty(\Omega)$ for the first estimate, the trilinear term $b^*(u, v, w)$ can be bounded by*

$$b^*(u, v, w) \leq \frac{1}{2}\left(\|u\| \|\nabla v\|_\infty \|w\| + \|u\| \|v\|_\infty \|\nabla w\|\right), \tag{2.7}$$

$$b^*(u, v, w) \leq C(\Omega) \|u\|^{1/2} \|\nabla u\|^{1/2} \|\nabla v\| \|\nabla w\|, \tag{2.8}$$

$$b^*(u, v, w) \leq C(\Omega) \|\nabla u\| \|\nabla v\| \|\nabla w\|. \tag{2.9}$$

Proof. The result of the first bound follows immediately from the definition of b^* and Holder's

inequality. The second follows from Holder's inequality, Ladyzhenskaya inequalities, and the Sobolev Embedding Theorem [33]. The third follows immediately from the second, due to the Poincare inequality. □

Lemma 2.0.4 (Discrete Gronwall Lemma)**.** *Let Δt, H, and a_n, b_n, c_n, d_n (for integers $n \geq 0$) be nonnegative numbers such that*

$$a_l + \Delta t \sum_{n=0}^{l} b_n \leq \Delta t \sum_{n=0}^{l-1} d_n a_n + \Delta t \sum_{n=0}^{l} c_n + H \quad for\ l \geq 0. \tag{2.10}$$

Then for all $\Delta t > 0$,

$$a_l + \Delta t \sum_{n=0}^{l} b_n \leq \exp\left(\Delta t \sum_{n=0}^{l-1} d_n\right)\left(\Delta t \sum_{n=0}^{l} c_n + H\right) \quad for\ l \geq 0. \tag{2.11}$$

Proof. The result can be found in [23]. □

2.1 Filtering and deconvolution

We define the discrete incompressible α-filter with a standard finite element implementation of (1.5)-(1.6), as in [43, 41, 12, 5]. We will assume the following definition of the filter unless otherwise noted:

Definition 2.1.1 (Discrete differential filter)**.** *Given $u \in (L^2(\Omega))^d$, for a given filtering radius $\alpha > 0$, $\bar{u}^h = F_h u$ is the unique solution in X_h of: Find $(\bar{u}^h, \lambda_h) \in (X_h, Q_h)$ satisfying*

$$\alpha^2(\nabla \bar{u}^h, \nabla v_h) + (\bar{u}^h, v_h) - (\lambda_h, \nabla \cdot v_h) + (\nabla \cdot \bar{u}^h, r_h) = (u, v_h) \ \ \forall (v_h, r_h) \in (X_h, Q_h). \tag{2.12}$$

Although mathematically the filtering radius α needs only to be chosen positive for the continuous model to be well-posed, in the discrete setting choosing $\alpha << O(h)$ leads to negligible effects of the filter, and thus the choice of $\alpha = O(h)$ is much more common, and we will make this choice throughout this work. Recall also that F_h is both a self-adjoint and positive operator [47].

We define the norms $\|\cdot\|_E$ and $\|\cdot\|_\epsilon$ by

$$\|\phi\|_E := (\phi, \overline{\phi}^h)^{1/2}, \tag{2.13}$$

$$\|\phi\|_\epsilon := (\nabla\phi, \nabla\overline{\phi}^h)^{1/2}. \tag{2.14}$$

That these operators are norms follows from the operator F_h being positive and self adjoint. The following result proves norm equivalences and inequalities for these norms. These results are proven in [29], and are important in the convergence analysis.

Lemma 2.1.2. *For $\phi \in X$, we have the following inequalities*

$$\|\overline{\phi}^h\| \leq \|\phi\|_E \leq \|\phi\|, \tag{2.15}$$

$$\|\nabla\overline{\phi}^h\| \leq \|\phi\|_\epsilon \leq \|\nabla\phi\|. \tag{2.16}$$

Furthermore, with $\alpha \leq O(h)$ and $\phi_h \in V_h$, the reverse inequalities hold up to a constant which is independent of h. Thus the the following norms are equivalent in V_h:

i) $\|\phi_h\|$, $\|\overline{\phi_h}^h\|$, and $\|\phi_h\|_E$

ii) $\|\nabla\phi_h\|$, $\|\nabla\overline{\phi_h}^h\|$, and $\|\phi\|_\epsilon$

The following lemma describes the filtering error, and is proven in [34].

Lemma 2.1.3. *For $\phi \in X$ and $\triangle\phi \in L^2(\Omega)$,*

$$\alpha^2||\nabla(\phi - \bar{\phi}^h)||^2 + ||\phi - \bar{\phi}^h||^2 \leq C\{\alpha^2 h^{2k}|\phi|^2_{k+1} + h^{2k+2}|\phi|^2_{k+1}\} + C\alpha^4||\triangle\phi||^2. \tag{2.17}$$

The next lemma is fundamental to establishing convergence rates.

Lemma 2.1.4. *For $\phi \in X \cap H^2(\Omega)$, and any $v_h \in V_h$,*

$$(\nabla(\overline{\phi}^h - \phi), \nabla v_h) = (\overline{\Delta_h\phi}^h - \Delta_h\phi, v_h). \tag{2.18}$$

Proof. We begin by noting that the continuous Laplacian commutes with the discrete filter, in a weak sense, due to Green's theorem, the definition of the discrete Laplacian, and the commutation

of the discrete Laplacian with the discrete filter, via

$$\begin{aligned}(\Delta\overline{\phi}^h, v_h) &= (\Delta_h\overline{\phi}^h, v_h)\\ &= (\overline{\Delta_h\phi}^h, v_h)\\ &= (\Delta_h\phi, \overline{v_h}^h)\\ &= (\Delta\phi, \overline{v_h}^h)\\ &= (\overline{\Delta\phi}^h, v_h)\ \forall v_h \in V_h. \end{aligned} \tag{2.19}$$

For (4.1.7), use the definition of the discrete Laplacian followed by the fact that discrete filtering commutes with the discrete Laplacian to get

$$\begin{aligned}(\nabla(\overline{\phi}^h - \phi), \nabla v_h) &= (\Delta_h\overline{\phi}^h - \Delta_h\phi, v_h)\\ &= (\overline{\Delta_h\phi}^h - \Delta_h\phi, v_h).\end{aligned}$$

□

Lemma 2.1.5. *Given a filtering radius $\alpha > 0$, and $\beta \leq \alpha$,*

$$-\nu(1-\beta^2\Delta)\Delta\bar{u} = -\nu\left(\left(1 - \frac{\alpha^2-\beta^2}{\alpha^2}\right)\Delta u + \frac{\alpha^2-\beta^2}{\alpha^2}\Delta\bar{u}\right). \tag{2.20}$$

Proof. This is shown in [29]. □

We now define the continuous and discrete Helmholtz filter.

Definition 2.1.6 (Continuous Helmholtz filter)**.** *Let $\phi \in L^2(\Omega)$. Then the Helmholtz filter of ϕ is the solution $\widetilde{\phi} \in X$ of*

$$\alpha^2(\nabla\widetilde{\phi}, \nabla v) + (\widetilde{\phi}, v) = (\phi, v) \quad \forall v \in X. \tag{2.21}$$

It will be notationally convenient to denote this filter also with F, with $F\phi := \widetilde{\phi}$. Discrete Helmholtz filtering is defined in an analogous manner.

Definition 2.1.7. *[Discrete Helmholtz filter] Let $\phi \in L^2(\Omega)$. Then the discrete Helmholtz filter of ϕ is the solution $\widetilde{\phi}^h \in X_h$ of*

$$\alpha^2(\nabla\widetilde{\phi}^h, \nabla\chi_h) + (\widetilde{\phi}^h, \chi_h) = (\phi, \chi_h)\ \forall \chi_h \in X_h. \tag{2.22}$$

We will also use the notation F_h to denote this filter, and define it by $F_h\phi := \tilde{\phi}^h$.

Next, we define discrete and continuous van Cittert deconvolution.

Definition 2.1.8. *The continuous and discrete van Cittert deconvolution operators D_N and D_N^h are defined by*

$$D_N := \sum_{n=0}^{N} (I - F)^n \,, \qquad D_N^h := \sum_{n=0}^{N} (I - F_h)^n. \tag{2.23}$$

From [13], we know that D_N acts as an approximate inverse to the filter F in the following sense:

$$\phi - D_N \widetilde{\phi} = (-1)^{N+1} \alpha^{2N+2} \Delta^{N+1} F^{N+1} \phi. \tag{2.24}$$

For the discrete deconvolution accuracy, we will utilize the following result from [34]:

Lemma 2.1.9. *For $\phi \in X \cap H^{2N+2}(\Omega) \cap H^{k+1}(\Omega)$,*

$$\|\phi - D_N^h \widetilde{\phi}^h\| \leq C \left((\alpha h^k + h^{k+1}) \left(\sum_{n=0}^{N} |F^n \widetilde{\phi}|_{k+1} \right) + \alpha^{2N+2} \|F^{N+1} \Delta^{N+1} \phi\| \right). \tag{2.25}$$

Remark 2.1.10. *The dependence of the terms $|F^n \widetilde{\phi}|_{k+1}$ on the right side of (2.25) on α is partially an open question. However, it is known from [34, 37] that in the periodic setting or if $\Delta^j \phi = 0$ on $\partial\Omega$ for $0 \leq j \leq \lceil \frac{m}{2} \rceil - 1$, they are independent of α. Otherwise, there exist C_i's independent of α satisfying*

$$\begin{aligned} \|F\phi\|_m &\leq C_1 \|\phi\|_m \qquad m = 0, 1, 2 \\ \|F^2\phi\|_m &\leq C_2 \|F\phi\|_m \qquad m = 0, 1, 2, 3, 4 \\ \|F^3\phi\|_m &\leq C_3 \|F^2\phi\|_m \quad m = 0, 1, 2, 3, 4, 5, 6 \end{aligned}$$

and so on. Thus for $k \geq 2$ and for any $N \geq 0$, the loss of a power of α cannot be ruled out.

Chapter 3

Improving accuracy in regularization models via adaptive nonlinear filtering

This chapter is a result of the work in [7]. We study a modification of the Leray$-\alpha$ model that employs a nonlinear filter. The filter we consider herein was first proposed in [38], and is based on the phenomenological idea that in laminar regions or where coherent structures persist, little or no filtering is needed because these regions are resolvable. This idea is implemented as the nonlinear filter (1.7).

The function $a(u)$ is meant to indicate where filtering should be applied, and thus we will refer to it as an *indicator function*. Herein we will study several possible choices of indicator functions, which were mentioned in the introduction, but will be precisely defined in this chapter. In [38], nonlinear filtering was used as part of an 'evolve, then filter, then relax' approach to evolution equations, and successful numerical results were shown for some small 2D problems. We extend the use of this type of filtering for use with the Leray regularization, and give several 2D numerical

examples to demonstrate its effectiveness. The system we study takes the form

$$\begin{aligned} v_t + \overline{v} \cdot \nabla v + \nabla p - \nu \Delta v &= f && (3.1) \\ \nabla \cdot v &= 0 && (3.2) \\ -\alpha^2 \nabla \cdot (a(v) \nabla \overline{v}) + \overline{v} + \nabla \lambda &= v && (3.3) \\ \nabla \cdot \overline{v} &= 0 && (3.4) \end{aligned}$$

We will present a numerical algorithm for the system (3.1)-(3.4) that decouples the conservation system (3.1)-(3.2) from the incompressible filter system (3.3)-(3.4), and provides an efficiently computable, well-posed, discrete system.

3.1 Indicator functions

Given an indicator function $a(\cdot)$, a fluid velocity $u \in X$, an averaging radius α (possibly varying with x), we redefine the filtered velocity $\overline{u}^h$ using a selected indicator function, $a(\cdot)$, as the solution of: Find $(\overline{u}^h, \lambda_h) \in X_h \times Q_h$ satisfying

$$\alpha^2 (a(u) \nabla \overline{u}^h, \nabla v_h) + (\overline{u}^h, v_h) - (\lambda_h, \nabla \cdot v_h) = (u, v_h) \quad \forall v_h \in X_h \,, \tag{3.5}$$

$$(\nabla \cdot \overline{u}^h, q) = 0 \quad \forall q \in Q_h. \tag{3.6}$$

As discussed in the introduction for the continuous case, the Lagrange multiplier term λ_h allows the solenoidal constraint to be enforced. Note that if the chosen element pair is used whose weak enforcement of mass conservation does not provide 'good' mass conservation, e.g. Taylor-Hood elements [10], then grad-div stabilization should be added to (3.5) to improve mass conservation and overall accuracy [36]. Consideration of mass conservation is particularly important in regularization models, where coarse meshes are used, and thus relying on global mass conservation may not be sufficient to provide physically relevant solutions.

When $u \in X$ is given input for the filter system (3.5)-(3.6), nonlinear filtering is made a linear problem. It is shown in [38] that solutions exist uniquely, and satisfy

$$2 \int_\Omega \alpha^2 a(u) |\nabla \overline{u}^h|^2 dx + ||\overline{u}^h||^2 \leq ||u||^2. \tag{3.7}$$

Error in discrete filtering is also considered in [38] and the following result is proven, which shows that what is lost through this discrete filtering is due only to discretization error and the filtering radius.

Theorem 3.1.1. *Consider the discrete nonlinear filter $\overline{u}^h$ given by (3.5), with $u \in X$. We have*

$$\int_\Omega \alpha^2 a(u)|\nabla(u-\overline{u}^h)|^2 dx + ||u-\overline{u}^h||^2$$
$$\leq C \inf_{\widetilde{u}\in X_h} \left\{ \int_\Omega \alpha^2 a(u)|\nabla(u-\widetilde{u})|^2 dx + ||u-\widetilde{u}||^2 \right\} + C\alpha^4 ||\nabla\cdot(a(u)\nabla u)||^2.$$

We consider the following indicator functions, for use with the filter (3.5)-(3.6).

1. The Q-criterion based indicator

   The most popular method for eduction of coherent vortices is the Q criterion, which was developed in [26], and is defined as follows. Define deformation and spin tensors by

   $$\nabla^s u := \frac{1}{2}\left(\nabla u + \nabla u^{tr}\right) \quad \text{and} \quad \nabla^{ss} u := \frac{1}{2}\left(\nabla u - \nabla u^{tr}\right).$$

   A persistent and coherent vortex is found at regions where spin (local rigid body rotation) dominates deformation, i.e. where

   $$Q(u,u) := \frac{1}{2}\left(\nabla^{ss}u : \nabla^{ss}u - \nabla^s u : \nabla^s u\right) > 0.$$

   It is a necessary condition (in 3D) and both necessary and sufficient (in 2D) for slower than exponential local separation of trajectories.

   We define a Q-criterion based indicator function so that $Q(u,u) > 0$ implies $a(u) \simeq 0$ (we note there are many ways to do this, and this way is certainly improvable), and is given by

   $$a_Q(u) := \frac{1}{2} - \frac{1}{\pi}\arctan\left(\alpha^{-1}\frac{Q(u,u)}{|Q(u,u)|+\alpha^2}\right).$$

2. Vreman's eddy viscosity based indicator

In [52], using only the gradient tensor, Vreman constructs an eddy viscosity coefficient formula that vanishes identically for 320 types of flow structures that are known to be coherent (non turbulent). Define

$$\begin{aligned} |\nabla u|_F^2 &= \sum_{i,j=1,2,3} (\frac{\partial u_j}{\partial x_i})^2, \beta_{ij} := \sum_{m=1,2,3} \frac{\partial u_i}{\partial x_m}\frac{\partial u_j}{\partial x_m}, \text{ and} \\ B(u) &: = \beta_{11}\beta_{22} - \beta_{12}^2 + \beta_{11}\beta_{33} - \beta_{13}^2 + \beta_{22}\beta_{33} - \beta_{23}^2. \end{aligned}$$

By construction, $B(u) = 0$ for different laminar flows. Since $0 \leq B(u)/|\nabla u|_F^4 \leq 1$ we take as an indicator function,

$$a_V(u) = \sqrt{\frac{B(u)}{|\nabla u|_F^4}}.$$

3. Synthesized methods

Given indicator functions a_i, constructing synthesized indicator functions can be easily done via

$$a_{ij}(u) := \left(a_i(u)a_j(u)\right)^{1/2}. \tag{3.8}$$

With this method, combining two indicator functions that have different selection criteria can produce a better indicator. In our numerical experiments, best results are usually obtained with a synthesized indicator. We note this was an idea of John Burkardt.

3.2 Numerical algorithm for nonlinear Leray model

We propose the following finite element algorithm to compute solutions to the Leray regularization model with adaptive nonlinear filtering.

Algorithm 3.2.1. *Given a forcing function $f \in L^\infty(0,T;H^{-1}(\Omega))$, initial velocity $u_0 \in V$, timestep $\Delta t > 0$, endtime T and integer M satisfying $T = M\Delta t$, define $u_h^{-1} = u_h^0$ to be the L^2 projection into V_h of u_0. Then for a fixed constant α chosen of the order of the mesh width, and given indicator*

function $0 \leq a(\cdot) \leq 1$, *find* $(u_h^n, p_h^n) \in (X_h, Q_h)$, $n = 1, 2, ..., M$ *satisfying,* $\forall (v_h, q_h) \in (X_h, Q_h)$,

$$\begin{aligned} \frac{1}{\Delta t}(v_h^{n+1} - v_h^n, \chi_h) + \left(\overline{U_h^n}^h \cdot \nabla v_h^{n+\frac{1}{2}}, \chi_h\right) & \\ -(p_h^{n+1/2}, \nabla \cdot \chi_h) + \nu(\nabla v_h^{n+\frac{1}{2}}, \nabla \chi_h) &= (f(t^{n+\frac{1}{2}}), \chi_h) \qquad (3.9) \\ (\nabla \cdot v_h^{n+1}, q_h) &= 0 \qquad (3.10) \end{aligned}$$

where $U_h^n := \frac{3}{2} v_h^n - \frac{1}{2} v_h^{n-1}$ *and* $\overline{\cdot}^h$ *is defined by (3.5)-(3.6).*

Remark 3.2.2. *An initial pressure is not needed, provided the first step is taken using a backward Euler type temporal discretization. Otherwise, pressure is solved for at half-time levels.*

Remark 3.2.3. *If a choice of* (X_h, Q_h) *is used that does not provide pointwise divergence-free solutions to the filtering problem (e.g. Taylor-Hood), then the nonlinear term in* (3.9) *should be skew-symmetrized as in [34], and grad-div stabilization should also be added to* (3.9).

There are several important properties of this discretization. By using a Crank-Nicolson temporal discretization and linear extrapolation of the filtered term, formal second order temporal accuracy is retained while decoupling the filter from the conservation law system and linearizing filter computations; hence at each timestep, two linear solves are needed. Moreover, this scheme is unconditionally stable with respect to timestep, as stated in the next lemma.

Lemma 3.2.4. *For any choice of time step* $\Delta t > 0$, *solutions to Algorithm 3.2.1 satisfy*

$$\|v_h^M\|^2 + \nu \Delta t \sum_{n=0}^{M-1} \|\nabla v_h^{n+1/2}\|^2 \leq C(data). \qquad (3.11)$$

Proof. Choose $\chi_h = v_h^{n+1/2}$. The nonlinear term(s) vanishes, due to skew symmetrization or directly, if the filtered extrapolated velocity is pointwise divergence-free. The pressure term vanishes since we can choose $q_h = p_h^{n+1}$ in (3.10). This leaves

$$\frac{1}{2\Delta t}\left(\|v_h^{n+1}\|^2 - \|v_h^n\|^2\right) + \nu \|\nabla v_h^{n+1/2}\|^2 = (f(t^{n+\frac{1}{2}}), v_h^{n+\frac{1}{2}}).$$

Applying Cauchy-Schwarz and Young's inequalities to the right-hand side, multiplying through by Δt, summing over time steps, and using the smoothness assumptions on the problem data gives the result. □

Remark 3.2.5. *Since the filter system is linear (since u_h^n, u_h^{n-1} are known) and stable, the result* (3.11) *is sufficient to show that Algorithm 3.2.1 is well-posed.*

For simplicity in stating the following convergence theorem, we summarize here the necessary regularity assumptions for the solution $(u(x,t), p(x,t))$ to the NSE

$$u \in L^\infty(0,T; H^{k+1}(\Omega)) \cap L^\infty(0,T; H^4(\Omega)) \tag{3.12}$$

$$u_{tt} \in L^2(0,T; H^1(\Omega)) \tag{3.13}$$

$$u_{ttt} \in L^2(0,T; L^2(\Omega)) \tag{3.14}$$

$$\Delta u_{tt} \in L^2(0,T; L^2(\Omega)). \tag{3.15}$$

Since the adaptive filter differs from the α-filter only by the indicator function which satisfies $0 < a(\cdot) \leq q$, solutions from Algorithm 3.2.1 must have consistency to the NSE at least as good as Leray-α solutions (i.e. when $a(\cdot) = 1$). We have the following convergence result for the algorithm:

Theorem 3.2.6. *Let $(u,p) \in (V,Q)$ be a smooth NSE solution on $\Omega \times (0,T]$ for a given set of data f, u_0, ν. Then if (u_n, p_n), $n = 0,1,...,M$ is the solution to Algorithm 3.2.1 using (P_k, P_{k-1}^{disc}) Scott-Vogelius elements, for $\Delta t > 0$, the velocity error satisfies*

$$\|u(T) - u_h^M\|^2 + \nu \Delta t \sum_{n=0}^{M-1} \|\nabla(u(t^{n+1/2}) - u_h^{n+1/2})\|^2 \leq C\left(\Delta t^4 + h^{2k} + \alpha^4\right), \tag{3.16}$$

where C is a constant dependent on data and the true solution.

Proof. This result follows the convergence proof for the usual Leray-α model given in [34, 5], but using the filter error result from Theorem 3.1.1. □

3.3 Numerical Experiments

In this section, we present several numerical experiments that illustrate the effectiveness of our proposed approach, in giving good coarse mesh approximations of incompressible flows. In particular, we will show this approach gives much better results than for the usual Leray-α model, and gives good approximations on meshes where the NSE is significantly underresolved when computed directly.

3.3.1 2D channel flow over a step

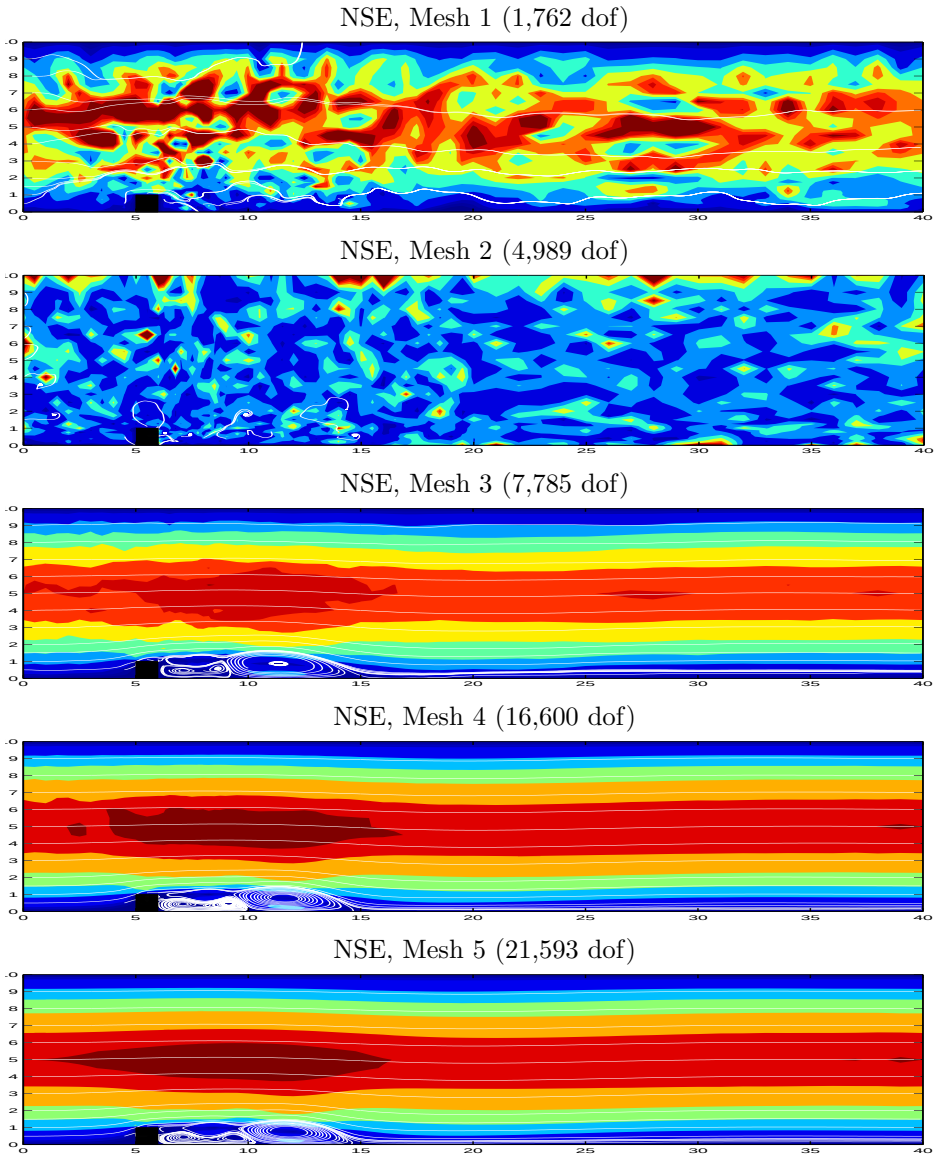

Figure 3.1: Shown above are the velocity solutions at $T = 40$ for 2D flow over a step, found by directly computing the Navier-Stokes equations (i.e. no filtering), on different meshes. Only the finest mesh correctly predicts the true solution.

Our first experiment is for two-dimensional flow over a forward and backward facing step. The domain is a 40 x 10 rectangular channel with a 1 x 1 step five units into the channel at the bottom. We assume no-slip boundary conditions on the top and bottom boundaries, a parabolic inflow profile given by $(y(10-y)/25, 0)^T$, and a zero-traction (do-nothing) outflow. The correct

behavior is a smooth velocity field away from the step, and for eddies to periodically form and shed behind the step.

We first present the results of computing the NSE directly. Computations were made on five successively finer meshes, using $\Delta t = 0.01$ and $\nu = 1/600$, and Taylor-Hood elements. Solutions at $T = 40$ are shown in Figure 3.1 as velocity streamlines over speed contours, and we observe only the finest mesh gets the correct solution, comparing to [34]. The solution is very under-resolved on the coarsest two meshes, and on meshes 3 and 4, the predicted solution captures the eddy formation and detachment, but oscillations are still observed in the speed contours.

We test the proposed model with Algorithm 3.2.1 on the two coarsest meshes, using the same parameters as for the coarse mesh NSE computation, and using indicator functions $a(u) = 1$, a_V, a_Q, and a_{VQ}. Results for Mesh 2 (which provides 4,989 dof) at $T = 40$ are shown in Figure 3.2. All four filters found a smooth flow field, but the Vreman filter and VQ-filter also capture the correct eddy detachment behind the step. Contour plots of the different indicator functions at $T = 40$ are shown for these computations in Figure 3.3. For this example, we see the V and VQ indicators have expected behavior in that little or no filtering is required away from the step. These two indicators suggest filtering is needed near the center of the channel, and we believe this to be a result of the laminar profiles predicted by NSE and regularization models to be slightly different [5], and so a mixing of the two could cause numerical artifacts. The Q indicator plot is quite different. It finds near the step areas to filter and not to filter, which is expected, but throughout the rest of the channel it gives values near 0.5. From the definition of our filter, the values near 0.5 correspond to $Q(u, u) = 0$, and so this suggests additional tuning of a_Q could be helpful (for this particular problem). We also present a plot of the velocity solution obtained using the VQ-filter on Mesh 1, in Figure 3.4. Here, with only 1,762 dof, a good approximation that predicts eddy detachment is found.

3.3.2 2D Flow around a cylinder

Our next numerical experiment is for two dimensional under-resolved channel flow around a cylinder, a well known benchmark problem taken from Shäfer and Turek [48] and John [27]. The flow patterns are driven by the interaction of a fluid with a wall which is an important scenario for many industrial flows. This simple flow is actually quite difficult to simulate successfully by a model with sufficient regularization to handle higher Reynolds number problems.

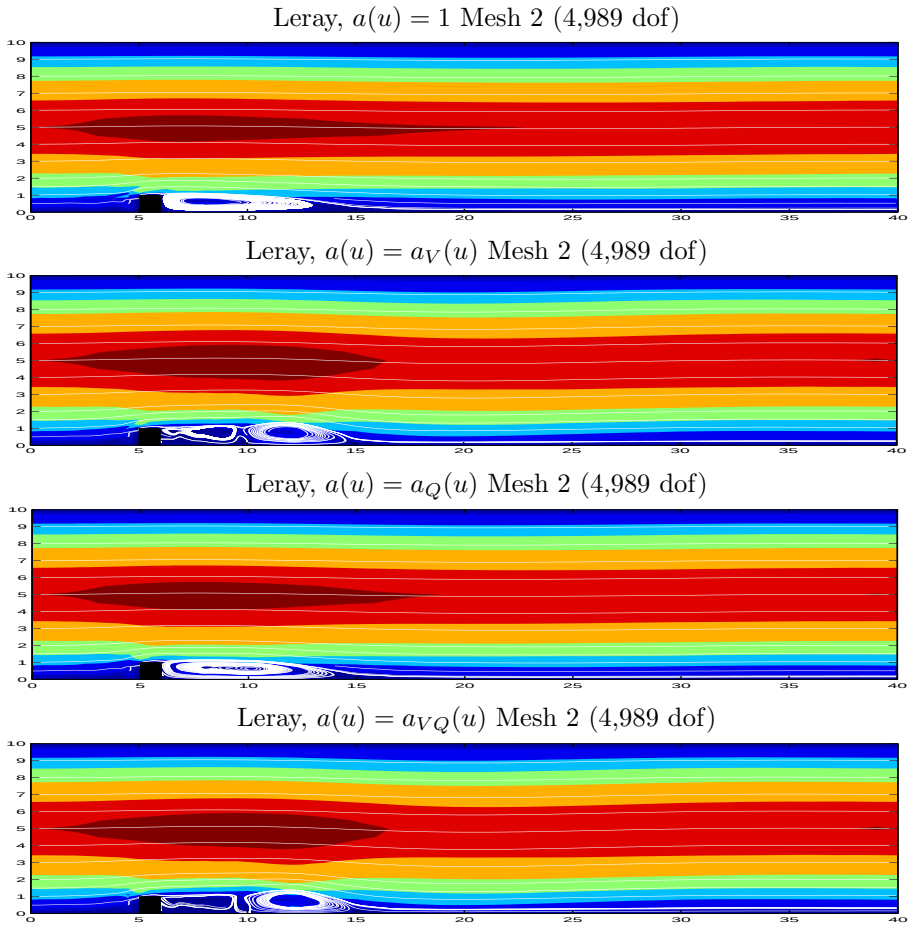

Figure 3.2: Shown above are the velocity solutions for $T = 40$ for 2D flow over a step, for the Leray model with the usual Leray-α model (top) and several choices of indicator functions, on mesh level 2.

The domain for the problem, illustrated in figure 3.5 is a 2.2×0.41 rectangular channel with a cylinder of radius 0.05 centered at $(0.2, 0.2)$ (taking the bottom left corner of the rectangle as the origin). The cylinder, top and bottom of the channel are prescribed no slip boundary conditions, and the time dependent inflow and outflow profile are

$$u_1(0, y, t) = u_1(2.2, y, t) = \frac{6}{0.41^2} \sin(\pi\, t/8) y(0.41 - y)\,,$$
$$u_2(0, y, t) = u_2(2.2, y, t) = 0.$$

The viscosity is set as $\nu = 10^{-3}$ and the external force $f = 0$. From time $t = 2$ to $t = 4$, the correct behavior is for two vortices to start to develop behind the cylinder. They then separate into the

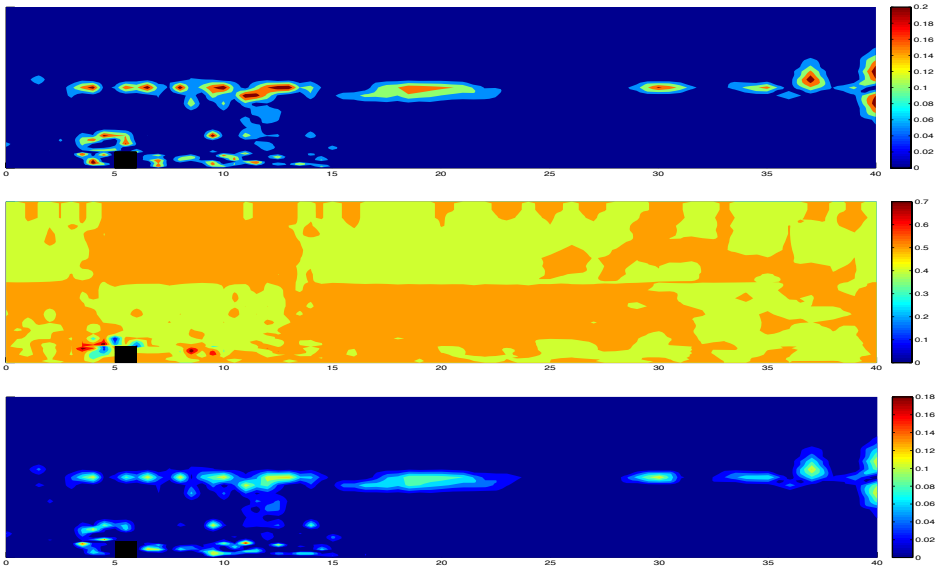

Figure 3.3: Contour plots of the Vreman Filter (top), Q-Filter (middle) and VQ-Filter (bottom), mesh 1, $T = 40$.

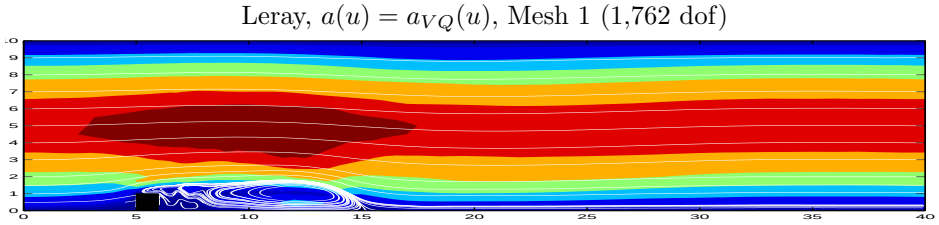

Figure 3.4: Shown above are the velocity solutions at $T = 40$ for 2D flow over a step, for the Leray model with the VQ indicator function, on mesh level 1.

flow, and soon after a vortex street forms which can be visible through the final time $T = 8$. A plot of the resolved $t = 6$ solution is shown in Figure 3.6.

We compute solutions to Algorithm 3.2.1 with Taylor-Hood elements on a triangular mesh providing 14,446 total degrees of freedom, with time step $\Delta t = 0.001$, and filtering radius α chosen to be the average mesh width, with varying indicator functions. These simulations are all under-resolved; fully resolved computations of the Navier-Stokes equations use upwards of 100,000 degrees of freedom and even smaller time steps. Thus we do not expect exact agreement with solutions of Algorithm 3.2.1 with the true solution or lift and drag reference values. However, we do expect answers to be close, if this model/algorithm is to be considered useful.

To evaluate the solutions, we compute values for the maximal drag $c_{d,max}$ and lift $c_{l,max}$

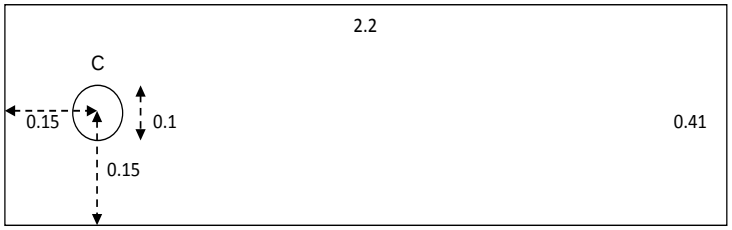

Figure 3.5: Domain for the $2D$ flow past an obstacle.

coefficients at the cylinder, and for the pressure difference $\Delta p(t)$ between the front and back of the cylinder at the final time $T = 8$. Lift and drag coefficients (using the one dimensional method described by V. John [27]) for fully resolved flows will lie in the reference intervals ([48])

$$c_{d,max}^{ref} \in [2.93,\, 2.97], \quad c_{l,max}^{ref} \in [0.47,\, 0.49], \quad \Delta p^{ref} \in [-0.115,\, -0.105]$$

We test Algorithm 3.2.1 with indicator functions $a(u) = 1,\ a_V,\ a_Q$, and a_{VQ}. The plots of velocity field and speed contour, figure 3.7, show that using $a(u) = 1$ does not capture the wake expected behind the cylinder, but $a(u) = a_{VQ}(u)$ does. We saw very similar results for a_Q and a_V (not pictured). The maximum lift and drag coefficients and pressure drop for the simulations are given in Table 3.1, and we see that our algorithm performs well with all three nonlinear filters, but is much less accurate when the linear filter is used. Even on a finer mesh with 56,477 the linear filter (i.e. usual α-filter) still does not perform as well as the nonlinear filters on the coarser mesh (Table 3.1).

Indicator	dof	$c_{d,max}$	$c_{l,max}$	Δp
$a(u) = 1$	14,446	2.2844	0.0176	-0.1267
$a_V(u)$	14,446	2.8472	0.4010	-0.1138
$a_Q(u)$	14,446	2.8574	0.4019	-0.1134
$a_{VQ}(u)$	14,446	2.8628	0.4051	-0.1135
$a(u) = 1$	56,477	2.6682	0.2879	-0.1067
DNS Reference Values	>100,000	[2.93,2.97]	[0.47,0.49]	[-0.115,-0.105]

Table 3.1: Lift, drag and pressure drop for the flow around a cylinder experiment with varying indicator functions used in the filtering.

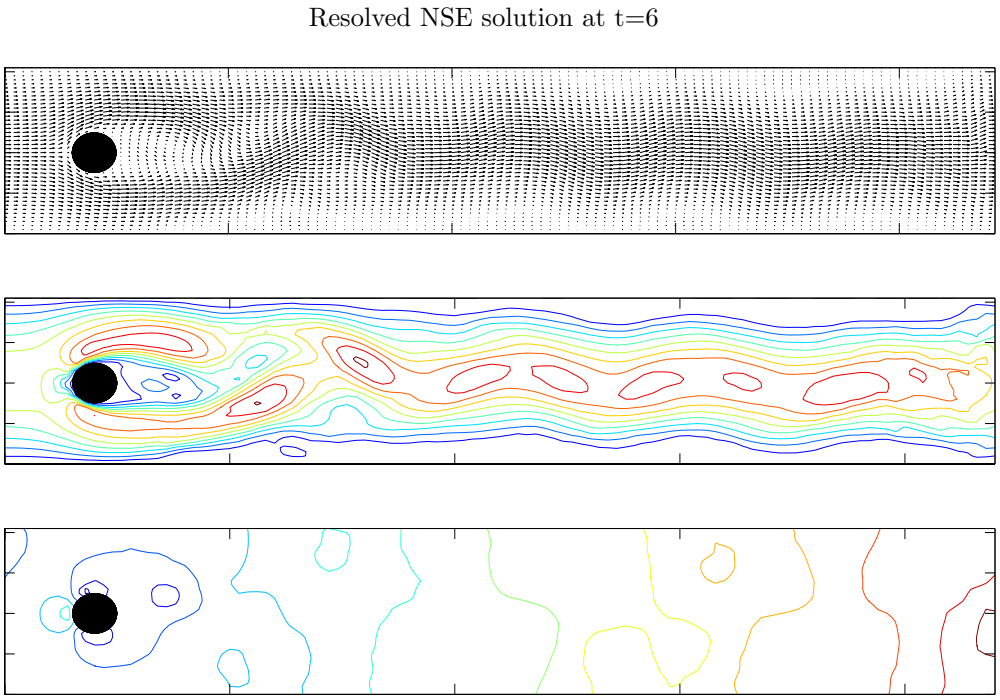

Figure 3.6: Shown above are the (top) velocity field, (middle) speed countours, and (bottom) pressure contours for the resolved $t = 6$ solution to the 2D channel flow around a cylinder problem.

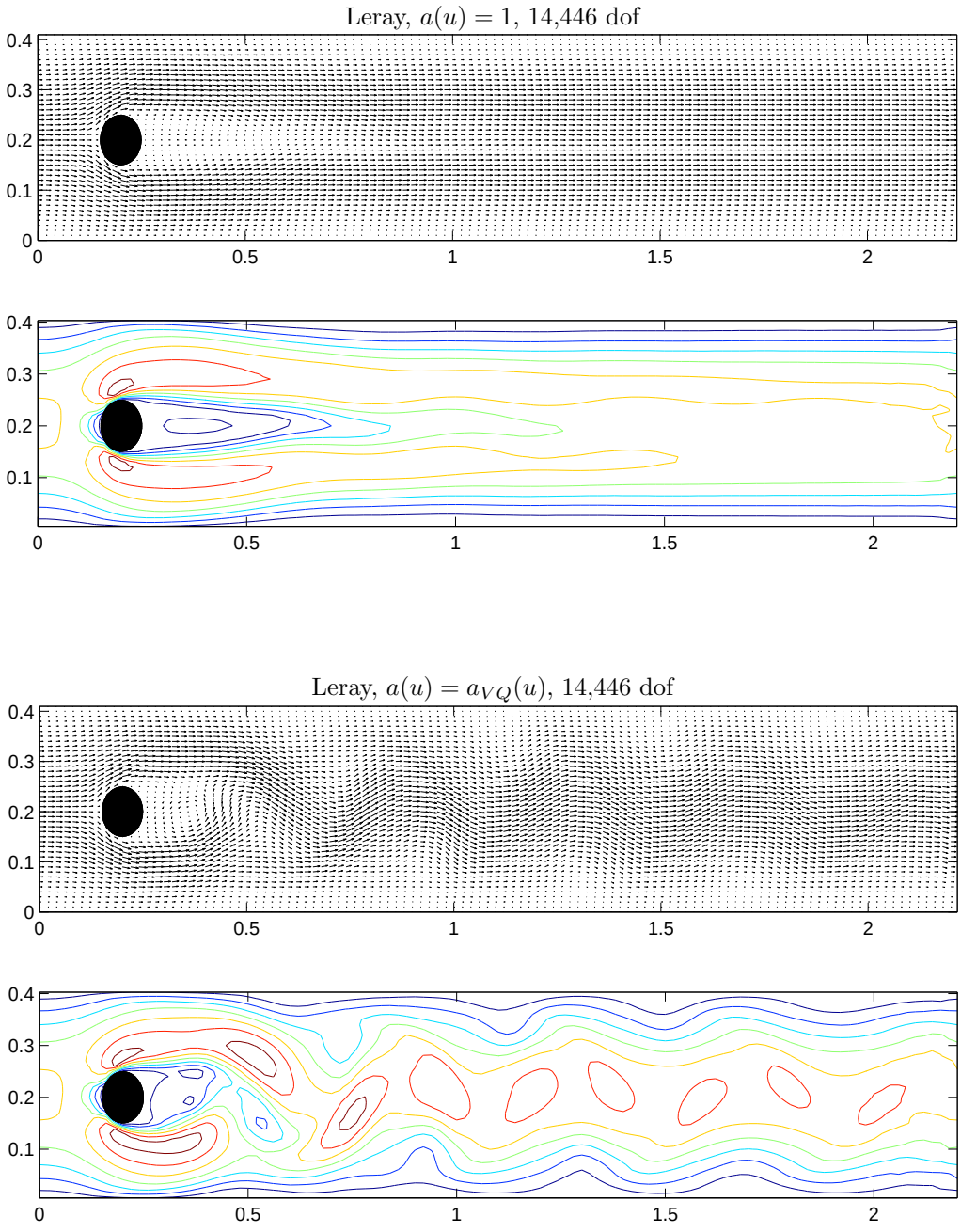

Figure 3.7: Shown above are the velocity field and speed contours for the Leray model with $a(u) = 1$ (top) and $a(u) = a_{VQ}(u)$ (bottom).

Chapter 4

Numerical study of a regularization model for incompressible flow with deconvolution-based adaptive nonlinear filtering

This chapter is a result of the work in [6]. We consider deconvolution-based indicator functions together with adaptive Leray regularization models, which were originally proposed and tested in [7], as stated in Chapter 3. These models use nonlinear filtering with indicator functions to identify regions where regularization is needed, and locally vary the spatial filtering radius accordingly. It is the purpose of this work to extend this methodology by i) developing a better indicator function which is based on mathematics instead of physical phenomenology, ii) providing a rigorous convergence theory to verify the robustness of the method, and iii) further numerical testing.

The purpose of a theory for any numerical method (i.e. proofs of stability and convergence rates) is to provide some sense of robustness for the method, and thus an expectation that it will work in more than only some specific, well-chosen, situations. In [7], simulations with (3.1)-(3.4) using physical phenomenology-based indicator functions were found to be quite successful, however it does not seem that any of those indicator function are able to be rigorously analyzed. This is not

to say that physical-phenomenology-based models are not good or accurate, instead we are simply saying that it is preferable to have a rigorous mathematical proof of accuracy. With this in mind, we propose herein a new indicator function defined by

$$a_{D_N}(u) := |u - D_N^h \widetilde{u}^h|,$$

where $\widetilde{u}^h$ denotes discrete linear Helmholtz filtering of u and D_N^h denotes order N van Cittert approximate deconvolution with the discrete linear Helmholtz filter (Definition 2.1.7). The accuracy of this indicator function is rooted in the accuracy of Richardson extrapolation, and we note the idea of using van Cittert approximate deconvolution in fluid models to increase accuracy is well established and mathematically grounded [1, 49, 13]. The main idea behind this indicator function is that, for continuous-level filtering and deconvolution, $\phi \approx D_N \widetilde{\phi}$ where ϕ is smooth. Hence, if we consider ϕ as a velocity field, then if ϕ is smooth, we expect no regularization is necessary in regions where $\phi \approx D_N \widetilde{\phi}$. However, an implementation of this idea must use discrete filtering and discrete approximate deconvolution, and so it turns out the analysis to prove convergence of the resulting numerical method is quite challenging.

4.1 Preliminaries

Definition 4.1.1. *We define as an indicator function*

$$a_{D_N}(u)(x) := |u(x) - D_N^h \widetilde{u}^h(x)|. \tag{4.1}$$

Remark 4.1.2. *The function a_{D_N} cannot be expected to exactly satisfy $a_{D_N}(x) \leq 1$, although in our experience, for flows which are normalized to have a characteristic velocity of 1, this relation has always been true. Due to the imprecision of α, it is not problematic for a flow to have a maximum $a_{D_N}(u)(x)$ slightly larger than one. Still, if it is not, an indicator of the form*

$$\hat{a}_{D_N}(u)(x) := \frac{a_{D_N}(u)(x)}{\max\{1, 2\|u\|_{L^\infty(0,T;L^\infty)}\}}$$

could be used instead, and all the theory provided herein will still hold. Hence, without loss of generality, we will assume $a_{D_N}(x) \leq 1$.

Adaptive filtering with the deconvolution based indicator function is defined as follows.

Definition 4.1.3 (Adaptive filtering using the deconvolution-based indicator function)**.** *Given $u \in L^2(\Omega)$ and an averaging radius $\alpha > 0$, we define the adaptively filtered velocity $\overline{u}^h \in V_h$ to be the solution of*

$$\alpha^2(a_{D_N}(u)\nabla\overline{u}^h, \nabla v_h) + (\overline{u}^h, v_h) = (u, v_h) \quad \forall v_h \in V_h. \tag{4.2}$$

The next lemmas prove bounds on adaptively filtered variables.

Lemma 4.1.4. *For $u \in X$,*

1.

$$2\alpha^2\|\sqrt{a_{D_N}(u)}\nabla\overline{u}^h\|^2 + \|\overline{u}^h\| \leq \|u\|. \tag{4.3}$$

2. If $L : X \to V_h$ is a linear operator such that

$$(Lw, v_h) = -(a_{D_N}(u)\nabla w, \nabla v_h) \ \forall v_h \in V_h, \tag{4.4}$$

then

$$2\alpha^2\|L\overline{u}^h\|^2 + \|\sqrt{a_{D_N}(u)}\nabla\overline{u}^h\|^2 \leq \|\nabla u\|^2. \tag{4.5}$$

Proof. For the first inequality, let $v_h = \overline{u}^h$ in (4.2), then apply Cauchy-Schwarz and Young's inequalities on the right hand side.

For the second estimate, in (4.2), choose $v_h = L\overline{u}^h$ to get

$$\alpha^2(a_{D_N}(u)\nabla\overline{u}^h, \nabla L\overline{u}^h) + (\overline{u}^h, L\overline{u}^h) = (P^{L^2}_{X_h}u, L\overline{u}^h). \tag{4.6}$$

Simplifying and using (4.4), we have

$$-\alpha^2\|L\overline{u}^h\|^2 - (a_{D_N}(u)\nabla\overline{u}^h, \nabla\overline{u}^h) = (\nabla P^{L^2}_{X_h}u, a_{D_N}(u)\nabla\overline{u}^h), \tag{4.7}$$

and thus

$$\alpha^2\|L\overline{u}^h\|^2 + \|\sqrt{a_{D_N}(u)}\nabla\overline{u}^h\|^2 \leq |a_{D_N}(u)\nabla P^{L^2}_{X_h}u, \nabla\overline{u}^h|. \tag{4.8}$$

Now using Cauchy-Schwarz, we get

$$\begin{aligned} 2\alpha^2\|L\overline{u}^h\|^2 + \|\sqrt{a_{D_N}(u)}\nabla\overline{u}^h\|^2 &\leq \|\sqrt{a_{D_N}(u)}\nabla P^{L^2}_{X_h}u\|^2 \\ &\leq \|\nabla P^{L^2}_{X_h}u\|^2 \\ &\leq C\|\nabla u\|^2. \end{aligned} \tag{4.9}$$

□

A key step in the convergence analysis of the method we propose in Section 4 is to bound $\|u - \overline{u_h}^h\|$. The next two lemmas accomplish this, but in two separate steps, then bring the results together with the triangle inequality. First, we define an intermediate filtering procedure 'between' the function and its adaptively filtered representation, to make for a cleaner analysis.

Definition 4.1.5. *For $\phi \in L^2(\Omega)$, $u_h \in V_h$, $\widehat{\phi}^{u_h} \in V_h$ is defined to be the solution of, $\forall v_h \in V_h$,*

$$\alpha^2(a_{D_N}(u_h)\nabla\widehat{\phi}^{u_h}, \nabla v_h) + (\widehat{\phi}^{u_h}, v_h) = (\phi, v_h). \tag{4.10}$$

Lemma 4.1.6. *For $u \in V \cap H^{k+1}(\Omega) \cap H^3(\Omega)$, and $\hat{u}^{h,u_h}$ satisfying (4.10) with $\alpha = O(h)$, we have*

$$\alpha^2\|\sqrt{a_{D_N}(u_h)}\nabla(u - \widehat{u}^{u_h})\|^2 + \|u - \widehat{u}^{u_h}\|^2 \leq C(\alpha^2 h^{2k} + \alpha^2\|a_{D_N}(u)\|^2 + h^{2k+2}) + C\alpha^2\|u - u_h\|^2. \tag{4.11}$$

Proof. Let $\widehat{u}^{u_h}$ satisfy (4.10). Add $\alpha^2(a_{D_N}(u_h)\nabla u, \nabla v_h)$ to both sides, and denote $e := u - \widehat{u}^{u_h}$ to get

$$\alpha^2(a_{D_N}(u_h)\nabla e, \nabla v_h) + (e, v_h) = \alpha^2(a_{D_N}(u_h)\nabla u, \nabla v_h). \tag{4.12}$$

For arbitrary $U_h \in V_h$, denote $e = u - U_h + U_h - \widehat{u}^{u_h} := \eta + \phi_h$. Choosing $v_h = \phi_h$ gives

$$\begin{aligned}
\alpha^2\|\sqrt{a_{D_N}(u_h)}\nabla\phi_h\|^2 + \|\phi_h\|^2 &= (\alpha^2 a_{D_N}(u_h)\nabla\eta, \nabla\phi_h) + (\eta, \phi_h) + \alpha^2(a_{D_N}(u_h)\nabla u, \nabla\phi_h) \\
&\leq \alpha^2\|\sqrt{a_{D_N}(u_h)}\nabla\eta\|\|\sqrt{a_{D_N}(u_h)}\nabla\phi_h\| + \|\eta\|\|\phi_h\| \\
&\quad + \alpha^2\|a_{D_N}(u_h)\nabla u\|\|\nabla\phi_h\| \\
&\leq \frac{\alpha^2}{2}\|\sqrt{a_{D_N}(u_h)}\nabla\eta\|^2 + \frac{\alpha^2}{2}\|\sqrt{a_{D_N}(u_h)}\nabla\phi_h\|^2 + \frac{1}{2}\|\eta\|^2 \\
&\quad + \frac{1}{2}\|\phi_h\|^2 + \alpha^2\|a_{D_N}(u_h)\nabla u\|\|\nabla\phi_h\|. \qquad (4.13)
\end{aligned}$$

Next, we reduce, and for the last term on the right hand side, we apply the inverse inequality and that $\alpha = O(h)$ to get

$$\begin{aligned}
\frac{\alpha^2}{2}\|\sqrt{a_{D_N}(u_h)}\nabla\phi_h\|^2 + \frac{1}{2}\|\phi_h\|^2 \leq \frac{\alpha^2}{2}\|\sqrt{a_{D_N}(u_h)}\nabla\eta\|^2 \\
+ \frac{1}{2}\|\eta\|^2 + C\alpha^2\|a_{D_N}(u_h)\nabla u\|^2 + \frac{1}{4}\|\phi_h\|^2. \qquad (4.14)
\end{aligned}$$

This reduces further using that $a_{D_N}(\cdot) \leq 1$ and the assumptions on the smoothness of u, yielding

$$\begin{aligned}
\alpha^2\|\sqrt{a_{D_N}(u)}\nabla\phi_h\|^2 + \|\phi_h\|^2 &\leq \alpha^2\|\sqrt{a_{D_N}(u_h)}\nabla\eta\|^2 + \|\eta\|^2 + \alpha^2\|a_{D_N}(u_h)\nabla u\|^2 \\
&\leq C\alpha^2\|a_{D_N}(u_h)\|_\infty^2\|\nabla\eta\|^2 + \|\eta\|^2 + C\alpha^2\|a_{D_N}(u_h)\|^2\|\nabla u\|_\infty^2 \\
&\leq \alpha^2\|\nabla\eta\|^2 + \|\eta\|^2 + C\alpha^2\|a_{D_N}(u_h)\|^2.
\end{aligned}$$

Finally, we write $a_{D_N}(u_h) = a_{D_N}(u) + a_{D_N}(e)$, and using that $\|a_{D_N}(e)\| \leq C\|e\|$ [37], we obtain

$$\begin{aligned}
\alpha^2\|\sqrt{a_{D_N}(u)}\nabla\phi_h\|^2 + \|\phi_h\|^2 &\leq \alpha^2\|\nabla\eta\|^2 + \|\eta\|^2 + C\alpha^2\|a_{D_N}(u)\|^2 + C\alpha^2\|a_{D_N}(e)\|^2 \\
&\leq C(\alpha^2 h^{2k} + h^{2k+2} + \alpha^2\|a_{D_N}(u)\|^2) + C\alpha^2\|u - u_h\|^2. \qquad (4.15)
\end{aligned}$$

Reducing and applying the triangle inequality finishes the proof. □

Lemma 4.1.7. *For $u \in V$ and $u_h \in V_h$,*

$$\|\widehat{u}^{u_h} - \overline{u_h}^h\| \leq \|u - u_h\|. \qquad (4.16)$$

Proof. Let $\widehat{u}^{u_h}$ satisfy (4.10). Then for $\overline{u_h}^h$ defined by (4.2), subtract the filter equation and denote

$e = u - u_h$ to get, $\forall v_h \in V_h$,

$$\alpha^2(a_{D_N}(u_h)\nabla(\widehat{u}^{u_h} - \overline{u_h}^h), \nabla v_h) + (\widehat{u}^{u_h} - \overline{u_h}^h, v_h) = (e, v_h). \tag{4.17}$$

Choosing $v_h = \widehat{u}^{u_h} - \overline{u_h}^h$ gives

$$\alpha^2 \|\sqrt{a_{D_N}(u_h)}\nabla(\widehat{u}^{u_h} - \overline{u_h}^h)\|^2 + \|\widehat{u}^{u_h} - \overline{u_h}^h\|^2 = (e, \widehat{u}^{u_h} - \overline{u_h}^h). \tag{4.18}$$

This implies

$$\begin{aligned} \|\widehat{u}^{u_h} - \overline{u_h}^h\|^2 &\leq (e, \widehat{u}^{u_h} - \overline{u_h}^h) \\ &\leq \|e\|\|\widehat{u}^{u_h} - \overline{u_h}^h\|, \end{aligned} \tag{4.19}$$

which proves the result after reducing and substituting in the definition of e. □

Remark 4.1.8. *Combining lemmas 4.1.6 and 4.1.7 provides the result: For $u \in V \cap H^{k+1}(\Omega) \cap H^3(\Omega)$, $u_h \in V_h$, and assuming $\alpha = O(h)$,*

$$\|u - \overline{u_h}^h\| \leq \|u - \widehat{u}^{u_h}\| + \|\overline{u_h}^h - \widehat{u}^{u_h}\| \leq C\left(\|u - u_h\| + \alpha h^k + \alpha\|a_{D_N}(u)\|\right). \tag{4.20}$$

4.2 Scheme and Stability

We now define the numerical scheme studied herein, and prove it is well-posed.

Algorithm 4.2.1. *Given a kinematic viscosity $\nu > 0$, an end-time $T > 0$, a timestep Δt chosen so that $\Delta t < T = M\Delta t$, $f \in L^\infty(0, T; H^{-1}(\Omega))$, initial conditions $u_h^{-1} = u_h^0 \in V_h$, filtering radius $\alpha \leq O(h)$, find $(u_h^n, p_h^n) \in (X_h, Q_h)$ for $n = 1, 2, ..., M$ satisfying, $\forall (v_h, q_h) \in (X_h, Q_h)$,*

$$\begin{aligned} \frac{1}{\Delta t}(u_h^{n+1} - u_h^n, v_h) + b^*\left(\overline{\frac{3}{2}u_h^n - \frac{1}{2}u_h^{n-1}}^h, u_h^{n+1/2}, v_h\right) - (p_h^{n+1/2}, \nabla \cdot v_h) & \\ +\nu(\nabla u_h^{n+1/2}, \nabla v_h) &= (f^{n+1/2}, v_h), \end{aligned} \tag{4.21}$$

$$(\nabla \cdot u_h^{n+1}, q_h) = 0. \tag{4.22}$$

Remark 4.2.2. *The filtered terms are treated explicitly in this timestepping scheme, so at each timestep one needs to perform one adaptive filter solve and one mass/momentum system solve. Note also that, in practice, one solves directly for $p_h^{n+1/2}$, and so no initial pressure is required.*

Lemma 4.2.3. *Solutions to Algorithm 4.2.1 exist uniquely.*

Proof. Observe that at each timestep we solve two finite dimensional and linear problems. It is clear that the filter system is well-posed, and so we consider only the momentum mass system. Assuming two solutions at timelevel $n+1$, (u_1, p_1) and (u_2, p_2), if we define $e := u_1 - u_2$ we have that

$$\frac{1}{\Delta t}(e, v_h) + \frac{1}{2}b^*\left(\overline{\frac{3}{2}u_h^n - \frac{1}{2}u_h^{n-1}}^h, e, v_h\right) - (p_1 - p_2, \nabla \cdot v_h) + \frac{\nu}{2}(\nabla e, \nabla v_h) = 0. \tag{4.23}$$

Now choosing $v_h = e$ vanishes the pressure and trilinear terms, which yields

$$\frac{1}{\Delta t}\|e\|^2 + \frac{\nu}{2}\|\nabla e\|^2 = 0.$$

Thus $\|\nabla e\| = \|e\| = 0$, and since e is finite dimensional, $u_1 = u_2$. Using this and the LBB assumption immediately shows $p_1 = p_2$. We have proven that solutions are unique at each time step, and since the problem is finite dimensional and linear, this implies solutions must exist as well. Since the chosen timestep level was arbitrary, and we started with a unique initial condition, the stated result follows. □

Next, we prove that these solutions are bounded by the problem data.

Lemma 4.2.4. *Solutions to Algorithm 4.2.1 satisfy*

$$\|u_h^M\|^2 + \Delta t\nu \sum_{n=0}^{M-1} \|\nabla u_h^{n+1/2}\|^2 \leq C(\nu, f, u_0, T). \tag{4.24}$$

Proof. Choose $v_h = u_h^{n+1/2}$ in (7.1). The trilinear and pressure terms vanish, leaving

$$\begin{aligned} \frac{1}{2\Delta t}(\|u_h^{n+1}\|^2 - \|u_h^n\|^2) + \nu\|\nabla u_h^{n+1/2}\|^2 &= (f^{n+1/2}, u_h^{n+1/2}) \\ &\leq \frac{1}{2\nu}\|f^{n+1/2}\|_{-1}^2 + \frac{\nu}{2}\|\nabla u_h^{n+1/2}\|^2, \end{aligned} \tag{4.25}$$

which reduces to

$$\frac{1}{2\Delta t}(\|u_h^{n+1}\|^2 - \|u_h^n\|^2) + \frac{\nu}{2}\|\nabla u_h^{n+1/2}\|^2 \leq \frac{1}{2\nu}\|f^{n+1/2}\|_{-1}^2. \tag{4.26}$$

Summing over timesteps and multiplying by $2\Delta t$ gives

$$\|u_h^M\|^2 + \Delta t\nu \sum_{n=0}^{M-1} \|\nabla u_h^{n+1/2}\|^2 \leq \nu^{-1}\Delta t \sum_{n=0}^{M-1} \|f^{n+1/2}\|_{-1}^2 + \|u_h^0\|^2, \tag{4.27}$$

which finishes the proof. □

4.3 Convergence

This section is devoted to proving convergence of the numerical scheme. For simplicity in stating the following theorem, we state here the regularity assumptions on the solution $(u(x,t), p(x,t))$ of the true Navier-Stokes solution, which we denote (u, p):

$$u \in L^\infty(0,T; H^{k+1}(\Omega) \cap H^3(\Omega) \cap V) \tag{4.28}$$

$$u_{tt} \in L^4(0,T; H^1(\Omega)) \tag{4.29}$$

$$u_{ttt} \in L^2(0,T; L^2(\Omega)) \tag{4.30}$$

$$p \in L^\infty(0,T; H^k(\Omega)). \tag{4.31}$$

We will denote $U_h^n := \frac{3}{2}u_h^n - \frac{1}{2}u_h^{n-1}$ and $U^n := \frac{3}{2}u(t^n) - \frac{1}{2}u(t^{n-1})$.

Theorem 4.3.1. *Let $(u(t), p(t))$ be a solution of the NSE satisfying no-slip boundary conditions, and (4.28)-(4.31), with given $f \in L^\infty(0,T; H^{-1}(\Omega))$ and $u_0 \in V_h$. Let (u_h^n, p_h^n), $n = 1, \ldots M$ be the solution of Algorithm 4.2.1, using (P_k, P_{k-1}) Taylor-Hood or (P_k, P_{k-1}^{disc}) Scott-Vogelius elements in a setting where they are LBB stable, and $\alpha \leq O(h)$, and without loss of generality $\alpha < 1$. Then for any $\Delta t > 0$, the error in the discrete solution satisfies*

$$\|u(T) - u_h^M\|^2 + \Delta t \sum_{n=0}^{M-1} \nu\|\nabla(u^{n+1/2} - u_h^{n+1/2})\|^2 \leq C(\Delta t^4 + \alpha^2 h^{2k} + \alpha^2\|a_{D_N}(u)\|^2 + h^{2k}),$$

where C is independent of $h, \alpha,\ \Delta t$, but depends on the data and NSE solution.

Remark 4.3.2. *If we assume $\Delta^j u = 0$ on $\partial\Omega$ for $0 \le j \le \lceil \frac{m}{2} \rceil - 1$, or periodic boundary conditions, then the result becomes*

$$\|u(T) - u_h^M\|^2 + \Delta t \sum_{n=0}^{M-1} \nu \|\nabla(u^{n+1/2} - u_h^{n+1/2})\|^2 \le C(\Delta t^4 + \alpha^2 h^{2k} + \alpha^{4N+6} + h^{2k}).$$

Proof. The NSE at time $t = t^{n+1/2}$, after denoting $u^{n+1/2} := \frac{u(t^{n+1}) + u(t^n)}{2}$, satisfies for all $v_h \in V_h$:

$$\left(\frac{u(t^{n+1}) - u(t^n)}{\Delta t}, v_h\right) + \nu(\nabla u^{n+1/2}, \nabla v_h) + b^*\left(\widehat{U^n}^{U_h^n}, u^{n+1/2}, v_h\right) - (p(t^{n+1/2}), \nabla \cdot v_h) = (f(t^{n+1/2}), v_h) + G(u, n, v_h), \quad (4.32)$$

where

$$G(u, n, v_h) := \left(\frac{u(t^{n+1}) - u(t^n)}{\Delta t} - u_t(t^{n+1/2}), v_h\right) + \nu(\nabla(u^{n+1/2} - u(t^{n+1/2})), v_h) \quad (4.33)$$

$$+ \quad b^*\left(\widehat{U^n}^{U_h^n}, u^{n+1/2}, v_h\right) - b^*(u(t^{n+1/2}), u(t^{n+1/2}), v_h). \quad (4.34)$$

Take $v_h \in V_h$ in (4.21), which vanishes the pressure term, and subtract the equation from (4.32) to get

$$\frac{1}{\Delta t}(e^{n+1} - e^n, v_h) + b^*\left(\overline{U_h^n}^h, u_h^{n+1/2}, v_h\right) - b^*\left(\widehat{U^n}^{U_h^n}, u^{n+1/2}, v_h\right) + \nu(\nabla e^{n+1/2}, \nabla v_h) = (p(t^{n+1/2}), \nabla \cdot v_h) + G(u, n, v_h).$$

Rewriting the nonlinearity gives

$$\frac{1}{\Delta t}(e^{n+1} - e^n, v_h) + b^*\left(\overline{U_h^n}^h, e^{n+1/2}, v_h\right) + b^*\left(\overline{U_h^n}^h - \widehat{U^n}^{U_h^n}, u^{n+1/2}, v_h\right) + \nu(\nabla e^{n+1/2}, \nabla v_h) = (p(t^{n+1/2}), \nabla \cdot v_h) + G(u, n, v_h).$$

Decompose the velocity error term as

$$e^n = (u(t^n) - P_{V_h}^{L^2}(u(t^n))) - (u_h^n - P_{V_h}^{L^2}(u(t^n))) =: \eta^n - \phi_h^n,$$

then choose $v_h = \phi_h^{n+\frac{1}{2}}$ to get, $\forall q_h \in Q_h$,

$$\frac{1}{2\Delta t}(\|\phi_h^{n+1}\|^2 - \|\phi_h^n\|^2) + \nu\|\nabla\phi_h^{n+1/2}\|^2 = (\nabla\eta^{n+1/2}, \nabla\phi_h^{n+1/2}) - b^*\left(\overline{U_h^n}^h, \eta^{n+1/2}, \phi_h^{n+1/2}\right)$$
$$- b^*\left(\overline{U_h^n}^h - \widehat{U^n}^{U_h^n}, u^{n+1/2}, \phi_h^{n+1/2}\right) + (p(t^{n+1/2}) - q_h, \nabla\cdot\phi_h^{n+1/2}) + G(u, n, \phi_h^{n+1/2}).$$

Applying Cauchy-Schwarz and Young inequalities yields

$$\frac{1}{2\Delta t}(\|\phi_h^{n+1}\|^2 - \|\phi_h^n\|^2) + \frac{\nu}{2}\|\nabla\phi_h^{n+1/2}\|^2 \le C\nu\|\nabla\eta^{n+1/2}\|^2 + C\nu^{-1}\inf_{q_h\in Q_h}\|p - q_h\|^2$$
$$+ b^*\left(\overline{U_h^n}^h, \eta^{n+1/2}, \phi_h^{n+1/2}\right) + b^*\left(\overline{U_h^n}^h - \widehat{U^n}^{U_h^n}, u^{n+1/2}, \phi_h^{n+1/2}\right) + G(u, n, \phi_h^{n+1/2}). \quad (4.35)$$

We now bound the first trilinear term, using Lemmas 4.2.4 and 4.1.7, Poincare's inequality, and decomposing U_h^n and U^n.

$$b^*\left(\overline{U_h^n}^h - \widehat{U^n}^{U_h^n}, u^{n+1/2}, \phi_h^{n+1/2}\right) \le C\|\overline{U_h^n}^h - \widehat{U^n}^{U_h^n}\|\|\nabla u^{n+1/2}\|_\infty\|\phi_h^{n+1/2}\|$$
$$\le C\|U_h^n - U^n\|\|u^{n+1/2}\|_3\|\nabla\phi_h^{n+1/2}\|$$
$$\le \frac{\nu}{8}\|\nabla\phi_h^{n+1/2}\|^2 + C\nu^{-1}\|u^{n+1/2}\|_3^2(\|\eta^n\|^2 + \|\eta^{n-1}\|^2 + \|\phi_h^n\|^2 + \|\phi_h^{n-1}\|^2). \quad (4.36)$$

We bound the remaining term using Remark 4.1.8 as follows:

$$\begin{aligned}
b^*\left(\overline{U_h^n}^h, \eta^{n+1/2}, \phi_h^{n+1/2}\right) &= b^*\left(\overline{U_h^n}^h - U^n, \eta^{n+1/2}, \phi_h^{n+1/2}\right) + b^*\left(U^n, \eta^{n+1/2}, \phi_h^{n+1/2}\right) \\
&\le C\|\overline{U_h^n}^h - U^n\|(\|\nabla\eta^{n+1/2}\|\|\phi_h^{n+1/2}\|_\infty + \|\eta^{n+1/2}\|\|\nabla\phi_h^{n+1/2}\|_\infty) \\
&\quad + C\|\nabla U^n\|\|\nabla\eta^{n+1/2}\|\|\nabla\phi_h^{n+1/2}\| \\
&\le C\|\overline{U_h^n}^h - U^n\|(h^{-1/2}\|\nabla\eta^{n+1/2}\|\|\nabla\phi_h^{n+1/2}\| + h^{-3/2}\|\eta^{n+1/2}\|\|\nabla\phi_h^{n+1/2}\|) \\
&\quad + \frac{\nu}{32}\|\nabla\phi_h^{n+1/2}\|^2 + C\nu^{-1}\|\nabla U^n\|^2\|\nabla\eta^{n+1/2}\|^2 \\
&\le \frac{\nu}{16}\|\nabla\phi_h^{n+1/2}\|^2 + C\nu^{-1}\|\overline{U_h^n}^h - U^n\|^2(h^{2k-1}|u|_{k+1}^2) + C\nu^{-1}\|\nabla\eta^{n+1/2}\|^2 \\
&\le \frac{\nu}{16}\|\nabla\phi_h^{n+1/2}\|^2 + C\nu^{-1}h^{2k-1}(\|\eta^{n-1}\|^2 + \|\eta^n\|^2 + \|\phi_h^{n-1}\|^2 + \|\phi_h^n\|^2 \\
&\quad + \alpha^2 h^{2k} + \alpha^2\|a_{D_N}(u)\|^2) + C\nu^{-1}\|\nabla\eta^{n+1/2}\|^2. \qquad (4.37)
\end{aligned}$$

We next bound the terms in $G(u, n, \phi_h^{n+1/2})$ following [33]. For the last two terms, we add $b^*\left(U^n, u^{n+1/2}, \phi_h^{n+1/2}\right)$

to the first one and subtract it from the second one. The second term is then bounded using Cauchy-Schwarz and Young inequalities and Lemma 4.1.6,

$$\begin{aligned}
&b^*(\widehat{U^n}^{U_h^n} - U^n, u^{n+1/2}, \phi_h^{n+1/2}) \\
&\quad\leq \quad C\|\widehat{U^n}^{U_h^n} - U^n\|\|\nabla u^{n+1/2}\|_\infty\|\phi_h^{n+1/2}\| \\
&\quad\leq \quad \frac{\nu}{16}\|\nabla\phi_h^{n+1/2}\|^2 + C\nu^{-1}\|u^{n+1/2}\|_3^2\|\widehat{U^n}^{U_h^n} - U^n\|^2 \\
&\quad\leq \quad \frac{\nu}{16}\|\nabla\phi_h^{n+1/2}\|^2 \\
&\qquad +C\nu^{-1}\|u^{n+1/2}\|_3^2(\alpha^2h^{2k} + \alpha^2\|a_{D_N}(u)\|^2 + h^{2k+2} + \alpha^2(\|\eta^{n-1}\|^2 + \|\eta^n\|^2 + \|\phi_h^{n-1}\|^2 + \|\phi_h^n\|^2)).
\end{aligned}$$

Combining the above estimates, summing over timesteps, multiplying by Δt, noting that $\|\phi_h^0\| = 0$, and applying regularity assumptions (4.28)-(4.31) yields

$$\begin{aligned}
\|\phi_h^M\|^2 + \Delta t\sum_{n=0}^{M-1}\nu\|\nabla\phi_h^{n+1/2}\|^2 \leq C\Bigg((1+\alpha^2)\Delta t\sum_{n=0}^{M-1}\nu^{-1}\|\phi_h^n\|^2 + \Delta t\sum_{n=0}^{M-1}\nu^{-1}\|\nabla\eta^n\|^2 \\
+ \Delta t^4 + \alpha^2h^{2k} + \alpha^2\|a_{D_N}(u)\|^2 + h^{2k+2}\Bigg). \quad (4.38)
\end{aligned}$$

Assuming (P_k, P_{k-1}) Taylor-Hood elements or (P_k, P_{k-1}^{disc}) Scott-Vogelius elements, and applying Gronwall's Lemma, for any $\Delta t > 0$ we get

$$\|\phi_h^M\|^2 + \Delta t\sum_{n=0}^{M-1}\nu\|\nabla\phi_h^{n+1/2}\|^2 \leq C(\Delta t^4 + \alpha^2h^{2k} + \alpha^2\|a_{D_N}(u)\|^2 + h^{2k}). \quad (4.39)$$

Applying the triangle inequality to (4.39), we get the stated result. □

4.4 Numerical Experiments

In this section we present numerical experiments which demonstrate the effectiveness of our approach. The first experiment confirms the convergence rates predicted by our analysis in the previous section. In our second two experiments, channel flow around a step and channel flow with two outlets and a contraction, we show our results are a significant improvement over those of the usual Leray-α model and give much more accurate results on coarse meshes than computing the NSE directly.

4.4.1 Convergence rate verification

Our first numerical experiment is to verify the rates predicted in the previous section for Algorithm 4.2.1. We compute approximations to the chosen solution

$$\begin{aligned} u_1(x,y,t) &= (1+0.01t)\sin(2\pi y) \\ u_2(x,y,t) &= (1+0.01t)\cos(2\pi x) \\ p(x,y,t) &= x+y \end{aligned}$$

on $\Omega = [0,1]^2$, $T = 0.01$, and $\Delta t = 0.001$. Here, the question we address is whether the spatial convergence is of order $h^{k-1/2}$ or h^k. To isolate the spatial error, we take a small end time and time steps to make the temporal effect on the error small.

We choose $\nu = 1$, calculate f from the NSE and the chosen solution, and choose u_h^0 to be the L^2 projection of $u(0)$ into V_h. Then, using Algorithm 4.2.1 with both (P_3, P_2) and (P_2, P_1) elements, we compute solutions on five successive mesh refinements using $\alpha = h$ and N=0 (our analysis shows that for these element choices, choosing $N > 0$ does not improve asymptotic accuracy over the N=0 case). Our analytical results predict, with $a(u) = a_{D_0}$, a rate of 2 for (P_2, P_1) elements, and 3 for (P_3, P_2). Table 4.4.1 shows our calculated errors and rates, and we do observe optimal convergence.

h	$\|u - u_h^{P2}\|_{2,1}$	Rate	$\|u - u_h^{P3}\|_{2,1}$	Rate
1/4	5.58e-02	-	5.63e-03	-
1/8	1.43e-02	1.962	8.06e-04	2.805
1/16	3.60e-03	1.990	1.17e-04	2.783
1/32	9.02e-04	1.998	1.42e-05	3.042
1/64	2.26e-04	1.999	1.72e-06	3.044

Table 4.1: $L^2(0,T;H^1(\Omega))$ errors and rates found with $a(u) = a_{D_0}(u)$. With (P_2, P_1) elements (LEFT), we observe a rate of 2, and with (P_3, P_2) elements (RIGHT), we observe a rate of 3.

4.4.2 2D Channel Flow

Our next numerical experiment is the benchmark 2D channel flow problem over a forward-backward facing step. The domain is a 40x10 rectangle with a 1x1 step five units into the channel at the bottom. We assume no slip, no penetration boundary conditions on the top and bottom, and parabolic inflow and outflow conditions given by $(y(10-y)/25, 0)^T$. The correct physical behavior with $f = 0$ and $\nu = 1/600$ is well known to be a smooth velocity profile with eddies forming and

shedding behind the step [34]. A resolved NSE solution is shown in figure 4.1, which requires 21,593 degrees of freedom to fully resolve with (P_2, P_1) Taylor-Hood elements.

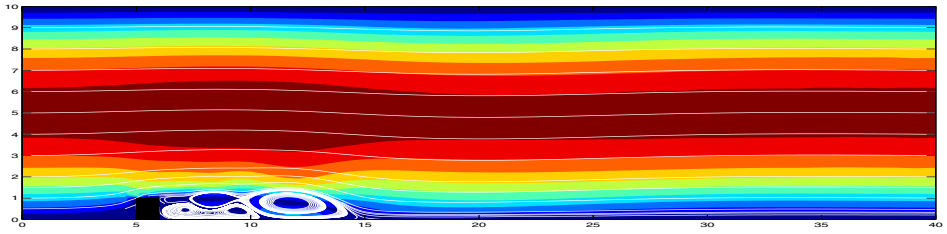

Figure 4.1: NSE fine mesh solution.

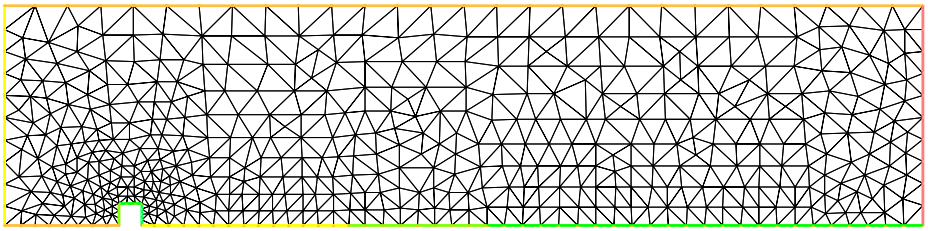

Figure 4.2: Coarse mesh used in computations for experiment 2.

Coarse mesh computations were made for the NSE (i.e. no model), Leray-α (i.e. $a(u)(x) := 1$), and Leray with nonlinear filtering and indicator functions a_{D_0} and a_{D_1}. Due to the success of the proposed model with the Vreman-based indicator function in [7] (which is based on an idea of A. Vreman from [52]), we also compare solutions to Leray with nonlinear filtering and indicator function a_V defined by

$$a_V(u) = \sqrt{\frac{B(u)}{|\nabla u|_F^4}},$$

where $|\cdot|_F$ denotes the Frobenius norm, and B is defined by

$$\begin{aligned} \beta_{ij} &:= \sum_{m=1,2,3} \frac{\partial u_i}{\partial x_m}\frac{\partial u_j}{\partial x_m} \\ B(u) &: = \beta_{11}\beta_{22} - \beta_{12}^2 + \beta_{11}\beta_{33} - \beta_{13}^2 + \beta_{22}\beta_{33} - \beta_{23}^2. \end{aligned}$$

On a coarse mesh that provides 4,603 degrees of freedom (dof) using (P_2, P_1) Taylor-Hood elements, using no numerical stabilization, $\nu = 1/600$, $\Delta t = 0.01$, $f = 0$, and $\alpha = 0.365$, we compute solutions using the proposed algorithm (and appropriate modifications for NSE (i.e. no filtering step reduces the algorithm to the well known linear extrapolated Crank-Nicolson method). Solutions at

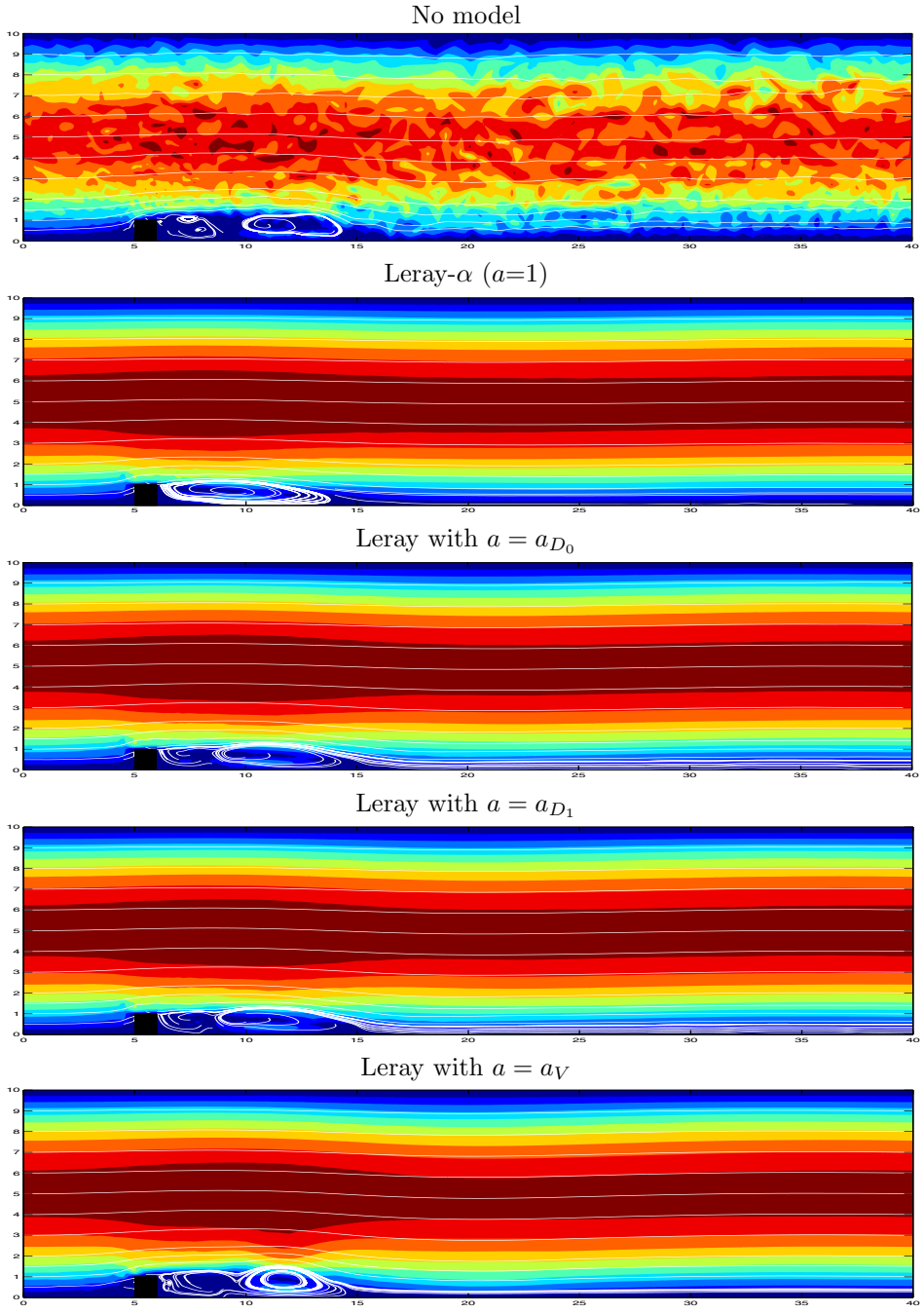

Figure 4.3: Velocity solutions of coarse mesh simulations for 2D flow over a step at T=40, from top to bottom, for NSE (no model), Leray-α, and Leray with nonlinear filter that used indicator function a_{D_0}, a_{D_1}, and a_V.

T=40 for each of the models is shown in figure 4.3 as velocity streamlines over speed contours. We observe the NSE solution (i.e. no model) is incorrect, as it exhibits significant oscillations. The

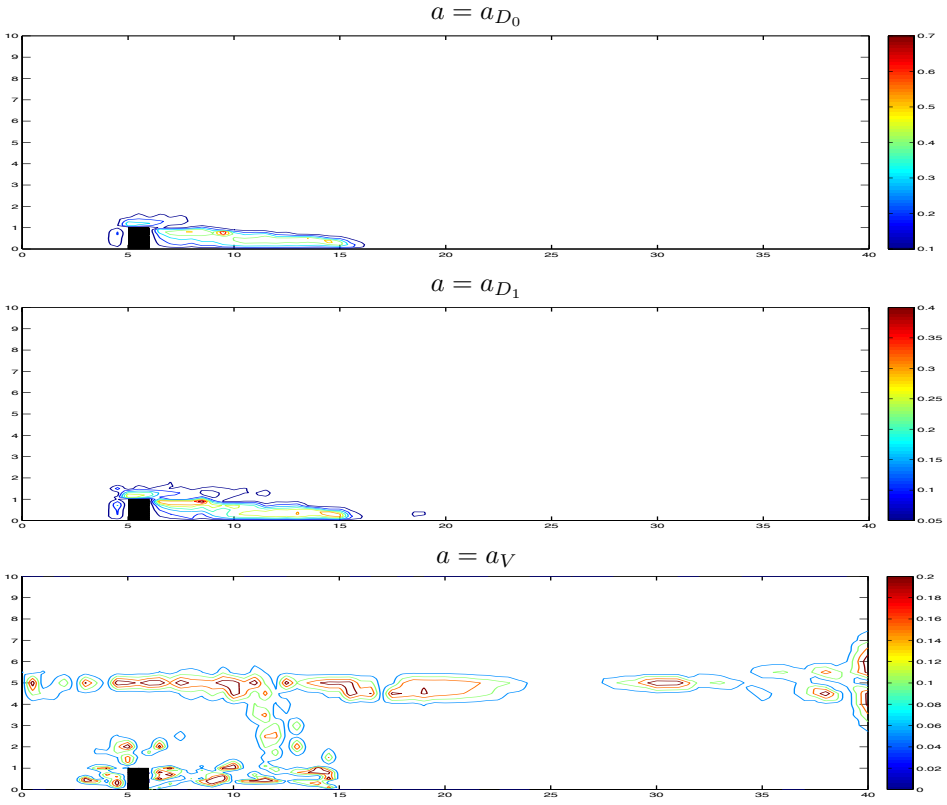

Figure 4.4: Contour plots of the indicator functions $a(u)$ for the 2D flow over a step test problem, at T=40.

usual Leray-α solution finds smooth channel flow but fails to capture eddy detachment. However, when our nonlinear filtering scheme is used, both with $N = 0$ and $N = 1$, we find smooth channel flow and eddy detachment. The nonlinear filter scheme with the Vreman indicator also correctly predicts smooth channel flow and eddy detachment. Figure 4.4 shows contour plots of a_{D_0}, a_{D_1}, and a_V at T=40 in their respective simulations. We observe each indicator provides $a \approx 0$ in most of the channel away from the step, which is what is desired. However, the a_V indicator gives large values of a near the center of the channel, which does not fit the intent of the indicator function, since the flow is laminar there. The deconvolution-based indicator functions are nonzero mainly near the step, which is exactly what is desired.

4.4.3 Channel flow with two outlets and a contraction

Our next numerical test is for a benchmark channel flow problem with a contraction, one inlet on the left hand side, and two outlets, at the top and at the right hand side. A diagram of the

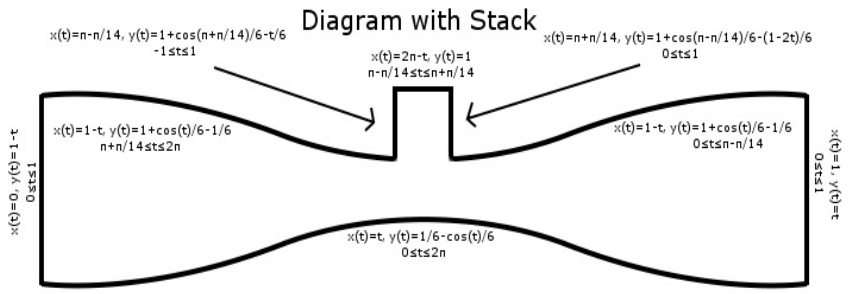

Figure 4.5: Shown above is a diagram of the domain for test problem 2.

flow domain is shown in Figure 4.5.

This problem was first studied by Turek et. al. in [24], and subsequently in [32]. We enforce no slip boundary conditions on all walls, a parabolic inflow profile with max velocity $u_{inlet}^{max} = 1$ at the center, and for the outflows, zero traction is enforced (with the 'do-nothing' condition). This flow has no external forcing (f=0), we set the kinematic viscosity $\nu = 0.001$, start the flow from rest, and ran the simulation to T=4.

Plots of the resolved NSE solution's speed contours are shown in figure 4.6 for T=1, 2, 3, and 4. This solution was found by computing the NSE directly using a timestep of $\Delta t = 0.01$ and grad-div stabilized (P_2, P_1) Taylor-Hood elements (see, e.g. [44])on a triangular mesh that provided 260,378 degrees of freedom.

We next test the NSE and the proposed method on a much coarser mesh that provides 18,076 velocity degrees of freedom, $\alpha = 0.075$, now using Taylor-Hood elements without any stabilization. Velocity solutions for each of the models is shown in Figure 4.7. The NSE coarse mesh solution is clearly incorrect. With the Leray-α model, we see a smooth solution, but appears to be oversmoothed and delayed in its development compared to the true solution. The solutions using the deconvolution-based indicator function nonlinear filtering performed better, yielding results quite similar to the DNS solution. The model with the Vreman based indicator also finds a good solution.

Figure 4.8 shows the contour plots of the indicator functions at T=4. The results are as we would hope for the deconvolution based indicators, in that $a_{D_N}(u)(x) \approx 0$ in the smooth flow regions, and $a_{D_N}(u)(x) > 0$ in the regions which appear less smooth, particularly near the contraction. The Vreman based indicator finds large a values in the middle of the channel, before the contraction, which is not a region we would expect to need filtering.

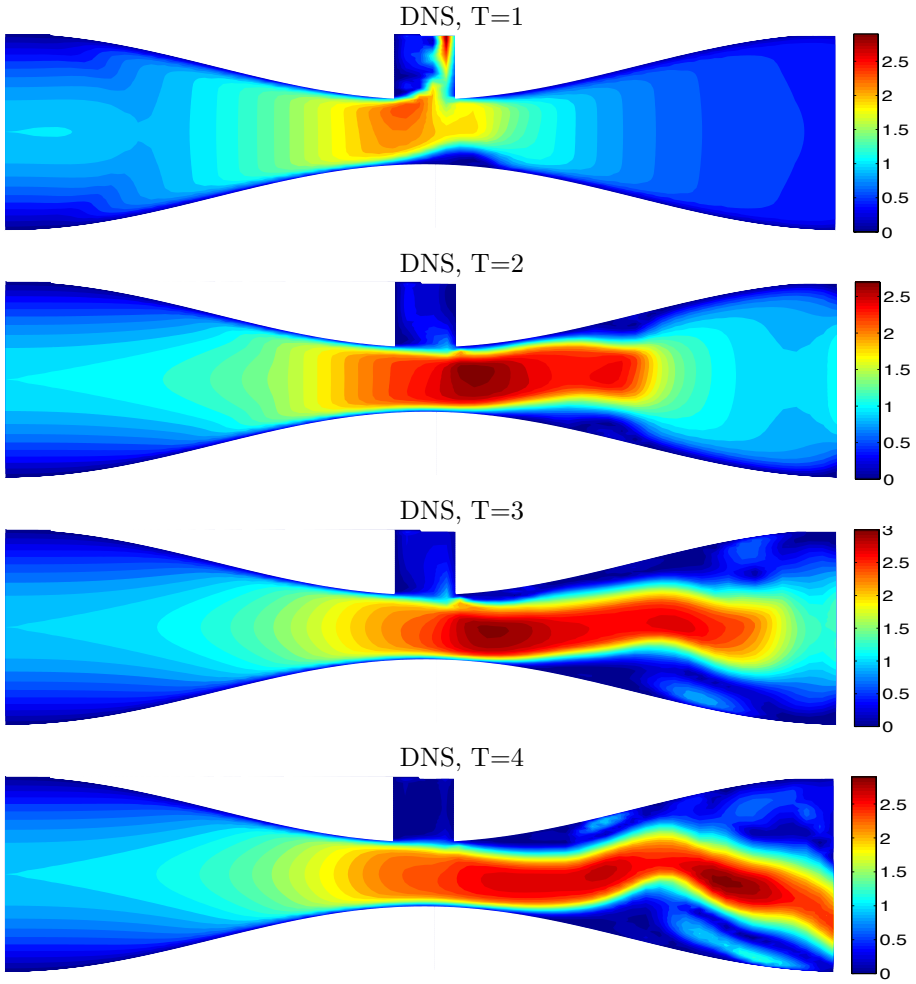

The fine mesh used for DNS

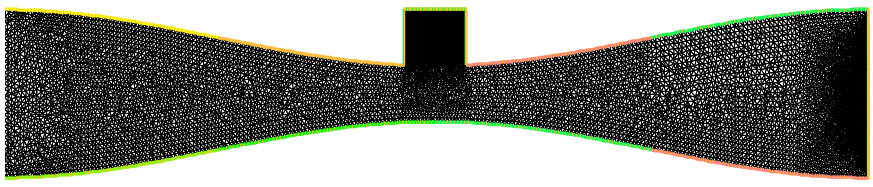

Figure 4.6: Shown above are contour plots of the speed of the resolved Navier-Stokes velocity solution at T=1,2,3,4, order from top to bottom.

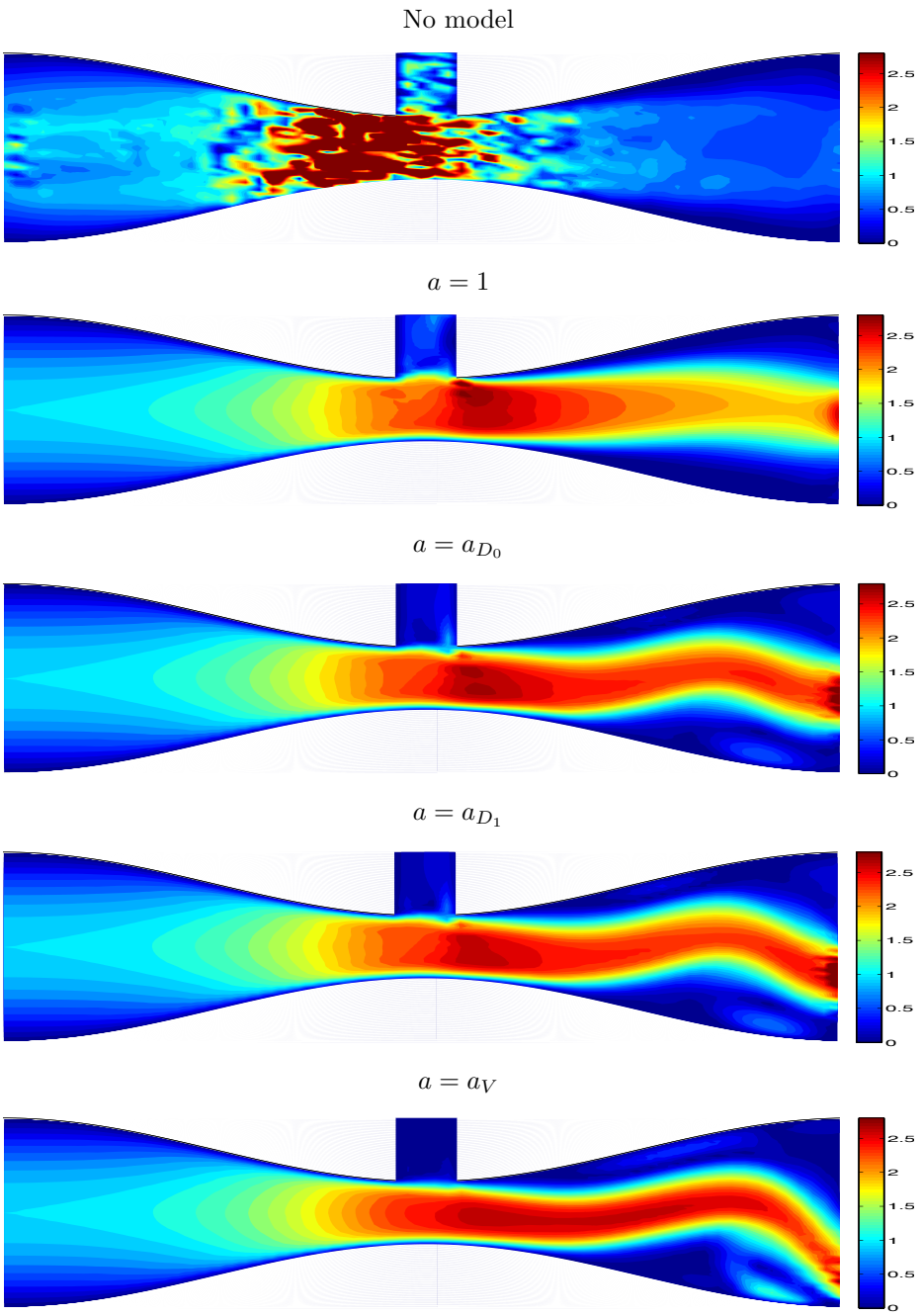

Figure 4.7: Velocity solutions of coarse mesh simulations for 2D flow with two outlets and a contraction at T=4, from top to bottom, for NSE (no model), Leray-α, and Leray with nonlinear filtering that use indicator functions a_{D_0}, a_{D_1}, and a_V.

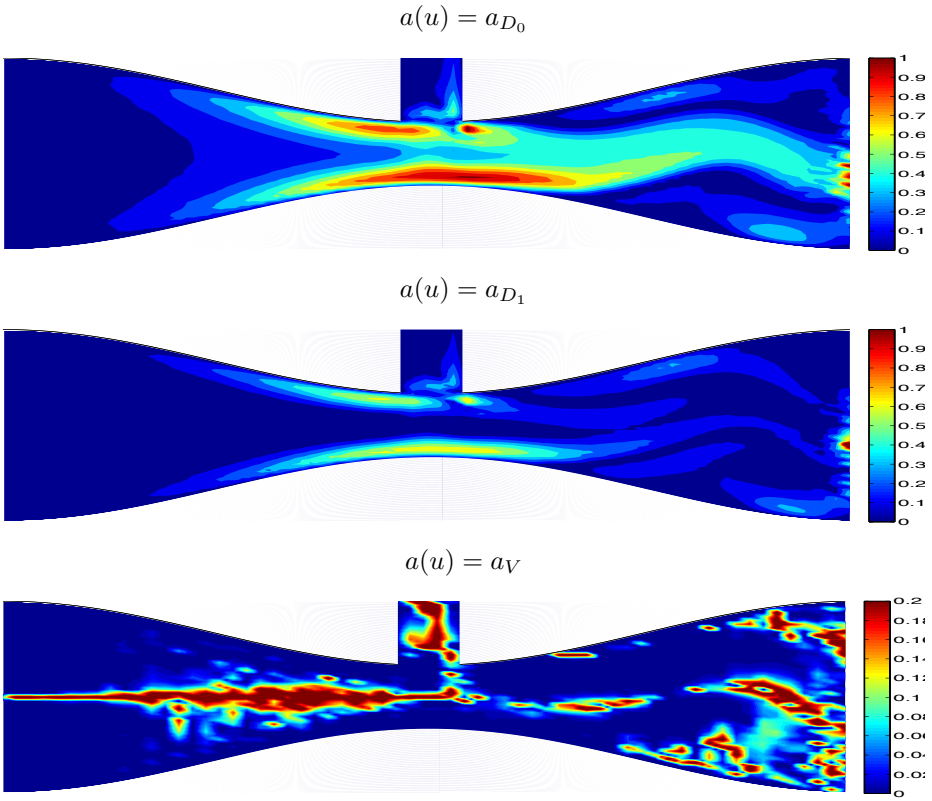

Figure 4.8: Contour plots of $a(u)$ in coarse mesh simulations for 2D flow with two outlets and a contraction at $T = 4$.

Chapter 5

Improving accuracy in the Leray model for the incompressible magnetohydrodynamic equations via adaptive deconvolution-based nonlinear filtering

Computations with the MHD equations can be very difficult. They are derived by coupling the Navier-Stokes equations (NSE) with Maxwell's equation. The NSE are currently unable to be resolved using direct numerical simulation (DNS) for complex flows, so the nonlinear coupling with Maxwell's equation makes DNS of the MHD equations even harder.

Regularization models are one way to approximate these equations at a lower computational

cost. The Leray-MHD equations are given by

$$u_t + \overline{u}\cdot\nabla u - s\overline{B}\cdot\nabla B - Re^{-1}\Delta u + \nabla p = f, \tag{5.1}$$

$$B_t - Re_m^{-1}\Delta B + \overline{u}\cdot\nabla B - \overline{B}\cdot\nabla u = \nabla\times g, \tag{5.2}$$

$$\nabla\cdot u = \nabla\cdot B = 0, \tag{5.3}$$

where $\overline{u}$ and $\overline{B}$ solve

$$-\alpha^2\Delta\overline{u} + \overline{u} = u, \quad -\alpha^2\Delta\overline{B} + \overline{B} = B, \tag{5.4}$$

and $\alpha > 0$ is the filtering radius. This model has been studied by Yu and Li [53], and shown to be well-posed, and convergent to the MHD, analogous to Leray's original result in 1934 [39].

We extend the work from the previous chapter by applying the nonlinear filter to the Leray-MHD model. The analysis performed on this indicator function with the Leray model can be easily extended to the MHD case.

5.1 Numerical Scheme

We now define the numerical scheme studied herein, and prove it is well-posed.

Algorithm 5.1.1. *Given an end-time $T > 0$, a timestep Δt chosen so that $\Delta t < T = M\Delta t$, $f \in L^\infty(0,T;H^{-1}(\Omega))$, initial conditions $u_h^0, B_h^0 \in V_h$, filtering radius $\alpha \le O(h)$, find $(u_h^n, p_h^n, B_h^n, \lambda_h^n) \in (X_h, Q_h, X_h, Q_h)$ for $n = 1, 2, ..., M$ satisfying, $\forall (v_h, q_h, \chi_h, r_h) \in (X_h, Q_h, X_h, Q_h)$,*

$$\begin{aligned}
&\frac{1}{\Delta t}(u_h^{n+1} - u_h^n, v_h) + Re^{-1}(\nabla u_h^{n+1/2}, \nabla v_h) - (p_h^{n+1/2}, \nabla\cdot v_h) \\
&+b^*\left(\overline{\frac{3}{2}u_h^n - \frac{1}{2}u_h^{n-1}}^h, u_h^{n+1/2}, v_h\right) - sb^*\left(\overline{\frac{3}{2}B_h^n - \frac{1}{2}B_h^{n-1}}^h, B_h^{n+1/2}, v_h\right) &= (f^{n+1/2}, v_h), \quad (5.5)\\
&(\nabla\cdot u_h^{n+1}, q_h) &= 0. \quad (5.6)\\
&\frac{1}{\Delta t}(B_h^{n+1} - B_h^n, \chi_h) + Re_m^{-1}(\nabla B_h^{n+1/2}, \nabla\chi_h) + (\lambda_h^{n+1/2}, \nabla\cdot\chi_h) \\
&-b^*\left(\overline{\frac{3}{2}B_h^n - \frac{1}{2}B_h^{n-1}}^h, u_h^{n+1/2}, \chi_h\right) + b^*\left(\overline{\frac{3}{2}u_h^n - \frac{1}{2}u_h^{n-1}}^h, B_h^{n+1/2}, \chi_h\right) &= (\nabla\times g^{n+1/2}, \chi_h), \quad (5.7)\\
&(\nabla\cdot B_h^{n+1}, r_h) &= 0 \quad (5.8)
\end{aligned}$$

Lemma 5.1.2. *Solutions to Algorithm 5.1.1 satisfy*

$$\begin{aligned}\|u_h^M\|^2 &+ \Delta t Re^{-1}\sum_{n=0}^{M-1}\|\nabla u_h^{n+1/2}\|^2 + s\|B_h^M\|^2 + \Delta t s Re_m^{-1}\sum_{n=0}^{M-1}\|\nabla B_h^{n+1/2}\|^2 \\ &\leq Re\Delta t\sum_{n=0}^{M-1}\|f^{n+1/2}\|_{-1}^2 + sRe_m\Delta t\sum_{n=0}^{M-1}\|\nabla\times g^{n+1/2}\|_{-1}^2 + \|u_h^0\|^2 + s\|B_h^0\|^2 \\ &\leq C(Re, Re_m, f, u_0, B_0, T). \end{aligned} \tag{5.9}$$

Proof. In (5.5), choose $v_h = u_h^{n+1/2}$ and in (5.7), choose $\chi_h = sB_h^{n+1/2}$. Several trilinear terms and the pressure terms vanish, leaving

$$\begin{aligned}\frac{1}{2\Delta t}(\|u_h^{n+1}\|^2 - \|u_h^n\|^2) + Re^{-1}\|\nabla u_h^{n+1/2}\|^2 & \\ -sb\left(\overline{\frac{3}{2}B_h^n - \frac{1}{2}B_h^{n-1}}^h, B_h^{n+1/2}, u_h^{n+1/2}\right) &= (f^{n+1/2}, u_h^{n+1/2}) \end{aligned} \tag{5.10}$$

$$\begin{aligned}\frac{s}{2\Delta t}(\|B_h^{n+1}\|^2 - \|B_h^n\|^2) + sRe_m^{-1}\|\nabla B_h^{n+1/2}\|^2 & \\ -sb\left(\overline{\frac{3}{2}B_h^n - \frac{1}{2}B_h^{n-1}}^h, u_h^{n+1/2}, B_h^{n+1/2}\right) &= s(\nabla\times g^{n+1/2}, B_h^{n+1/2}). \end{aligned} \tag{5.11}$$

Adding these together, we get

$$\begin{aligned}\frac{1}{2\Delta t}(\|u_h^{n+1}\|^2 - \|u_h^n\|^2) + Re^{-1}\|\nabla u_h^{n+1/2}\|^2 + \frac{s}{2\Delta t}(\|B_h^{n+1}\|^2 - \|B_h^n\|^2) + sRe_m^{-1}\|\nabla B_h^{n+1/2}\|^2 & \\ = (f^{n+1/2}, u_h^{n+1/2}) + s(\nabla\times g^{n+1/2}, B_h^{n+1/2}). \end{aligned} \tag{5.12}$$

Using Cauchy-Schwarz and Young's inequalities we have

$$\begin{aligned}\frac{1}{2\Delta t}(\|u_h^{n+1}\|^2 - \|u_h^n\|^2) + \frac{Re^{-1}}{2}\|\nabla u_h^{n+1/2}\|^2 + \frac{s}{2\Delta t}(\|B_h^{n+1}\|^2 - \|B_h^n\|^2) + \frac{sRe_m^{-1}}{2}\|\nabla B_h^{n+1/2}\|^2 & \\ \leq \frac{Re}{2}\|f^{n+1/2}\|_{-1}^2 + \frac{sRe_m}{2}\|\nabla\times g^{n+1/2}\|_{-1}^2. \end{aligned} \tag{5.13}$$

Summing over time steps and multiplying by Δt yields

$$\begin{aligned}\|u_h^M\|^2 + s\|B_h^M\|^2 + \Delta t Re^{-1}\sum_{n=0}^{M-1}\|\nabla u_h^{n+1/2}\|^2 + \Delta t s Re_m^{-1}\sum_{n=0}^{M-1}\|\nabla B_h^{n+1/2}\|^2 & \\ \leq Re\Delta t\sum_{n=0}^{M-1}\|f^{n+1/2}\|_{-1}^2 + sRe_m\Delta t\sum_{n=0}^{M-1}\|\nabla\times g^{n+1/2}\|_{-1}^2 + \|u_h^0\|^2 + s\|B_h^0\|^2. \end{aligned} \tag{5.14}$$

□

Lemma 5.1.3. *Solutions to (5.5)-(5.8) admit the following conservation laws*

1. *Global energy conservation*

$$\frac{1}{2}\|u_h^M\|^2 + \frac{s}{2}\|B_h^{n+1}\|^2 + \Delta t \sum_{n=0}^{M-1}\left(Re^{-1}\|\nabla u_h^{n+1/2}\|^2 + sRe_m^{-1}\|\nabla B_h^{n+1/2}\|^2\right)$$
$$= \frac{1}{2}\|u_h^0\|^2 + \frac{1}{2}\|B_h^0\|^2 + \Delta t \sum_{n=0}^{M-1}\left((f(t^{n+1/2}), u_h^{n1+/2}) + s(\nabla \times g(t^{n+1/2}), B_h^{n1+/2})\right). \quad (5.15)$$

2. *Global cross-helicity conservation*

$$(u_h^M, B_h^M) + \Delta t \sum_{n=}^{M-1}(Re^{-1} + Re_m^{-1})(\nabla u_h^{n+1/2}, \nabla B_h^{n+1/2})$$
$$= (u_h^0, B_h^0) + \sum_{n=0}^{M-1}((f(t^{n+1/2}), B_h^{n+1/2}) + (\nabla \times g(t^{n+1/2}), u_h^{n+1/2})). \quad (5.16)$$

Proof. To prove 1, choose $v_h = u_h^{n+1/2}$ in (5.5) and $\chi_h = sB_h^{n+1/2}$ in (5.7). This leaves

$$\frac{1}{2\Delta t}(\|u_h^{n+1}\|^2 - \|u_h^n\|^2) + Re^{-1}\|\nabla u_h^{n+1/2}\|^2 - sb^*\left(\overline{\frac{3}{2}B_h^n - \frac{1}{2}B_h^{n-1}}^h, B_h^{n+1/2}, u_h^{n+1/2}\right)$$
$$= (f(t^{n+1/2}), u_h^{n1+/2}). \quad (5.17)$$

$$\frac{s}{2\Delta t}(\|B_h^{n+1}\|^2 - \|B_h^n\|^2) + sRe_m^{-1}\|\nabla B_h^{n+1/2}\|^2 - sb^*\left(\overline{\frac{3}{2}B_h^n - \frac{1}{2}B_h^{n-1}}^h, u_h^{n+1/2}, B_h^{n+1/2}\right)$$
$$= s(\nabla \times g(t^{n+1/2}), B_h^{n1+/2}). \quad (5.18)$$

Adding the above together, the two remaining nonlinear terms vanish, leaving

$$\frac{1}{2\Delta t}(\|u_h^{n+1}\|^2 - \|u_h^n\|^2) + \frac{s}{2\Delta t}(\|B_h^{n+1}\|^2 - \|B_h^n\|^2) + Re^{-1}\|\nabla u_h^{n+1/2}\|^2 + sRe_m^{-1}\|\nabla B_h^{n+1/2}\|^2$$
$$= (f(t^{n+1/2}), u_h^{n1+/2}) + s(\nabla \times g(t^{n+1/2}), B_h^{n1+/2}). \quad (5.19)$$

To finish the proof, we multiply by Δt and sum over time steps. To prove the second result, choose

$v_h = B_h^{n+1/2}$ in (5.5) and $\chi_h = u_h^{n+1/2}$ in (5.7), which gives

$$\frac{1}{\Delta t}(u_h^{n+1} - u_h^n, B_h^{n+1/2}) + Re^{-1}(\nabla u_h^{n+1/2}, \nabla B_h^{n+1/2}) + b^*\left(\overline{\frac{3}{2}u_h^n - \frac{1}{2}u_h^{n-1}}^h, u_h^{n+1/2}, B_h^{n+1/2}\right) = (f(t^{n+1/2}), B_h^{n+1/2}). \quad (5.20)$$

$$\frac{1}{\Delta t}(B_h^{n+1} - B_h^n, u_h^{n+1/2}) + Re_m^{-1}(\nabla B_h^{n+1/2}, \nabla u_h^{n+1/2}) + b^*\left(\overline{\frac{3}{2}u_h^n - \frac{1}{2}u_h^{n-1}}^h, B_h^{n+1/2}, u_h^{n+1/2}\right) = (\nabla \times g(t^{n+1/2}), u_h^{n+1/2}). \quad (5.21)$$

Adding the above together cancels the remaining two nonlinear terms, leaving

$$\frac{1}{\Delta t}(u_h^{n+1} - u_h^n, B_h^{n+1/2}) + \frac{1}{\Delta t}(B_h^{n+1} - B_h^n, u_h^{n+1/2}) + (Re^{-1} + Re_m^{-1})(\nabla u_h^{n+1/2}, \nabla B_h^{n+1/2}) = (f(t^{n+1/2}), B_h^{n+1/2}) + (\nabla \times g(t^{n+1/2}), u_h^{n+1/2}). \quad (5.22)$$

We can rewrite the first two terms as

$$\frac{1}{\Delta t}(u_h^{n+1} - u_h^n, B_h^{n+1/2}) + \frac{1}{\Delta t}(B_h^{n+1} - B_h^n, u_h^{n+1/2}) = \frac{1}{2\Delta t}((u_h^{n+1}, B_h^{n+1} - (u_h^n, B_h^n)) + \frac{1}{2\Delta t}((u_h^{n+1}, B_h^n - (u_h^n, B_h^{n+1})) + \frac{1}{2\Delta t}((B_h^{n+1}, u_h^{n+1} - (B_h^n, u_h^n)) - \frac{1}{2\Delta t}((B_h^{n+1}, u_h^n - (B_h^n, u_h^{n+1})), \quad (5.23)$$

which reduces to

$$\frac{1}{\Delta t}((u_h^{n+1}, B_h^{n+1} - (u_h^n, B_h^n)) + (Re^{-1} + Re_m^{-1})(\nabla u_h^{n+1/2}, \nabla B_h^{n+1/2}) = (f(t^{n+1/2}), B_h^{n+1/2}) + (\nabla \times g(t^{n+1/2}), u_h^{n+1/2}). \quad (5.24)$$

Multiplying by Δt and summing over time steps completes the proof. □

5.2 Convergence

This section is devoted to proving convergence of the numerical scheme. For simplicity in stating the following theorem, we state here the regularity assumptions of the solution $(u(x,t), p(x,t), B(x,t), \lambda(x,t))$ of the true MHD solutions:

$$u, B \in L^\infty(0,T; H^{k+1} \cap V) \tag{5.25}$$

$$u_{tt}, B_{tt} \in L^2(0,T; H^1(\Omega)) \tag{5.26}$$

$$u_{ttt}, B_{ttt} \in L^2(0,T; L^2(\Omega)) \tag{5.27}$$

$$p, \lambda \in L^\infty(0,T; H^k(\Omega)). \tag{5.28}$$

We will denote $U_h^n := \frac{3}{2}u_h^n - \frac{1}{2}u_h^{n-1}$, $U^n := \frac{3}{2}u(t^n) - \frac{1}{2}u(t^{n-1})$, $\tilde{B}_h^n := \frac{3}{2}B_h^n - \frac{1}{2}B_h^{n-1}$, and $\tilde{B}^n := \frac{3}{2}B(t^n) - \frac{1}{2}B(t^{n-1})$.

Theorem 5.2.1. *Let $(u(t), p(t), B(t), \lambda(t))$ be a solution of the MHD satisfying no-slip boundary conditions, and (5.25)-(5.28), with given $f \in L^\infty(0,T; H^{-1}(\Omega))$ and $u_0, B_0 \in V_h$. Let $(u_h^n, p_h^n, B_H^n, \lambda_H^n)$, $n = 0, 1, \dots M$ be the solution of Algorithm 5.1.1, using (P_k, P_{k-1}) Taylor-Hood or (P_k, P_{k-1}^{disc}) Scott-Vogelius elements in a setting where they are LBB stable, and $\alpha \leq O(h)$. Then for any $\Delta t > 0$, the error in the discrete solution satisfies*

$$\|u_h^M - u(T)\|^2 + s\|B_h^M - B(T)\|^2 + \Delta t \sum_{n=0}^{M-1} Re^{-1}\|\nabla(u_h^{n+1/2} - u(t^{n+1/2})\|^2$$
$$+\Delta t \sum_{n=0}^{M-1} sRe_m^{-1}\|\nabla(B_h^{n+1/2} - B(t^{n+1/2})\|^2 \leq C\left(\Delta t^4 + \alpha^2 h^{2k} + \alpha^2\|a_{D_N}(u)\|^2 + \alpha^2\|a_{D_N}(B)\|^2 + h^{2k}\right), \tag{5.29}$$

where C is a constant independent of α, h, and Δt.

Proof. The first equation of the MHD at time $t = t^{n+1/2}$, after denoting $u^{n+1/2} := \frac{u(t^{n+1}) + u(t^n)}{2}$ and $B^{n+1/2} := \frac{B(t^{n+1}) + B(t^n)}{2}$, satisfies for all $v_h \in V_h$:

$$\left(\frac{u(t^{n+1}) - u(t^n)}{\Delta t}, v_h\right) + Re^{-1}(\nabla u^{n+1/2}, \nabla v_h) + b^*\left(\widehat{U^n}^{U_h^n}, u^{n+1/2}, v_h\right)$$
$$- sb^*\left(\widehat{\tilde{B}^n}^{\tilde{B}_h^n}, B^{n+1/2}, v_h\right) - (p(t^{n+1/2}), \nabla \cdot v_h) = (f(t^{n+1/2}), v_h) + G(u, B, n, v_h), \tag{5.30}$$

where

$$\begin{aligned} G(u,B,n,v_h) &:= \left(\frac{u(t^{n+1})-u(t^n)}{\Delta t} - u_t(t^{n+1/2}), v_h\right) + Re^{-1}(\nabla(u^{n+1/2}-u(t^{n+1/2})), v_h) \\ &+ b^*\left(\widehat{U^n}^{U_h^n}, u^{n+1/2}, v_h\right) - b^*(u(t^{n+1/2}), u(t^{n+1/2}), v_h) \\ &- sb^*\left(\widehat{\tilde{B}^n}^{\tilde{B_h^n}}, B^{n+1/2}, v_h\right) + sb^*(B(t^{n+1/2}), B(t^{n+1/2}), v_h). \end{aligned} \tag{5.31}$$

Take $v_h \in V_h$ in (7.1) which vanishes the pressure term. Denote $e_u^n := u_h^n - u(t^n)$ and $e_B^n := B_h^n - B(t^n)$ and subtract (5.30) from (7.1) to get

$$\begin{aligned} &\frac{1}{\Delta t}(e_u^{n+1}-e_u^n, v_h) + b^*\left(\overline{U_h^n}^h, u_h^{n+1/2}, v_h\right) - b^*\left(\widehat{U^n}^{U_h^n}, u^{n+1/2}, v_h\right) - sb^*\left(\overline{\tilde{B}_h^n}^h, B_h^{n+1/2}, v_h\right) \\ &+ sb^*\left(\widehat{\tilde{B}^n}^{B_h^n}, B^{n+1/2}, v_h\right) + Re^{-1}(\nabla e_u^{n+1/2}, \nabla v_h) = (p(t^{n+1/2}), \nabla\cdot v_h) + G(u,B,n,v_h). \end{aligned} \tag{5.32}$$

Rewriting the nonlinear terms gives

$$\begin{aligned} &\frac{1}{\Delta t}(e_u^{n+1}-e_u^n, v_h) + b^*\left(\overline{U_h^n}^h, e_u^{n+1/2}, v_h\right) + b^*\left(\overline{U_h^n}^h - \widehat{U^n}^{U_h^n}, u^{n+1/2}, v_h\right) \\ &\quad + sb^*\left(\widehat{\tilde{B}^n}^{B_h^n} - \overline{\tilde{B}_h^n}^h, B^{n+1/2}, v_h\right) + sb^*\left(\overline{\tilde{B}^n}^h, e_B^{n+1/2}, v_h\right) + Re^{-1}(\nabla e_u^{n+1/2}, \nabla v_h) \\ &\quad = (p(t^{n+1/2}), \nabla\cdot v_h) + G(u,B,n,v_h). \end{aligned} \tag{5.33}$$

Decompose the error terms as

$$e_u^n = (u(t^n) - P_{V_h}^{L^2}(u(t^n))) - (u_h^n - P_{V_h}^{L^2}(u(t^n))) =: \eta_u^n - \phi_u^n,$$

$$e_B^n = (B(t^n) - P_{V_h}^{L^2}(B(t^n))) - (B_h^n - P_{V_h}^{L^2}(B(t^n))) =: \eta_B^n - \phi_B^n,$$

then choose $v_h = \phi_u^{n+1/2}$ to get, $\forall q_h \in Q_h$,

$$\frac{1}{\Delta t}(\|\phi_u^{n+1}\|^2 - \|\phi_u^n\|^2) + b^*\left(\overline{U_h^n}^h, \eta_u^{n+1/2}, \phi_u^{n+1/2}\right) + b^*\left(\overline{U_h^n}^h - \widehat{U^n}^{U_h^n}, u^{n+1/2}, \phi_u^{n+1/2}\right)$$
$$+ sb^*\left(\widehat{\tilde{B}^n}^{B_h^n} - \overline{\tilde{B}_h^n}^h, B^{n+1/2}, \phi_u^{n+1/2}\right) + sb^*\left(\overline{\tilde{B}^n}^h, \eta_B^{n+1/2}, \phi_u^{n+1/2}\right) + sb^*\left(\overline{\tilde{B}^n}^h, \phi_B^{n+1/2}, \phi_u^{n+1/2}\right)$$
$$+ Re^{-1}\|\nabla\phi_u^{n+1/2}\|^2 + Re^{-1}(\nabla\eta_u^{n+1/2}, \nabla\phi_u^{n+1/2}) = (p(t^{n+1/2}) - q_h, \nabla\cdot\phi_u^{n+1/2}) + G(u, B, n, \phi_u^{n+1/2}). \tag{5.34}$$

Now, the second equation of the MHD at time $t = t^{n+1/2}$ satisfies, for all $v_h \in V_h$,

$$\left(\frac{B(t^{n+1}) - B(t^n)}{\Delta t}, \chi_h\right) + Re_m^{-1}(\nabla B^{n+1/2}, \nabla\chi_h) + b^*\left(\widehat{U^n}^{U_h^n}, B^{n+1/2}, \chi_h\right)$$
$$- b^*\left(\widehat{\tilde{B}^n}^{\tilde{B}_h^n}, u^{n+1/2}, \chi_h\right) - (\lambda(t^{n+1/2}), \nabla\cdot\chi_h) = (\nabla\times g(t^{n+1/2}), \chi_h) + F(u, B, n, \chi_h), \tag{5.35}$$

where

$$\begin{aligned} F(u, B, n, v_h) \quad &:= \quad \left(\frac{B(t^{n+1}) - B(t^n)}{\Delta t} - B_t(t^{n+1/2}), \chi_h\right) + Re_m^{-1}(\nabla(B^{n+1/2} - B(t^{n+1/2})), \chi_h) \\ &+ \quad b^*\left(\widehat{U^n}^{U_h^n}, B^{n+1/2}, \chi_h\right) - b^*(u(t^{n+1/2}), B(t^{n+1/2}), \chi_h) \\ &- \quad b^*\left(\widehat{\tilde{B}^n}^{\tilde{B}_h^n}, u^{n+1/2}, \chi_h\right) + b^*(B(t^{n+1/2}), u(t^{n+1/2}), \chi_h). \end{aligned} \tag{5.36}$$

Take $v_h \in V_h$ in (5.7) which vanishes the pressure term, and subtract (5.35) from (5.7) to get

$$\frac{1}{\Delta t}(e_B^{n+1} - e_B^n, \chi_h) + Re_m^{-1}(\nabla e_B^{n+1/2}, \nabla\chi_h) + b^*\left(\overline{U_h^n}^h, B_h^{n+1/2}, \chi_h\right)$$
$$- b^*\left(\widehat{U^n}^{U_h^n}, B^{n+1/2}, \chi_h\right) - b^*\left(\overline{\tilde{B}_h^n}^h, u_h^{n+1/2}, \chi_h\right) + b^*\left(\widehat{\tilde{B}^n}^{\tilde{B}_h^n}, u^{n+1/2}, \chi_h\right)$$
$$= (\lambda(t^{n+1/2}), \nabla\cdot\chi_h) + F(u, B, n, \chi_h). \tag{5.37}$$

Rewriting the nonlinear terms gives

$$\frac{1}{\Delta t}(e_B^{n+1}-e_B^n,\chi_h)+Re_m^{-1}(\nabla e_B^{n+1/2},\nabla\chi_h)+b^*\left(\overline{U_h^n}^h,e_B^{n+1/2},\chi_h\right)$$
$$+b^*\left(\overline{U_h^n}^h-\widehat{U^n}^{U_h^n},B^{n+1/2},\chi_h\right)+b^*\left(\overline{\tilde{B}^n}^h,e_u^{n+1/2},\chi_h\right)+b^*\left(\widehat{\tilde{B}^n}^{\tilde{B_h^n}}-\overline{\tilde{B}_h^n}^h,u^{n+1/2},\chi_h\right)$$
$$=(\lambda(t^{n+1/2}),\nabla\cdot\chi_h)+F(u,B,n,\chi_h). \quad (5.38)$$

Decompose the error as above, and choose $\chi_h=s\phi_B^{n+1/2}$, which yields, $\forall r_h\in Q_h$,

$$\frac{s}{\Delta t}(\|\phi_B^{n+1}\|^2-\|\phi_B^n\|^2)+sRe_m^{-1}\|\nabla\phi_B^{n+1/2}\|^2+Re_m^{-1}(\nabla\eta_B^{n+1/2},\nabla\phi_B^{n+1/2})+sb^*\left(\overline{U_h^n}^h,\eta_B^{n+1/2},\phi_B^{n+1/2}\right)$$
$$+sb^*\left(\overline{U_h^n}^h-\widehat{U^n}^{U_h^n},B^{n+1/2},\phi_B^{n+1/2}\right)+sb^*\left(\overline{\tilde{B}^n}^h,\eta_u^{n+1/2},\phi_B^{n+1/2}\right)+sb^*\left(\overline{\tilde{B}^n}^h,\phi_u^{n+1/2},\phi_B^{n+1/2}\right)$$
$$+sb^*\left(\widehat{\tilde{B}^n}^{\tilde{B_h^n}}-\overline{\tilde{B}_h^n}^h,u^{n+1/2},\phi_B^{n+1/2}\right)=s(\lambda(t^{n+1/2})-r_h,\nabla\cdot\phi_B^{n+1/2})+sF(u,B,n,\phi_B^{n+1/2}). \quad (5.39)$$

Now add (5.34) to (5.39) to obtain

$$\frac{1}{\Delta t}(\|\phi_u^{n+1}\|^2-\|\phi_u^n\|^2)+\frac{s}{\Delta t}(\|\phi_B^{n+1}\|^2-\|\phi_B^n\|^2)+Re^{-1}\|\nabla\phi_u^{n+1/2}\|^2+sRe_m^{-1}\|\nabla\phi_B^{n+1/2}\|^2$$
$$+b^*\left(\overline{U_h^n}^h,\eta_u^{n+1/2},\phi_u^{n+1/2}\right)+b^*\left(\overline{U_h^n}^h-\widehat{U^n}^{U_h^n},u^{n+1/2},\phi_u^{n+1/2}\right)+sb^*\left(\widehat{\tilde{B}^n}^{B_h^n}-\overline{\tilde{B}_h^n}^h,B^{n+1/2},\phi_u^{n+1/2}\right)$$
$$+sb^*\left(\overline{\tilde{B}^n}^h,\eta_B^{n+1/2},\phi_u^{n+1/2}\right)+sb^*\left(\overline{U_h^n}^h,\eta_B^{n+1/2},\phi_B^{n+1/2}\right)+sb^*\left(\overline{U_h^n}^h-\widehat{U^n}^{U_h^n},B^{n+1/2},\phi_B^{n+1/2}\right)$$
$$+sb^*\left(\overline{\tilde{B}^n}^h,\eta_u^{n+1/2},\phi_B^{n+1/2}\right)+sb^*\left(\widehat{\tilde{B}^n}^{\tilde{B_h^n}}-\overline{\tilde{B}_h^n}^h,u^{n+1/2},\phi_B^{n+1/2}\right)+Re^{-1}(\nabla\eta_u^{n+1/2},\nabla\phi_u^{n+1/2})$$
$$+Re_m^{-1}(\nabla\eta_B^{n+1/2},\nabla\phi_B^{n+1/2})=(p(t^{n+1/2})-q_h,\nabla\cdot\phi_u^{n+1/2})+s(\lambda(t^{n+1/2})-r_h,\nabla\cdot\phi_B^{n+1/2})$$
$$+G(u,B,n,\phi_u^{n+1/2})+sF(u,B,n,\phi_B^{n+1/2}). \quad (5.40)$$

Applying Cauchy-Schwarz and Young inequalities yields

$$\begin{aligned}
&\frac{1}{\Delta t}(\|\phi_u^{n+1}\|^2-\|\phi_u^n\|^2)+\frac{s}{\Delta t}(\|\phi_B^{n+1}\|^2-\|\phi_B^n\|^2)+\frac{Re^{-1}}{2}\|\nabla\phi_u^{n+1/2}\|^2+\frac{sRe_m^{-1}}{2}\|\nabla\phi_B^{n+1/2}\|^2\\
&\le b^*\left(\overline{U_h^n}^h,\eta_u^{n+1/2},\phi_u^{n+1/2}\right)+b^*\left(\overline{U_h^n}^h-\widehat{U^n}^{U_h^n},u^{n+1/2},\phi_u^{n+1/2}\right)+sb^*\left(\widehat{\tilde{B}^n}^{B_h^n}-\overline{\tilde{B}_h^n}^h,B^{n+1/2},\phi_u^{n+1/2}\right)\\
&+sb^*\left(\overline{\tilde{B}^n}^h,\eta_B^{n+1/2},\phi_u^{n+1/2}\right)+sb^*\left(\overline{U_h^n}^h,\eta_B^{n+1/2},\phi_B^{n+1/2}\right)+sb^*\left(\overline{U_h^n}^h-\widehat{U^n}^{U_h^n},B^{n+1/2},\phi_B^{n+1/2}\right)\\
&+sb^*\left(\overline{\tilde{B}^n}^h,\eta_u^{n+1/2},\phi_B^{n+1/2}\right)+sb^*\left(\widehat{\tilde{B}^n}^{\tilde{B}_h^n}-\overline{\tilde{B}_h^n}^h,u^{n+1/2},\phi_B^{n+1/2}\right)+CRe\inf_{q_h\in Q_h}\|p(t^{n+1/2})-q_h\|^2\\
&+CsRe_m\inf_{r_h\in Q_h}\|\lambda(t^{n+1/2})-r_h\|^2+Re\|\nabla\eta_u^{n+1/2}\|^2+Re_m\|\nabla\eta_B^{n+1/2}\|^2\\
&+G(u,B,n,\phi_u^{n+1/2})+sF(u,B,n,\phi_B^{n+1/2}). \quad (5.41)
\end{aligned}$$

We now bound the nonlinear terms:

$$\begin{aligned}
b^*\left(\overline{U_h^n}^h-\widehat{U^n}^{U_h^n},u^{n+1/2},\phi_u^{n+1/2}\right)&\le\|\overline{U_h^n}^h-\widehat{U^n}^{U_h^n}\|\|u^{n+1/2}\|_\infty\|\phi_u^{n+1/2}\|\\
&\le\|U_h^n-U^n\|\|u^{n+1/2}\|_\infty\|\nabla\phi_u^{n+1/2}\|\\
&\le\frac{Re^{-1}}{32}\|\nabla\phi_u^{n+1/2}\|^2+CRe\|u^{n+1/2}\|_\infty^2(\|\eta_u^n\|^2+\|\eta_u^{n-1}\|^2+\|\phi_u^n\|^2+\|\phi_u^{n-1}\|^2) \quad (5.42)
\end{aligned}$$

$$\begin{aligned}
sb^*\left(\overline{U_h^n}^h-\widehat{U^n}^{U_h^n},B^{n+1/2},\phi_B^{n+1/2}\right)&\le s\|\overline{U_h^n}^h-\widehat{U^n}^{U_h^n}\|\|B^{n+1/2}\|_\infty\|\phi_B^{n+1/2}\|\\
&\le s\|U_h^n-U^n\|\|B^{n+1/2}\|_\infty\|\nabla\phi_B^{n+1/2}\|\\
&\le\frac{Re_m^{-1}}{32}\|\nabla\phi_B^{n+1/2}\|^2+Cs^2Re_m\|B^{n+1/2}\|_\infty^2(\|\eta_u^n\|^2+\|\eta_u^{n-1}\|^2+\|\phi_u^n\|^2+\|\phi_u^{n-1}\|^2) \quad (5.43)
\end{aligned}$$

$$\begin{aligned}
sb^*\left(\widehat{\tilde{B}^n}^{B_h^n}-\overline{\tilde{B}_h^n}^h,B^{n+1/2},\phi_u^{n+1/2}\right)&\le s\|\widehat{\tilde{B}^n}^{B_h^n}-\overline{\tilde{B}_h^n}^h\|\|B^{n+1/2}\|_\infty\|\phi_u^{n+1/2}\|\\
&\le s\|\tilde{B}^n-\tilde{B}_h^n\|\|B^{n+1/2}\|_\infty\|\nabla\phi_u^{n+1/2}\|\\
&\le\frac{Re^{-1}}{32}\|\nabla\phi_u^{n+1/2}\|^2+Cs^2Re\|B^{n+1/2}\|_\infty^2(\|\eta_B^n\|^2+\|\eta_B^{n-1}\|^2+\|\phi_B^n\|^2+\|\phi_B^{n-1}\|^2) \quad (5.44)
\end{aligned}$$

$$sb^*\left(\widehat{\tilde{B}^n}^{B_h^n} - \overline{\tilde{B}_h^n}^h, u^{n+1/2}, \phi_B^{n+1/2}\right) \leq s\|\widehat{\tilde{B}^n}^{B_h^n} - \overline{\tilde{B}_h^n}^h\|\|u^{n+1/2}\|_\infty\|\phi_B^{n+1/2}\|$$

$$\leq s\|\tilde{B^n} - \tilde{B_h^n}\|\|u^{n+1/2}\|_\infty\|\nabla\phi_B^{n+1/2}\|$$

$$\leq \frac{Re_m^{-1}}{32}\|\nabla\phi_B^{n+1/2}\|^2 + Cs^2Re_m\|u^{n+1/2}\|_\infty^2(\|\eta_B^n\|^2 + \|\eta_B^{n-1}\|^2 + \|\phi_B^n\|^2 + \|\phi_B^{n-1}\|^2). \quad (5.45)$$

We bound the remaining trilinear terms using Remark 4.1.8.

$$\begin{aligned}
b^*\left(\overline{U_h^n}^h, \eta_u^{n+1/2}, \phi_u^{n+1/2}\right) &= b^*\left(\overline{U_h^n}^h - U^n, \eta_u^{n+1/2}, \phi_u^{n+1/2}\right) + b^*\left(U^n, \eta_u^{n+1/2}, \phi_u^{n+1/2}\right) \\
&\leq C\|\overline{U_h^n}^h - U^n\|(\|\nabla\eta_u^{n+1/2}\|\|\phi_u^{n+1/2}\|_\infty + \|\eta_u^{n+1/2}\|\|\nabla\phi_u^{n+1/2}\|_\infty) \\
&\quad +C\|\nabla U^n\|\|\nabla\eta_u^{n+1/2}\|\|\nabla\phi_u^{n+1/2}\| \\
&\leq C\|\overline{U_h^n}^h - U^n\|(h^{-1/2}\|\nabla\eta_u^{n+1/2}\|\|\nabla\phi_u^{n+1/2}\| + h^{-3/2}\|\eta_u^{n+1/2}\|\|\nabla\phi_u^{n+1/2}\|) \\
&\quad +\frac{Re^{-1}}{32}\|\nabla\phi_u^{n+1/2}\|^2 + CRe\|\nabla U^n\|^2\|\nabla\eta_u^{n+1/2}\|^2 \\
&\leq \frac{Re^{-1}}{32}\|\nabla\phi_u^{n+1/2}\|^2 + CRe\|\overline{U_h^n}^h - U^n\|^2(h^{2k-1}|u|_{k+1}^2) + CRe\|\nabla\eta_u^{n+1/2}\|^2 \\
&\leq \frac{Re^{-1}}{32}\|\nabla\phi_u^{n+1/2}\|^2 + CReh^{2k-1}(\|\eta_u^{n-1}\|^2 + \|\eta_u^n\|^2 + \|\phi_u^{n-1}\|^2 + \|\phi_u^n\|^2 \\
&\quad +\alpha^2h^{2k} + \alpha^2\|a_{D_N}(u)\|^2) + CRe\|\nabla\eta_u^{n+1/2}\|^2 \qquad (5.46)
\end{aligned}$$

$$\begin{aligned}
sb^*\left(\overline{U_h^n}^h, \eta_B^{n+1/2}, \phi_B^{n+1/2}\right) &= sb^*\left(\overline{U_h^n}^h - U^n, \eta_B^{n+1/2}, \phi_B^{n+1/2}\right) + sb^*\left(U^n, \eta_B^{n+1/2}, \phi_B^{n+1/2}\right) \\
&\leq \frac{Re_m^{-1}}{32}\|\nabla\phi_B^{n+1/2}\|^2 + CRe_ms^2h^{2k-1}(\|\eta_B^{n-1}\|^2 + \|\eta_B^n\|^2 + \|\phi_B^{n-1}\|^2 + \|\phi_B^n\|^2 \\
&\quad +\alpha^2h^{2k} + \alpha^2\|a_{D_N}(u)\|^2) + CRe_ms^2\|\nabla\eta_B^{n+1/2}\|^2 \qquad (5.47)
\end{aligned}$$

$$\begin{aligned}
sb^*\left(\overline{B_h^n}^h, \eta_B^{n+1/2}, \phi_u^{n+1/2}\right) &= sb^*\left(\overline{B_h^n}^h - B^n, \eta_B^{n+1/2}, \phi_u^{n+1/2}\right) + sb^*\left(B^n, \eta_B^{n+1/2}, \phi_u^{n+1/2}\right) \\
&\leq \frac{Re^{-1}}{32}\|\nabla\phi_u^{n+1/2}\|^2 + CRes^2h^{2k-1}(\|\eta_B^{n-1}\|^2 + \|\eta_B^n\|^2 + \|\phi_u^{n-1}\|^2 + \|\phi_u^n\|^2 \\
&\quad +\alpha^2h^{2k} + \alpha^2\|a_{D_N}(B)\|^2) + CRes^2\|\nabla\eta_B^{n+1/2}\|^2 \qquad (5.48)
\end{aligned}$$

$$\begin{aligned}
sb^*\left(\overline{B_h^n}^h, \eta_u^{n+1/2}, \phi_B^{n+1/2}\right) &= sb^*\left(\overline{B_h^n}^h - B^n, \eta_u^{n+1/2}, \phi_B^{n+1/2}\right) + sb^*\left(B^n, \eta_u^{n+1/2}, \phi_B^{n+1/2}\right) \\
&\leq \frac{Re_m^{-1}}{32}\|\nabla\phi_B^{n+1/2}\|^2 + CRe_ms^2h^{2k-1}(\|\eta_u^{n-1}\|^2 + \|\eta_u^n\|^2 + \|\phi_B^{n-1}\|^2 + \|\phi_B^n\|^2 \\
&\quad +\alpha^2h^{2k} + \alpha^2\|a_{D_N}(B)\|^2) + CRe_ms^2\|\nabla\eta_u^{n+1/2}\|^2. \qquad (5.49)
\end{aligned}$$

Combining, we have

$$\frac{1}{\Delta t}(\|\phi_u^{n+1}\|^2 - \|\phi_u^n\|^2) + \frac{s}{\Delta t}(\|\phi_B^{n+1}\|^2 - \|\phi_B^n\|^2) + \frac{Re^{-1}}{2}\|\nabla\phi_u^{n+1/2}\|^2 + \frac{sRe_m^{-1}}{2}\|\nabla\phi_B^{n+1/2}\|^2$$
$$\leq CRe \inf_{q_h\in Q_h}\|p(t^{n+1/2}) - q_h\|^2 + CsRe_m \inf_{r_h\in Q_h}\|\lambda(t^{n+1/2}) - r_h\|^2 + Re\|\nabla\eta_u^{n+1/2}\|^2 + Re_m\|\nabla\eta_B^{n+1/2}\|^2$$
$$+ CRe\|u^{n+1/2}\|_\infty^2(\|\eta_u^n\|^2 + \|\eta_u^{n-1}\|^2 + \|\phi_u^n\|^2 + \|\phi_u^{n-1}\|^2)$$
$$+ Cs^2Re_m\|B^{n+1/2}\|_\infty^2(\|\eta_u^n\|^2 + \|\eta_u^{n-1}\|^2 + \|\phi_u^n\|^2 + \|\phi_u^{n-1}\|^2)$$
$$+ Cs^2Re\|B^{n+1/2}\|_\infty^2(\|\eta_B^n\|^2 + \|\eta_B^{n-1}\|^2 + \|\phi_B^n\|^2 + \|\phi_B^{n-1}\|^2)$$
$$+ Cs^2Re_m\|u^{n+1/2}\|_\infty^2(\|\eta_B^n\|^2 + \|\eta_B^{n-1}\|^2 + \|\phi_B^n\|^2 + \|\phi_B^{n-1}\|^2)$$
$$+ CReh^{2k-1}(\|\eta_u^{n-1}\|^2 + \|\eta_u^n\|^2 + \|\phi_u^{n-1}\|^2 + \|\phi_u^n\|^2 + \alpha^2h^{2k} + \alpha^2\|a_{D_N}(u)\|^2)$$
$$+ CRe_ms^2h^{2k-1}(\|\eta_B^{n-1}\|^2 + \|\eta_B^n\|^2 + \|\phi_B^{n-1}\|^2 + \|\phi_B^n\|^2 + \alpha^2h^{2k} + \alpha^2\|a_{D_N}(u)\|^2)$$
$$+ CRes^2h^{2k-1}(\|\eta_B^{n-1}\|^2 + \|\eta_B^n\|^2 + \|\phi_u^{n-1}\|^2 + \|\phi_u^n\|^2 + \alpha^2h^{2k} + \alpha^2\|a_{D_N}(B)\|^2)$$
$$+ CRe_ms^2h^{2k-1}(\|\eta_u^{n-1}\|^2 + \|\eta_u^n\|^2 + \|\phi_B^{n-1}\|^2 + \|\phi_B^n\|^2 + \alpha^2h^{2k} + \alpha^2\|a_{D_N}(B)\|^2)$$
$$+ G(u, B, n, \phi_u^{n+1/2}) + sF(u, B, n, \phi_B^{n+1/2}). \quad (5.50)$$

We next bound the terms in $G(u, B, n, \phi_u^{n+1/2})$ and $F(u, B, n, \phi_B^{n+1/2}$ using the bounds in [33]. We have

$$\left(\frac{u(t^{n+1}) - u(t^n)}{\Delta t} - u_t(t^{n+1/2}), \phi_u^{n+1/2}\right) \leq \frac{1}{2}\|\phi_u^{n+1}\|^2 + \frac{1}{2}\|\phi_u^n\|^2 + C(\Delta t)^3\int_{t^n}^{t^{n+1}}\|u_{ttt}\|^2dt \quad (5.51)$$

$$\left(\frac{B(t^{n+1}) - B(t^n)}{\Delta t} - B_t(t^{n+1/2}), \phi_B^{n+1/2}\right) \leq \frac{1}{2}\|\phi_B^{n+1}\|^2 + \frac{1}{2}\|\phi_B^n\|^2 + C(\Delta t)^3\int_{t^n}^{t^{n+1}}\|B_{ttt}\|^2dt \quad (5.52)$$

$$\nu(\nabla(u^{n+1/2} - u(t^{n+1/2})), \phi_u^{n+1/2}) \leq \frac{Re^{-1}}{32}\|\nabla\phi_u^{n+1/2}\|^2 + CRe(\Delta t)^3\int_{t^n}^{t^{n+1/2}}\|\nabla u_{tt}\|^2dt \quad (5.53)$$

$$\nu(\nabla(B^{n+1/2} - B(t^{n+1/2})), \phi_B^{n+1/2}) \leq \frac{Re_m^{-1}}{32}\|\nabla\phi_B^{n+1/2}\|^2 + CRe_m(\Delta t)^3\int_{t^n}^{t^{n+1/2}}\|\nabla B_{tt}\|^2dt. \quad (5.54)$$

We add to $b^*\left(U^n, u^{n+1/2}, \phi_u^{n+1/2}\right)$ to one of the terms and subtract it from another, bounding the resulting differences as

$$b^*\left(U^n, u^{n+1/2}, \phi_u^{n+1/2}\right) - b^*(u(t^{n+1/2}), u(t^{n+1/2}), \phi_u^{n+1/2}) \leq \frac{Re^{-1}}{32}\|\nabla\phi_u^{n+1/2}\|^2$$
$$+ CRe(\Delta t)^4(\|\nabla(u(t^n)+u(t^{n-1}))\|^4 + \|\nabla u^{n+1/2}\|^4) + CRe(\Delta t)^3\int_{t^n}^{t^{n+1}}\|\nabla u_{tt}\|^4 dt, \quad (5.55)$$

and, using Cauchy-Schwarz and Young inequalities and Lemma 4.1.6,

$$b^*(\widehat{U^n}^{h,U_h^n} - U^n, u^{n+1/2}, \phi_u^{n+1/2}) \leq C\|\widehat{U^n}^{h,U_h^n} - U^n\|\|\nabla u^{n+1/2}\|_\infty\|\phi_u^{n+1/2}\|$$
$$\leq \frac{Re^{-1}}{32}\|\nabla\phi_u^{n+1/2}\|^2 + CRe\|u^{n+1/2}\|_3^2\|\widehat{U^n}^{h,U_h^n} - U^n\|^2$$
$$\leq \frac{Re^{-1}}{32}\|\nabla\phi_u^{n+1/2}\|^2 + CRe\|u^{n+1/2}\|_3^2(\alpha^2h^{2k}$$
$$+ \alpha^2\|a_{D_N}(u)\|^2 + h^{2k+2} + \alpha^2(\|\eta_u^{n-1}\|^2 + \|\eta_u^n\|^2 + \|\phi_u^{n-1}\|^2 + \|\phi_u^n\|^2)). \quad (5.56)$$

We now add to $sb^*\left(\tilde{B^n}, B^{n+1/2}, \phi_u^{n+1/2}\right)$ to one of the terms and subtract it from another, bounding the resulting differences as

$$sb^*\left(B^n, B^{n+1/2}, \phi_u^{n+1/2}\right) - sb^*(B(t^{n+1/2}), B(t^{n+1/2}), \phi_u^{n+1/2}) \leq \frac{Re^{-1}}{32}\|\nabla\phi_u^{n+1/2}\|^2$$
$$+ Cs^2Re(\Delta t)^4(\|\nabla(B(t^n)+B(t^{n-1}))\|^4 + \|\nabla B^{n+1/2}\|^4) + Cs^2Re(\Delta t)^3\int_{t^n}^{t^{n+1}}\|\nabla B_{tt}\|^4 dt. \quad (5.57)$$

and, using Cauchy-Schwarz and Young inequalities and Lemma 4.1.6,

$$b^*(\widehat{\tilde{B^n}}^{h,B_h^n} - B^n, B^{n+1/2}, \phi_u^{n+1/2}) \leq Cs\|\widehat{\tilde{B^n}}^{h,B_h^n} - B^n\|\|\nabla B^{n+1/2}\|_\infty\|\phi_u^{n+1/2}\|$$
$$\leq \frac{Re^{-1}}{32}\|\nabla\phi_u^{n+1/2}\|^2 + Cs^2Re\|B^{n+1/2}\|_3^2(\alpha^2h^{2k}$$
$$+ \alpha^2\|a_{D_N}(B)\|^2 + h^{2k+2} + \alpha^2(\|\eta_B^{n-1}\|^2 + \|\eta_B^n\|^2 + \|\phi_B^{n-1}\|^2 + \|\phi_B^n\|^2)). \quad (5.58)$$

Next, add and subtract $sb^*\left(U^n, B^{n+1/2}, \phi_B^{n+1/2}\right)$ to one of the term and subtract it from another,

bounding the resulting differences as

$$sb^*\left(U^n, B^{n+1/2}, \phi_B^{n+1/2}\right) - sb^*(U(t^{n+1/2}), B(t^{n+1/2}), \phi_B^{n+1/2}) \leq \frac{Re_m^{-1}}{32}\|\nabla\phi_B^{n+1/2}\|^2 + CRe_m(\Delta t)^3\left(\|\nabla(u(t^n)+u(t^{n-1}))\|^2\int_{t^n}^{t^{n+1}}\|\nabla B_{tt}\|^4 dt + \|\nabla B(t^{n+1/2})\|^2\int_{t^n}^{t^{n+1}}\|\nabla u_{tt}\|^2\right), \tag{5.59}$$

and, using Cauchy-Schwarz and Young inequalities and Lemma 4.1.6,

$$\begin{aligned} sb^*(\widehat{U^n}^{h,U_h^n} - U^n, B^{n+1/2}, \phi_B^{n+1/2}) &\leq C\|\widehat{U^n}^{h,U_h^n} - U^n\|\|\nabla B^{n+1/2}\|_\infty\|\phi_B^{n+1/2}\| \\ &\leq \frac{Re_m^{-1}}{32}\|\nabla\phi_B^{n+1/2}\|^2 + CRe_m\|B^{n+1/2}\|_3^2(\alpha^2h^{2k} \\ &\quad + \alpha^2\|a_{D_N}(u)\|^2 + h^{2k+2} + \alpha^2(\|\eta_u^{n-1}\|^2 + \|\eta_u^n\|^2 + \|\phi_u^{n-1}\|^2 + \|\phi_u^n\|^2)). \end{aligned} \tag{5.60}$$

Finally, add and subtract $sb^*\left(\tilde{B}^n, u^{n+1/2}, \phi_B^{n+1/2}\right)$ and bound the differences as

$$sb^*\left(\tilde{B}^n, u^{n+1/2}, \phi_B^{n+1/2}\right) - sb^*(B(t^{n+1/2}), u(t^{n+1/2}), \phi_B^{n+1/2}) \leq \frac{Re_m^{-1}}{32}\|\nabla\phi_B^{n+1/2}\|^2 + CRe_m(\Delta t)^3\left(\|\nabla(B(t^n)+B(t^{n-1}))\|^2\int_{t^n}^{t^{n+1}}\|\nabla u_{tt}\|^4 dt + \|\nabla u(t^{n+1/2})\|^2\int_{t^n}^{t^{n+1}}\|\nabla B_{tt}\|^2\right), \tag{5.61}$$

and, using Cauchy-Schwarz and Young inequalities and Lemma 4.1.6,

$$\begin{aligned} sb^*(\widehat{U^n}^{h,U_h^n} - U^n, B^{n+1/2}, \phi_B^{n+1/2}) &\leq C\|\widehat{U^n}^{h,U_h^n} - U^n\|\|\nabla B^{n+1/2}\|_\infty\|\phi_B^{n+1/2}\| \\ &\leq \frac{Re_m^{-1}}{32}\|\nabla\phi_B^{n+1/2}\|^2 + CRe_m\|B^{n+1/2}\|_3^2(\alpha^2h^{2k} \\ &\quad + \alpha^2\|a_{D_N}(u)\|^2 + h^{2k+2} + \alpha^2(\|\eta_u^{n-1}\|^2 + \|\eta_u^n\|^2 + \|\phi_u^{n-1}\|^2 + \|\phi_u^n\|^2)). \end{aligned} \tag{5.62}$$

Combining all these bounds with (5.50) and using regularity assumptions (7.7)-(7.10), we obtain

$$\begin{aligned}\frac{1}{\Delta t}(\|\phi_u^{n+1}\|^2-\|\phi_u^n\|^2)+\frac{s}{\Delta t}(\|\phi_B^{n+1}\|^2-\|\phi_B^n\|^2)+\frac{Re^{-1}}{2}\|\nabla\phi_u^{n+1/2}\|^2+\frac{sRe_m^{-1}}{2}\|\nabla\phi_B^{n+1/2}\|^2\\ \leq Re\|\nabla\eta_u^{n+1/2}\|^2+Re_m\|\nabla\eta_B^{n+1/2}\|^2+CRe\bigg(\alpha^2h^{2k}+\alpha^2\|a_{D_N}(u)\|^2+h^{2k+2}\\ +\alpha^2(\|\eta_u^{n-1}\|^2+\|\eta_u^n\|^2+\|\phi_u^{n-1}\|^2+\|\phi_u^n\|^2)\bigg)\\ CRe_m\bigg(\alpha^2h^{2k}+\alpha^2\|a_{D_N}(B)\|^2+h^{2k+2}+\alpha^2(\|\eta_B^{n-1}\|^2+\|\eta_B^n\|^2+\|\phi_B^{n-1}\|^2+\|\phi_B^n\|^2)\bigg). \quad (5.63)\end{aligned}$$

Summing over timesteps, multiplying by Δt and noting that $\|u_h^0\|=\|B_h^0\|=0$ gives

$$\begin{aligned}\|\phi_u^M\|^2+s\|\phi_B^M\|^2+\Delta t\sum_{n=0}^{M-1}Re^{-1}\|\nabla\phi_u^{n+1/2}\|^2+\Delta t\sum_{n=0}^{M-1}sRe_m^{-1}\|\nabla\phi_B^{n+1/2}\|^2\\ \leq\Delta t\sum_{n=0}^{M-1}Re\|\nabla\eta_u^{n+1/2}\|^2+\Delta t\sum_{n=0}^{M-1}Re_m\|\nabla\eta_B^{n+1/2}\|^2+C\bigg(\alpha^2h^{2k}+\alpha^2\|a_{D_N}(u)\|^2+\alpha^2\|a_{D_N}(B)\|^2+h^{2k+2}\\ +\Delta t\sum_{n=0}^{M-1}\alpha^2\|\eta_u^n\|^2+\Delta t\sum_{n=0}^{M-1}\alpha^2\|\phi_u^n\|^2+\Delta t\sum_{n=0}^{M-1}\alpha^2\|\eta_B^n\|^2+\Delta t\sum_{n=0}^{M-1}\alpha^2\|\phi_B^n\|^2\bigg). \quad (5.64)\end{aligned}$$

Assuming (P_k,P_{k-1}) Taylor-Hood or (P_k,P_{k-1}^{disc}) Scott-Vogelius elements, we have

$$\begin{aligned}\|\phi_u^M\|^2+s\|\phi_B^M\|^2+\Delta t\sum_{n=0}^{M-1}Re^{-1}\|\nabla\phi_u^{n+1/2}\|^2+\Delta t\sum_{n=0}^{M-1}sRe_m^{-1}\|\nabla\phi_B^{n+1/2}\|^2\leq C\bigg(\Delta t^4+\alpha^2h^{2k}\\ +\alpha^2\|a_{D_N}(u)\|^2+\alpha^2\|a_{D_N}(B)\|^2+h^{2k}+\Delta t\sum_{n=0}^{M-1}\alpha^2\|\phi_u^n\|^2+\Delta t\sum_{n=0}^{M-1}\alpha^2\|\phi_B^n\|^2\bigg). \quad (5.65)\end{aligned}$$

Applying Gronwall's inequality yields

$$\begin{aligned}\|\phi_u^M\|^2+s\|\phi_B^M\|^2+\Delta t\sum_{n=0}^{M-1}Re^{-1}\|\nabla\phi_u^{n+1/2}\|^2+\Delta t\sum_{n=0}^{M-1}sRe_m^{-1}\|\nabla\phi_B^{n+1/2}\|^2\\ \leq C\bigg(\Delta t^4+\alpha^2h^{2k}+\alpha^2\|a_{D_N}(u)\|^2+\alpha^2\|a_{D_N}(B)\|^2+h^{2k}\bigg). \quad (5.66)\end{aligned}$$

Applying the triangle inequality gives the stated result. □

5.3 Numerical Experiments

In this section we verify the rates predicted in section 5.2 for Algorithm 5.1.1. We compute approximations to the chosen solution

$$\begin{aligned} u_1(x,y,t) &= (1+0.01t)\cos(y), \qquad B_1(x,y) = (1-0.01t)\sin(y) \\ u_2(x,y,t) &= (1+0.01t)\sin(x), \qquad B_2(x,y) = (1-0.01t)\cos(x) \\ p(x,y,t) &= x+y \end{aligned}$$

on $\Omega = [0,1]^2$ and $T = 1$. We choose $Re^{-1} = Re_m^{-1} = 1$, $s = 1$ calculate f and $\nabla \times g$ from the MHD and the chosen solution. Then, using Algorithm 5.1.1 with both (P_3, P_2) and (P_2, P_1) elements, we compute solutions on five successive mesh refinements using $\alpha = h$ and N=0 (our analysis shows that for these element choices, choosing $N > 0$ does not improve asymptotic accuracy over the N=0 case). Our analytical results predict that for (P_3, P_2) elements, with $a(\cdot) = a_{D_0}$, a rate of 3 and with $a(\cdot) = 1$ (the usual Leray model), a rate of 2. Tables 5.1 and 5.2 show our calculated errors and rates, and we do observe optimal convergence in both u and B.

h	Δt	$\|u - u_h\|_{2,1}$	Rate	$\|B - B_h\|_{2,1}$	Rate
1/4	1	1.49e-03	-	5.86e-04	-
1/8	1/3	2.16e-04	2.782	9.17e-05	2.676
1/16	1/9	3.15e-05	2.783	1.83e-05	2.327
1/32	1/27	5.18e-06	2.602	4.04e-06	2.177
1/64	1/81	1.04e-06	2.313	9.65e-07	2.066

Table 5.1: $L^2(0,T;H^1(\Omega))$ errors and rates for u and B found with Leray. We observe a rate of 2.

h	Δt	$\|u - u_h\|_{2,1}$	Rate	$\|B - B_h\|_{2,1}$	Rate
1/4	1	1.60e-03	-	8.51e-04	-
1/8	1/3	2.15e-04	2.896	9.04e-05	3.234
1/16	1/9	2.73e-05	2.974	9.70e-06	3.219
1/32	1/27	3.45e-06	2.987	1.15e-06	3.075
1/64	1/81	4.28e-07	3.011	1.43e-07	3.014

Table 5.2: $L^2(0,T;H^1(\Omega))$ errors and rates for u and B found with $a(\cdot) = a_{D_0}$. We observe a rate of 3.

Chapter 6

The Leray-$\alpha\beta$-deconvolution model

The work presented in this chapter is a result of [4]. Dissipation scale modeling in regularizations via the 'β-method' was introduced by Fried and Gurtin [15, 16, 17] for the Navier–Stokes-α (NS-α) model, as a way to model the inherent separation between the inertial (modeled below with the parameter α) and dissipation range scales (modeled below by the parameter β). Numerical studies due to Kim et al. [28, 29, 30] demonstrated that introducing the dissipation scale $\beta < \alpha$ improves accuracy of velocity scale prediction in the dissipation range for simulations of three-dimensional isotropic turbulent flows with periodic and non-periodic boundary conditions. It is the purpose of this paper to study analogous dissipation scale modeling in the context of the Leray-α model with deconvolution for viscous and incompressible fluid flow.

From the computational point of view, Leray-type models are more attractive than NS-α type models due to their ability to be linearized in time-stepping schemes without sacrificing unconditional stability with respect to time-step size [34, 35]. On the other hand, from the physical point of view, NS-α type models are more attractive because they conserve helicity and are frame–invariant, while Leray-type models are not [14, 20, 46]. However, we believe that computational advantages of Leray-type models outweigh the advantages of NS-α type models, particularly when deconvolution is used. This belief is founded on the observation that the consistency of the nonlinearity of (1.12) to that of the NSE is $O(\alpha^{2N+2})$, and thus that the deviation of the model from frame invariance and helicity conservation is also $O(\alpha^{2N+2})$. Moreover, since frame–invariance and helicity conservation are not typically exactly enforced in computations (due to discretization procedures), the greater *physical accuracy* of the NS-α type models over the Leray-type models may not be realized

in computed solutions.

6.1 Numerical algorithms for Leray-$\alpha\beta$-deconvolution

The system (1.12)-(1.15) is a fourth order system, and so does not easily lend itself to efficient computations. However, we can rewrite (1.12) by

$$u_t + D_N(\bar{u}) \cdot \nabla u + \nabla p - \nu \left(1 - \frac{\alpha^2 - \beta^2}{\alpha^2}\right) \Delta u - \nu \frac{\alpha^2 - \beta^2}{\alpha^2} \Delta \bar{u} = f, \tag{6.1}$$

which is second order and thus can be computed with C^0 mixed finite elements. This section presents and analyzes a finite element algorithm for our model.

6.1.1 A finite-element scheme for the Leray-$\alpha\beta$-deconvolution model

We now present an algorithm for Leray-$\alpha\beta$-deconvolution. The scheme uses a trapezoidal temporal discretization.

Algorithm 6.1.1. *Given a kinematic viscosity $\nu > 0$, and end-time $T > 0$, a time step Δt chosen so that $\Delta t < T = M\Delta t$, $f \in L^\infty(0,T;(L^2(\Omega))^d)$, a solenoidal initial condition $u_0 \in X$, parameters $\alpha \geq \beta > 0$ with $\alpha \leq O(h)$, $u_0 = u_h^0 \in V_h$, $\overline{u_h^0}^h = F_h(u_h^0)$, find $(u_h^n, \overline{u_h^n}^h, p_h^n, \lambda_h^n) \in (X_h, X_h, Q_h, Q_h)$ for $n = 1, 2, ..., M$ satisfying, $\forall (v_h, w_h, q_h, r_h) \in (X_h, X_h, Q_h, Q_h)$,*

$$\begin{aligned}
\frac{1}{\Delta t}(u_h^{n+1} - u_h^n, v_h) + (D_N^h \overline{u_h^{n+1/2}}^h \cdot \nabla u_h^{n+1/2}, v_h) &- (p_h^{n+1}, \nabla \cdot v_h) \\
+\nu \left(1 - \frac{\alpha^2 - \beta^2}{\alpha^2}\right) (\nabla u_h^{n+1/2}, \nabla v_h) & \\
+\nu \left(\frac{\alpha^2 - \beta^2}{\alpha^2}\right) (\nabla \overline{u_h^{n+1/2}}^h, \nabla v_h) &= (f^{n+1/2}, v_h), \qquad (6.2) \\
(\nabla \cdot u_h^{n+1}, q_h) &= 0, \qquad (6.3) \\
\alpha^2 (\nabla \overline{u_h^{n+1}}^h, \nabla w_h) + (\overline{u_h^{n+1}}^h, w_h) - (\lambda_h^{n+1}, \nabla \cdot w_h) - (u_h^{n+1}, w_h) &= 0, \qquad (6.4) \\
(\nabla \cdot \overline{u_h^{n+1}}^h, r_h) &= 0. \qquad (6.5)
\end{aligned}$$

It will be notationally convenient to instead study the equivalent V_h formulation: $\forall v_h,\ w_h \in$

V_h,

$$\begin{aligned}\frac{1}{\Delta t}(u_h^{n+1}-u_h^n,v_h)+(D_N^h\overline{u_h^{n+1/2}}^h\cdot\nabla u_h^{n+1/2},v_h) &+ \nu\left(1-\frac{\alpha^2-\beta^2}{\alpha^2}\right)(\nabla u_h^{n+1/2},\nabla v_h)\\ +\nu\left(\frac{\alpha^2-\beta^2}{\alpha^2}\right)(\nabla\overline{u_h^{n+1/2}}^h,\nabla v_h) &= (f^{n+1/2},v_h), \qquad (6.6)\\ \alpha^2(\nabla\overline{u_h^{n+1}}^h,\nabla w_h)+(\overline{u_h^{n+1}}^h,w_h)-(u_h^{n+1},w_h) &= 0. \qquad (6.7)\end{aligned}$$

We now prove the algorithm is unconditionally stable with respect to the time step.

Lemma 6.1.2. *Solutions to Algorithm (6.1.1) are unconditionally stable: for any $\Delta t > 0$, they satisfy*

$$\|u_h^M\|^2+\nu\Delta t\sum_{n=0}^{M-1}\|\nabla u_h^{n+1/2}\|^2\le C(data). \qquad (6.8)$$

Proof. We start the proof by choosing $v_h = u_h^{n+1/2}$ in (6.6). This immediately causes the nonlinear term to vanish, leaving

$$\begin{aligned}\frac{1}{\Delta t}(u_h^{n+1}-u_h^n,u_h^{n+1/2})+\nu\left(1-\frac{\alpha^2-\beta^2}{\alpha^2}\right)\|\nabla u_h^{n+1/2}\|^2&\\ +\nu\left(\frac{\alpha^2-\beta^2}{\alpha^2}\right)\|u_h^{n+1/2}\|_\epsilon^2=(f^{n+1/2},u_h^{n+1/2}). \qquad (6.9)&\end{aligned}$$

Using the identity

$$\frac{1}{\Delta t}(u_h^{n+1}-u_h^n,u_h^{n+\frac12})=\frac{1}{2\Delta t}(u_h^{n+1}-u_h^n,u_h^{n+1}+u_h^n)=\frac{1}{2\Delta t}(\|u_h^{n+1}\|^2-\|u_h^n\|^2)$$

with (6.9), and Lemma 2.1.2, we get

$$\frac{1}{2\Delta t}(\|u_h^{n+1}\|^2-\|u_h^n\|^2)+\nu\|u_h^{n+1/2}\|_\epsilon^2\le(f^{n+1/2},u_h^{n+1/2}). \qquad (6.10)$$

Using Lemma 2.1.2 on the left hand side (i.e. the equivalence of norms), then majorizing the righthand side with Cauchy-Schwarz and Young's inequalities yields

$$\begin{aligned}\frac{1}{2\Delta t}(\|u_h^{n+1}\|^2-\|u_h^n\|^2) &+ C_1\nu\|\nabla u_h^{n+1/2}\|^2\le\|f(t^{n+1/2})\|_{-1}\|\nabla u_h^{n+1/2}\|\\ &\le \frac{C}{2\nu}\|f(t^{n+1/2})\|_{-1}^2+\frac{C_1\nu}{2}\|\nabla u_h^{n+1/2}\|^2. \qquad (6.11)\end{aligned}$$

Reducing, summing over time steps and multiplying by Δt gives

$$\|u_h^M\|^2 + \nu\Delta t \sum_{n=0}^{M-1} \|\nabla u_h^{n+1/2}\|^2 \leq C\left(\nu^{-1}\Delta t \sum_{n=0}^{M-1} \|f(t^{n+1/2})\|_{-1}^2 + \|u_h^0\|^2\right), \tag{6.12}$$

which completes the proof. □

Remark 6.1.3. *These bounds are sufficient to establish the existence of the solution at each time step using the Leray–Schauder fixed-point theorem [33]. Uniqueness of discrete solutions can be proven in the usual way, but requires a data-dependent restriction on the timestep of $\Delta t \leq O(\nu^{-3})$. This restriction arises from the use of the discrete Gronwall inequality, and it is not believed to be sharp.*

6.1.2 Convergence Analysis

Theorem 6.1.4. *Let $(w(t), q(t))$ be a smooth, strong solution of the NSE, additionally satisfying $w \in L^\infty(0,T;H^{k+1}(\Omega))$ and the smoothness assumptions of Lemma 2.1.4. If (u_h, p_h) is a solution to Algorithm 6.1.1 with $N = 0$ or 1, then for Δt sufficiently small, there is a constant C, independent of h and Δt, such that*

$$\|w(T) - u_h^M\|^2 + \nu\Delta t \sum_{n=0}^{M-1} \|\nabla\left(\frac{w(t^n) + w(t^{n+1})}{2}\right) - u_h^{n+1/2}\|^2$$
$$\leq C(\Delta t^4 + \alpha^{4N+4} + h^{2k} + \nu^2(\alpha^2 - \beta^2)^2). \tag{6.13}$$

Proof. At time $t^{n+1/2}$, the solution of the NSE (w, q) satisfies

$$\left(\frac{w^{n+1} - w^n}{\Delta t}, v_h\right) - (D_N^h \overline{w^{n+1/2}}^h \cdot \nabla w^{n+1/2}, v_h) + \nu\left(1 - \frac{\alpha^2 - \beta^2}{\alpha^2}\right)(\nabla w^{n+1/2}, \nabla v_h)$$
$$+\nu\left(\frac{\alpha^2 - \beta^2}{\alpha^2}\right)(\nabla \overline{w^{n+1/2}}^h, \nabla v_h) = (f(t^{n+1/2}), v_h) + Intp(w^n, v_h), \quad \forall v_h \in V_h, \tag{6.14}$$

The term $Intp(w^n, v_h)$, given by

$$\begin{aligned} Intp(w^n, v_h) &= \left(\frac{w^{n+1}-w^n}{\Delta t} - w_t(t^{n+1/2}), v_h\right) \\ &+\nu(\nabla\left(\frac{w(t^n)+w(t^{n+1})}{2}\right) - \nabla w(t^{n+1/2}), \nabla v_h) \\ &+\nu\left(\frac{\alpha^2-\beta^2}{\alpha^2}\right)(\nabla\overline{\left(\frac{w(t^n)+w(t^{n+1})}{2}\right)}^h - \nabla\left(\frac{w(t^n)+w(t^{n+1})}{2}\right), \nabla v_h) \\ &-(D_N^h\overline{\left(\frac{w(t^n)+w(t^{n+1})}{2}\right)}^h \cdot \nabla\left(\frac{w(t^n)+w(t^{n+1})}{2}\right), v_h) \\ &+(D_N^h w(t^{n+1/2})\cdot\nabla w(t^{n+1/2}), v_h) + (f(t^{n+1/2}) - f^{n+1/2}, v_h), \end{aligned} \tag{6.15}$$

collects the interpolation error, the filtering error, and the consistency error. The pressure terms vanish since we are using SV elements that are pointwise div-free. Now, subtracting (6.2) from (6.14) and letting $e^n = w(t^n) - u_h^n$, we have

$$\begin{aligned} &\frac{1}{\Delta t}(e^{n+1}-e^n, v_h) - (D_N^h\overline{e^{n+1/2}}^h\cdot\nabla w^{n+1/2}, v_h) + (D_N^h\overline{u_h^{n+1/2}}^h\cdot\nabla e^{n+1/2}, v_h) \\ &\quad+\nu\left(1-\frac{\alpha^2-\beta^2}{\alpha^2}\right)(\nabla e^{n+1/2}, \nabla v_h) + \nu\left(\frac{\alpha^2-\beta^2}{\alpha^2}\right)(\nabla\overline{e^{n+1/2}}^h, \nabla v_h) = Intp(w^n, v_h). \end{aligned} \tag{6.16}$$

Decompose the error as $e^n = (w^n - U^n) - (v_h^n - U^n) := \eta^n - \phi_h^n$ where $\phi_h^n \in V_h$, and U is the L^2 projection of u in V_h.

$$\begin{aligned} &\frac{1}{\Delta t}(\phi_h^{n+1}-\phi_h^n, v_h) + \nu\left(1-\frac{\alpha^2-\beta^2}{\alpha^2}\right)(\nabla\phi_h^{n+1/2}, \nabla v_h) + \nu\left(\frac{\alpha^2-\beta^2}{\alpha^2}\right)(\nabla\overline{\phi_h^{n+1/2}}^h, \nabla v_h) \\ &\quad= \frac{1}{\Delta t}(\eta^{n+1}-\eta^n, v_h) + (D_N^h\overline{\eta^{n+1/2}}^h\cdot\nabla u^{n+1/2}, v_h) - (D_N^h\overline{\phi_h^{n+1/2}}^h\cdot\nabla u^{n+1/2}, v_h) \\ &\qquad- (D_N^h\overline{u_h^{n+1/2}}^h\cdot\nabla\eta^{n+1/2}, v_h) + (D_N^h\overline{u_h^{n+1/2}}^h\cdot\nabla\phi_h^{n+1/2}, v_h) \\ &\quad+\nu\left(1-\frac{\alpha^2-\beta^2}{\alpha^2}\right)(\nabla\eta^{n+1/2}, \nabla v_h) + \nu\left(\frac{\alpha^2-\beta^2}{\alpha^2}\right)(\nabla\overline{\eta^{n+1/2}}^h, \nabla v_h) + Intp(w^n, v_h). \end{aligned} \tag{6.17}$$

Setting $v_h = \phi_h^{n+1/2}$ in (6.17), we obtain

$$\begin{aligned}
&\frac{1}{\Delta t}(\|\phi_h^{n+1}\|^2 - \|\phi_h^n\|^2) + \nu\left(1 - \frac{\alpha^2-\beta^2}{\alpha^2}\right)\|\nabla\phi_h^{n+1/2}\|^2 + \nu\left(\frac{\alpha^2-\beta^2}{\alpha^2}\right)\|\phi_h\|_\epsilon^2 \\
&= \frac{1}{\Delta t}(\eta^{n+1} - \eta^n, \phi_h^{n+1/2}) + (D_N^h\overline{\eta^{n+1/2}}^h \cdot \nabla u^{n+1/2}, \phi_h^{n+1/2}) - (D_N^h\overline{\phi_h^{n+1/2}}^h \cdot \nabla u^{n+1/2}, \phi_h^{n+1/2}) \\
&\qquad - (D_N^h\overline{u_h^{n+1/2}}^h \cdot \nabla\eta^{n+1/2}, \phi_h^{n+1/2}) + \nu\left(1 - \frac{\alpha^2-\beta^2}{\alpha^2}\right)(\nabla\eta^{n+1/2}, \nabla\phi_h^{n+1/2}) \\
&\qquad\qquad + \nu\left(\frac{\alpha^2-\beta^2}{\alpha^2}\right)(\nabla\overline{\eta^{n+1/2}}^h, \nabla\phi_h^{n+1/2}) + Intp(w^n, \phi_h^{n+1/2}). \quad (6.18)
\end{aligned}$$

The first term form the right hand side vanishes based on its projection definition. We bound the rest of the right hand side terms as follows.

$$\begin{aligned}
(D_N^h\overline{\eta^{n+1/2}}^h \cdot \nabla u^{n+1/2}, \phi_h^{n+1/2}) &\leq C\|D_N^h\overline{\eta^{n+1/2}}^h\|\|\nabla u^{n+1/2}\|_\infty\|\phi_h^{n+1/2}\| \\
&\leq C(N)\|\eta^{n+1/2}\|\|u^{n+1/2}\|_{H^3}\|\phi_h^{n+1/2}\| \\
&\leq \frac{\nu}{4}\|\nabla\phi_h^{n+1/2}\|^2 + C(N)\nu^{-1}\|\eta^{n+1/2}\|^2\|u^{n+1/2}\|_{H^3}^2,
\end{aligned}$$

$$\begin{aligned}
(D_N^h\overline{\phi_h^{n+1/2}}^h \cdot \nabla u^{n+1/2}, \phi_h^{n+1/2}) &\leq C\|D_N^h\overline{\phi_h^{n+1/2}}^h\|\|\nabla u^{n+1/2}\|_\infty\|\phi_h^{n+1/2}\| \\
&\leq C(N)\|u^{n+1/2}\|_{H^3}\|\phi_h^{n+1/2}\|^2,
\end{aligned}$$

$$(D_N^h\overline{u_h^{n+1/2}}^h \cdot \nabla\eta^{n+1/2}, \phi_h^{n+1/2}) \leq \frac{\nu}{4}\|\nabla\phi_h^{n+1/2}\|^2 + C(N)\nu^{-1}\|\nabla\eta^{n+1/2}\|^2\|\nabla u_h^{n+1/2}\|^2,$$

$$\begin{aligned}
\nu\left(1 - \frac{\alpha^2-\beta^2}{\alpha^2}\right)(\nabla\eta^{n+1/2}, \nabla\phi_h^{n+1/2}) \leq \frac{\nu}{2}\left(1 - \frac{\alpha^2-\beta^2}{\alpha^2}\right)\|\nabla\phi_h^{n+1/2}\|^2 + \\
C\nu^{-1}\left(1 - \frac{\alpha^2-\beta^2}{\alpha^2}\right)\|\nabla\eta^{n+1/2}\|^2,
\end{aligned}$$

and

$$\begin{aligned}
&\nu\left(\frac{\alpha^2-\beta^2}{\alpha^2}\right)(\nabla\overline{\eta^{n+1/2}}^h, \nabla\phi_h^{n+1/2}) \\
&\qquad\qquad \leq \frac{\nu}{2}\left(\frac{\alpha^2-\beta^2}{\alpha^2}\right)\|\nabla\phi_h^{n+1/2}\|^2 + C\nu^{-1}\left(\frac{\alpha^2-\beta^2}{\alpha^2}\right)\|\nabla\eta^{n+1/2}\|^2.
\end{aligned}$$

Combine the above and use norm equivalences from Lemma 2.1.2 on the left hand side to obtain

$$\frac{1}{2\Delta t}(\|\phi_h^{n+1}\|^2 - \|\phi_h^n\|^2) + \frac{\nu}{2}\|\nabla\phi_h^{n+1/2}\|^2 \leq C\nu^{-1}\|\nabla\eta^{n+1/2}\|^2 + C\nu^{-1}\|\eta^{n+1/2}\|^2\|u^{n+1/2}\|_{H^3}^2 + C\nu^{-1}\|\phi_h^{n+1/2}\|^2\|u^{n+1/2}\|_{H^3}^2 + C\nu^{-1}\|\nabla\eta^{n+1/2}\|^2\|\nabla u_h^{n+1/2}\|^2 + CIntp(w^n, \phi_h^{n+1/2}). \quad (6.19)$$

The interpolation error is bounded in the usual way ([34, 35, 29]), and using Lemmas 2.1.2 and 2.1.9, and the regularity assumptions on the true solution, we find

$$|Intp(w^n, \phi_h^{n+1/2})| \leq C(\Delta t^4 + \alpha^{4N+4} + h^{2k} + \nu^2(\alpha^2 - \beta^2)^2) + \|\phi_h^{n+1}\|^2 + \|\phi_h^n\|^2. \quad (6.20)$$

Summing over time steps, multiplying by Δt, using $\|\phi_h^0\| = 0$, then under regularity assumptions we obtain

$$\|\phi_h^M\|^2 + \frac{\Delta t\nu}{2}\sum_{n=0}^{M-1}\|\nabla\phi_h^{n+1/2}\|^2 \leq C(1+\nu^{-1})\Delta t\sum_{n=0}^{M}\|\phi_h^n\|^2 + C\Bigg(\Delta t\sum_{n=0}^{M-1}\nu^{-1}\|\eta^{n+1/2}\|^2 + \Delta t^4 + \alpha^{4N+4} + h^{2k} + \nu^2(\alpha^2-\beta^2)^2) + \Delta t\sum_{n=0}^{M-1}\nu^{-1}\|\nabla\eta^{n+1/2}\|^2\|\nabla u_h^{n+1/2}\|^2\Bigg). \quad (6.21)$$

Continuing to bound the right hand side terms,

$$\begin{aligned} C\Delta t\nu^{-1}\sum_{n=0}^{M-1}\|\nabla\eta^{n+1/2}\|^2 &\leq C\Delta t\nu^{-1}\sum_{n=0}^{M}\|\nabla\eta^n\|^2 \\ &\leq C\Delta t\nu^{-1}\sum_{n=0}^{M}h^{2k}|u(t^n)|_{k+1}^2 \\ &\leq C\nu^{-1}h^{2k}. \end{aligned} \quad (6.22)$$

Since we assume $((P_k)^d, P_{k-1}^{disc})$ elements, then using the stability result gives

$$\begin{aligned}
& \Delta t \sum_{n=0}^{M-1} \nu^{-1} \|\nabla u_h^{n+1/2}\|^2 \|\nabla \eta^{n+1/2}\|^2 \\
= \quad & \Delta t \sum_{n=0}^{M-1} \nu^{-1} \|\nabla u_h^{n+1/2}\|^2 \inf_{v_h \in V_h} \|\nabla(u^{n+1/2}) - v_h)\|^2 \\
\leq \quad & \Delta t \sum_{n=0}^{M-1} \nu^{-1} \|\nabla u_h^{n+1/2}\|^2 (Ch^{2k} |u|_{k+1}^2) \\
\leq \quad & C\nu^{-1} h^{2k} \Delta t \sum_{n=0}^{M-1} \|\nabla u_h^{n+1/2}\|^2 \\
\leq \quad & C\nu^{-2} h^{2k}. \qquad (6.23)
\end{aligned}$$

Combining (6.21) with (6.22)-(6.23), and using (2.2) and (2.3) gives

$$\begin{aligned}
& \|\phi_h^M\|^2 + \frac{\Delta t \nu}{2} \sum_{n=0}^{M-1} \|\nabla \phi_h^{n+1/2}\|^2 \\
& \qquad \leq C(1+\nu^{-1}) \Delta t \sum_{n=0}^{M} \|\phi_h^n\|^2 + C(\nu^{-2} h^{2k} + \Delta t^4 + \alpha^{4N+4} + h^{2k} + \nu^2 (\alpha^2 - \beta^2)^2). \qquad (6.24)
\end{aligned}$$

For Δt small enough, applying Gronwall's inequality yields

$$\|\phi_h^M\|^2 + \frac{\Delta t \nu}{2} \sum_{n=0}^{M-1} \|\nabla \phi_h^{n+1/2}\|^2 \leq C(\Delta t^4 + \alpha^{4N+4} + h^{2k} + \nu^2 (\alpha^2 - \beta^2)^2). \qquad (6.25)$$

Finally, applying the triangle inequality gives the result. □

6.1.3 Linearized Scheme

Algorithm 6.1.1 can be more efficiently computed in the following way, by linearizing through time-lagging and extrapolation of the filtered terms, which decouples filtering and deconvolution from the system. Although unconditional stability is lost, the resulting stability condition for the time-step is mild, and easily justified by the gain in efficiency since the linear systems for the filtering and mass/momentum are decoupled and need solved only once at each time-step.

Algorithm 6.1.5. *Given a kinematic viscosity $\nu > 0$, and end-time $T > 0$, a time step Δt chosen so that $\Delta t < T = M\Delta t$, $f \in L^\infty(0, T; (L^2(\Omega))^d)$, the initial condition $u_0 \in V$, parameters $0 < \beta \leq \alpha \leq O(h)$, first find $u_h^0 \in V_h$ to be the L^2 projection of u_0 into V_h, then find $(u_h^n, \overline{u_h^n}^h) \in (V_h, V_h)$ by*

linear two-step process, for $n = 1, 2, ..., M$

Step 1: For all $v_h \in V_h$,

$$\frac{1}{\Delta t}(u_h^{n+1} - u_h^n, v_h) - (D_N^h \overline{\frac{3}{2}u_h^n - \frac{1}{2}u_h^{n-1}}^h \cdot \nabla u_h^{n+1/2}, v_h) + \nu\left(1 - \frac{\alpha^2 - \beta^2}{\alpha^2}\right)(\nabla u_h^{n+1/2}, \nabla v_h) + \nu\left(\frac{\alpha^2 - \beta^2}{\alpha^2}\right)(\nabla \overline{u_h^n}^h, \nabla v_h) = (f^{n+1/2}, v_h), \quad (6.26)$$

Step 2: For all $w_h \in V_h$,

$$\alpha^2(\nabla \overline{u_h^{n+1}}^h, \nabla w_h) + (\overline{u_h^{n+1}}^h, w_h) - (u_h^{n+1}, w_h) = 0, \quad (6.27)$$

For $n = 1$, $u_h^{-1} := u_h^0$.

This scheme is conditionally stable, with a mild time-step restriction when $\beta < \alpha$.

Lemma 6.1.6. *For a given mesh and parameters, if the time-step satisfies*

$$1 - \frac{C_i^2 \nu h^{-2} \Delta t}{2} \frac{\alpha^2 - \beta^2}{\alpha^2} > 0,$$

(i.e. $\Delta t < O\left(\frac{h^2}{\nu}\right)$*), solutions to Algorithm 6.1.5 satisfy*

$$\|u_h^M\|^2 + \nu \Delta t \sum_{n=0}^{M-1} \|\nabla u_h^{n+1/2}\|^2 \leq C(data). \quad (6.28)$$

Remark 6.1.7. *Since this scheme is linear, provided the time-step restriction, the stability result implies existence and uniqueness of solutions, without any further assumptions. Also, a convergence result similar to that proven for the nonlinear scheme holds for this scheme as well, but with the* Δt^4 *term in Theorem 6.1.4 reducing to a* $\nu^2 \Delta t^2$ *due the time lagging in the viscous term. If an extrapolation of this term was used instead, it would increase the accuracy, but currently we are unable to prove a stability result of practical use for such an alteration.*

Proof. Set $v_h = u_h^{n+1/2}$ in (6.26). This vanishes the nonlinearity, and leaves

$$\frac{1}{2\Delta t}\left(\|u_h^{n+1}\|^2 - \|u_h^n\|^2\right) + \nu\left(1 - \frac{\alpha^2 - \beta^2}{\alpha^2}\right)\|\nabla u_h^{n+1/2}\|^2 + \nu\left(\frac{\alpha^2 - \beta^2}{\alpha^2}\right)(\nabla \overline{u_h^n}^h, \nabla u_h^{n+1/2}) = (f^{n+1/2}, u_h^{n+1/2}). \quad (6.29)$$

The third term in the left hand side of (6.29) reduces as

$$\begin{aligned}(\nabla\overline{u_h^n}^h, \nabla u_h^{n+1/2}) &= (\nabla\overline{u_h^n}^h \pm \nabla\overline{u_h^{n+1/2}}^h, \nabla u_h^{n+1/2}) \\ &= \|u_h^{n+1/2}\|_\epsilon^2 + (\nabla\overline{u_h^n}^h - \nabla\overline{u_h^{n+1/2}}^h, \nabla u_h^{n+1/2}) \\ &= \|u_h^{n+1/2}\|_\epsilon^2 - \frac{1}{2}(\nabla\overline{u_h^{n+1}}^h - \nabla\overline{u_h^n}^h, \nabla u_h^{n+1/2}) \\ &= \|u_h^{n+1/2}\|_\epsilon^2 - \frac{1}{4}\left(\|u_h^{n+1}\|_\epsilon^2 - \|u_h^n\|_\epsilon^2\right), \end{aligned} \tag{6.30}$$

with the final equality holding since the filter is self-adjoint in the L^2 inner product, and so we can now rewrite (6.29) as

$$\begin{aligned}&\frac{1}{2\Delta t}\left(\|u_h^{n+1}\|^2 - \|u_h^n\|^2\right) + \nu\left(1 - \frac{\alpha^2-\beta^2}{\alpha^2}\right)\|\nabla u_h^{n+1/2}\|^2 \\ &\qquad + \nu\left(\frac{\alpha^2-\beta^2}{\alpha^2}\right)\|u_h^{n+1/2}\|_\epsilon^2 = (f^{n+1/2}, u_h^{n+1/2}) + \frac{\nu}{4}\frac{\alpha^2-\beta^2}{\alpha^2}\left(\|u_h^{n+1}\|_\epsilon^2 - \|u_h^n\|_\epsilon^2\right). \end{aligned} \tag{6.31}$$

For the forcing term in (6.31), using Cauchy-Schwarz, Young and norm equivalences from Lemma 2.1.2, we have the bounds

$$\begin{aligned}(f^{n+\frac{1}{2}}, u_h^{n+\frac{1}{2}}) &\le \|f^{n+\frac{1}{2}}\|_{-1}\|\nabla u_h^{n+\frac{1}{2}}\| \\ &\le \frac{\nu}{2}\left(1 - \frac{\alpha^2-\beta^2}{\alpha^2}\right)\|\nabla u_h^{n+\frac{1}{2}}\|^2 + \frac{1}{2\nu}\left(1 - \frac{\alpha^2-\beta^2}{\alpha^2}\right)^{-1}\|f^{n+\frac{1}{2}}\|_{-1}^2, \end{aligned} \tag{6.32}$$

and

$$\begin{aligned}(f^{n+\frac{1}{2}}, u_h^{n+\frac{1}{2}}) &\le \|f^{n+\frac{1}{2}}\|_{-1}\|\nabla u_h^{n+\frac{1}{2}}\| \le C\|f^{n+\frac{1}{2}}\|_{-1}\|u_h^{n+\frac{1}{2}}\|_\epsilon \\ &\le \frac{\nu}{2}\frac{\alpha^2-\beta^2}{\alpha^2}\|u_h^{n+\frac{1}{2}}\|_\epsilon^2 + \frac{C^2}{2\nu}\frac{\alpha^2}{\alpha^2-\beta^2}\|f^{n+\frac{1}{2}}\|_{-1}^2 \end{aligned} \tag{6.33}$$

Combining (6.31)-(6.33) provides

$$\begin{aligned}&\frac{1}{\Delta t}\left(\|u_h^{n+1}\|^2 - \|u_h^n\|^2\right) + \nu\left(1 - \frac{\alpha^2-\beta^2}{\alpha^2}\right)\|\nabla u_h^{n+1/2}\|^2 + \nu\frac{\alpha^2-\beta^2}{\alpha^2}\|u_h^{n+1/2}\|_\epsilon^2 \\ &\quad \le \frac{\nu}{4}\frac{\alpha^2-\beta^2}{\alpha^2}\left(\|u_h^{n+1}\|_\epsilon^2 - \|u_h^n\|_\epsilon^2\right) + \frac{1}{\nu}\|f^{n+\frac{1}{2}}\|_{-1}^2 \min\{C^2\left(\frac{\alpha^2-\beta^2}{\alpha^2}\right)^{-1}, \left(1 - \frac{\alpha^2-\beta^2}{\alpha^2}\right)^{-1}\}. \end{aligned} \tag{6.34}$$

Note the min on the right hand side of (6.34) is bounded by $2C^2$, since the two numbers being inverted are positive and sum to 1, so one of them must be bigger than or equal to $1/2$. Thus we have

$$\frac{1}{\Delta t}\left(\|u_h^{n+1}\|^2 - \|u_h^n\|^2\right) + \nu\left(1 - \frac{\alpha^2-\beta^2}{\alpha^2}\right)\|\nabla u_h^{n+1/2}\|^2 + \nu\frac{\alpha^2-\beta^2}{\alpha^2}\|u_h^{n+1/2}\|_\epsilon^2 \\ \leq \frac{\nu}{2}\frac{\alpha^2-\beta^2}{\alpha^2}\left(\|u_h^{n+1}\|_\epsilon^2 - \|u_h^n\|_\epsilon^2\right) + \frac{2C^2}{\nu}\|f^{n+\frac{1}{2}}\|_{-1}^2. \quad (6.35)$$

Multiplying by Δt and summing over time-steps yields

$$\left(\|u_h^M\|^2 - \|u_h^0\|^2\right) + \nu\Delta t\sum_{n=0}^{M-1}\left(\left(1 - \frac{\alpha^2-\beta^2}{\alpha^2}\right)\|\nabla u_h^{n+1/2}\|^2 + \frac{\alpha^2-\beta^2}{\alpha^2}\|u_h^{n+1/2}\|_\epsilon^2\right) \\ \leq \frac{\nu}{2}\frac{\alpha^2-\beta^2}{\alpha^2}\Delta t\left(\|u_h^M\|_\epsilon^2 - \|u_h^0\|_\epsilon^2\right) + \frac{2C^2}{\nu}\Delta t\sum_{n=0}^{M-1}\|f^{n+\frac{1}{2}}\|_{-1}^2, \quad (6.36)$$

which reduces using Lemma 2.1.2 and the inverse inequality to

$$\|u_h^M\|^2 + \nu\Delta t\sum_{n=0}^{M-1}\left(\left(1 - \frac{\alpha^2-\beta^2}{\alpha^2}\right)\|\nabla u_h^{n+1/2}\|^2 + \frac{\alpha^2-\beta^2}{\alpha^2}\|u_h^{n+1/2}\|_\epsilon^2\right) \\ \leq \frac{\nu\Delta t}{2}\frac{\alpha^2-\beta^2}{\alpha^2}\|u_h^M\|_\epsilon^2 + \frac{2C^2}{\nu}\Delta t\sum_{n=0}^{M-1}\|f^{n+\frac{1}{2}}\|_{-1}^2 + \|u_h^0\|^2 \\ \leq \frac{\nu\Delta t}{2}\frac{\alpha^2-\beta^2}{\alpha^2}\|\nabla u_h^M\|^2 + \frac{2C^2}{\nu}\Delta t\sum_{n=0}^{M-1}\|f^{n+\frac{1}{2}}\|_{-1}^2 + \|u_h^0\|^2 \\ \leq \frac{C_i^2\nu h^{-2}\Delta t}{2}\frac{\alpha^2-\beta^2}{\alpha^2}\|u_h^M\|^2 + \frac{2C^2}{\nu}\Delta t\sum_{n=0}^{M-1}\|f^{n+\frac{1}{2}}\|_{-1}^2 + \|u_h^0\|^2. \quad (6.37)$$

Taking with $\alpha = \beta$, or $\alpha > \beta$ with

$$1 - \frac{C_i^2\nu h^{-2}\Delta t}{2}\frac{\alpha^2-\beta^2}{\alpha^2} > 0,$$

along with norm equivalences, completes the proof. □

6.2 Finite Element Numerical Experiments

In this section, we present two numerical experiments on benchmark problems that illustrate the effectiveness of the proposed approach, in giving good coarse mesh approximations. All computations are done using Algorithm 6.1.5.

6.2.1 2D Flow around a cylinder

Our first numerical experiment is for two dimensional under-resolved channel flow around a cylinder, as described in chapter 3.

For our models to be successful, they should be able to approximate the true solution well, on a coarser mesh. Hence for these simulations, a barycenter-refined mesh providing 18,780 total degrees of freedom with $((P_3)^2, P_2^{disc})$ Scott-Vogelius elements, a time step of $\Delta t = 0.001$, and filtering radius α chosen to be the average mesh width, is used. Results are shown at $t = 6$ for $N = 0,\ 1$ and for $\beta = \alpha, \alpha/2$, in Figure 6.1. From these plots, we see that without deconvolution or β-modeling (i.e. the Leray-α model), the simulation fails to predict the vortex street. With either deconvolution or using $\beta = \alpha/2$, improvement is seen, but the combination of deconvolution $N = 1$ and $\beta = \alpha/2$ gives a result that matches well the DNS of Figure 3.6 in that the vortex street continues to the end of the channel.

N	β	c_d^{max}	c_l^{max}	Δp
0	α	2.173	0.034	-0.124
0	$\alpha/2$	1.950	0.182	-0.114
1	α	2.510	0.234	-0.097
1	$\alpha/2$	2.447	0.315	-0.114

Table 6.1: Maximum lift and drag coefficients and pressure drop for four model settings on a coarse mesh.

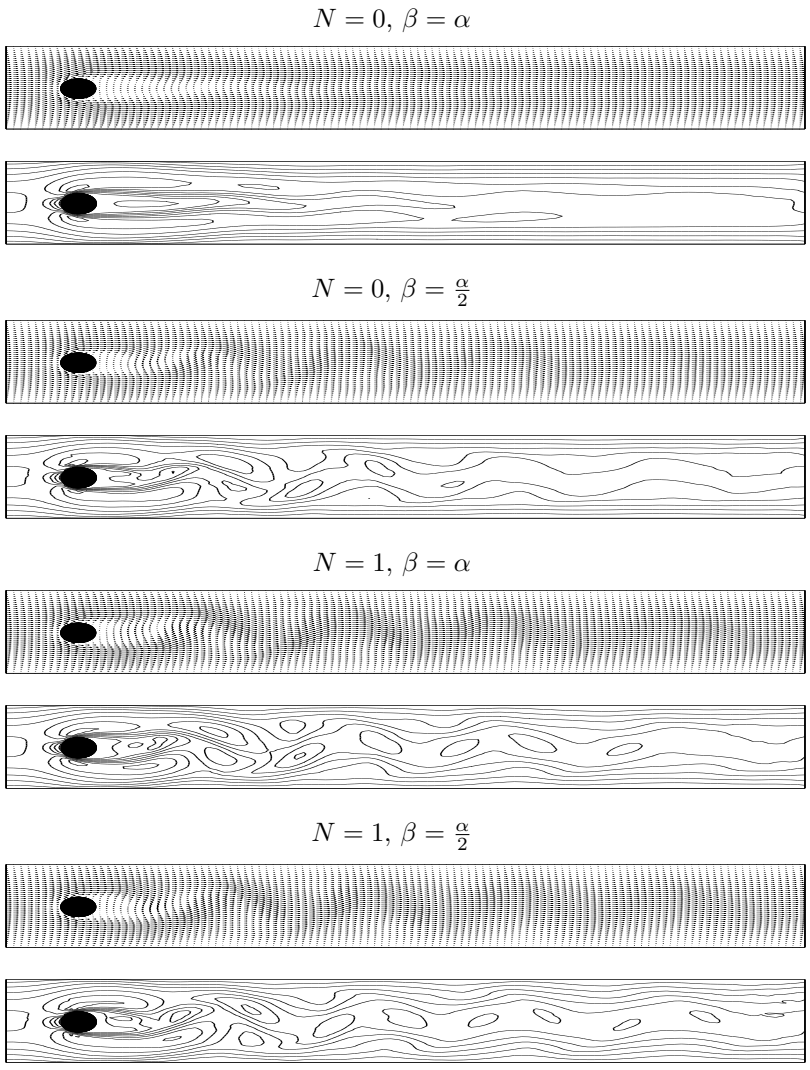

Figure 6.1: Shown above are the velocity field and speed contours of the models' computed solutions at $t = 6$ for the channel flow around a cylinder test problem.

Chapter 7

Numerical approximation of a multiscale Leray model for incompressible, viscous flow

The work presented in this chapter is a result of [3]. We study a modification of the Leray-α model. We will filter on a finer mesh, which allows smoothing of the solution to be more localized, causing less damping at coherent flow structures. The filter system is decoupled from the mass/momentum system, and even though it is solved on a finer mesh, the filter solve can be considered as equivalent to a well conditioned Stokes problem, as we are solving the same matrix at every timestep.

We present an efficient numerical method for the model that is unconditionally stable and optimally convergent, and which decouples the mass/momentum system from the filter system, improving the efficiency of the system solves.

7.1 Scheme and Stability

Algorithm 7.1.1. *Given a kinematic viscosity $\nu > 0$, an end-time $T > 0$, a time step Δt chosen so that $\Delta t < T = M\Delta t$, $f \in L^\infty(0,T;(L^2(\Omega))^d)$, initial condition $u_0 \in X$, filtering radius $\alpha \leq O(\hat{h})$,*

find $(u_h^n, p_h^n) \in (X_h, Q_h)$ *for* $n = 1, 2, ..., M$ *satisfying,* $\forall (v_h, q_h) \in (X_h, Q_h)$,

$$\frac{1}{\Delta t}(u_h^{n+1} - u_h^n, v_h) + b^*(\overline{u_h^{n+1/2}}^{\hat{h}}, u_h^{n+1/2}, v_h) - (p_h^{n+1}, \nabla \cdot v_h)$$
$$+\nu(\nabla u_h^{n+1/2}, \nabla v_h) = (f^{n+1/2}, v_h), \tag{7.1}$$
$$(\nabla \cdot u_h^{n+1}, q_h) = 0. \tag{7.2}$$

Lemma 7.1.2. *Solutions to Algorithm (7.1.1) exist, are unique, and satisfy*

$$\|u_h^M\|^2 + \Delta t \sum_{n=0}^{M-1} \nu \|\nabla u_h^{n+1/2}\|^2 \leq C(\nu, f, u_h^0, T). \tag{7.3}$$

Proof. Begin by choosing $v_h = u_h^{n+1/2}$ in (7.1). The trilinear term vanishes, leaving

$$\frac{1}{2\Delta t}(\|u_h^{n+1}\|^2 - \|u_h^n\|^2) + \nu \|\nabla u_h^{n+1/2}\|^2 = (f^{n+1/2}, u_h^{n+1/2}) \leq C\nu^{-1}\|f^{n+1/2}\|^2 + \frac{\nu}{2}\|\nabla u_h^{n+1/2}\|^2, \tag{7.4}$$

which reduces to

$$\frac{1}{2\Delta t}(\|u_h^{n+1}\|^2 - \|u_h^n\|^2) + \frac{\nu}{2}\|\nabla u_h^{n+1/2}\|^2 \leq C\nu^{-1}\|f^{n+1/2}\|^2. \tag{7.5}$$

Summing over timesteps and multiplying by $2\Delta t$ yields

$$\|u_h^M\|^2 + \Delta t \sum_{n=0}^{M-1} \nu \|\nabla u_h^{n+1/2}\|^2 \leq C\nu^{-1} \sum_{n=0}^{M-1} \|f^{n+1/2}\|^2 + \|u_h^0\|^2. \tag{7.6}$$

□

7.2 Convergence

This section proves convergence of the scheme to the NSE solution. The result gives guidance in choice of parameter α to achieve optimal accuracy. For simplicity in stating the following convergence theorem, we summarize here the necessary regularity assumptions for the solution

$(u(x,t), p(x,t))$ to the NSE

$$u \in L^\infty(0,T;H^{k+1}(\Omega)), \tag{7.7}$$

$$u \in L^\infty(0,T;H^{2N+2}(\Omega)), \tag{7.8}$$

$$u_{tt} \in L^4(0,T;H^1(\Omega)), \tag{7.9}$$

$$u_{ttt} \in L^2(0,T;L^2(\Omega)), \tag{7.10}$$

$$p \in L^\infty(0,T;H^k(\Omega)). \tag{7.11}$$

Theorem 7.2.1. *Let $(u(t), p(t))$ be a solution of the NSE satisfying no-slip boundary conditions, and (7.7)-(7.11), with given $f \in L^\infty(0,T;H^{-1}(\Omega))$ and $u_0 \in H^1(\Omega)$. Let (u_h^n, p_h^n), $n = 0, 1, \ldots M$ be the solution of Algorithm (7.1), using (P_k, P_{k-1}) elements. Then for Δt small enough, the error in the discrete solution satisfies*

$$\|u(T) - u_h^M\|^2 + \Delta t \sum_{n=0}^{M-1} \nu \|\nabla(u^{n+1/2} - u_h^{n+1/2})\|^2 \leq C(\Delta t^4 + h^{2k} + \alpha^4 + \alpha^2 \hat{h}^{2k} + \hat{h}^{2k+2})$$

Remark 7.2.2. *With $\alpha = O(\hat{h})$ (which is believed to be the optimal choice [34],[47],[43],[41]), estimate of the theorem reduces to*

$$\|u(T) - u_h^M\| + \Delta t \sum_{n=0}^{M-1} \nu \|\nabla(u^{n+1/2} - u_h^{n+1/2})\| \leq C(\Delta t^2 + h^k + \hat{h}^2)$$

Hence, using degree polynomial $k = 3$, $\hat{h} = O(h^{3/2})$ will provide optimal convergence.

Proof. We begin by multiplying the NSE at $t = t^{n+\frac{1}{2}}$ by $v_h \in V_h$. Then integrate to get, $\forall v_h \in V_h$,

$$\left(\frac{u(t^{n+1}) - u(t^n)}{\Delta t}, v_h\right) - (p(t^{n+1/2}), \nabla \cdot v_h) + \nu(\nabla u^{n+1/2}, \nabla v_h) + b^*(\overline{u^{n+1/2}}^{\hat{h}}, u^{n+1/2}, v_h) = (f(t^{n+1/2}), v_h) + G(u, n, v_h), \tag{7.12}$$

where

$$G(u,n,v_h) := \left(\frac{u(t^{n+1}) - u(t^n)}{\Delta t} - u_t(t^{n+1/2}), v_h\right) + \nu(\nabla(u^{n+1/2} - u(t^{n+2/2})), v_h) + b^*(\overline{u^{n+1/2}}^{\hat{h}}, u^{n+1/2}, v_h) - b^*(u(t^{n+1/2}), u(t^{n+1/2}), v_h). \tag{7.13}$$

Denote $e^n = u(t^n) - u_h^n$ and subtract (7.12) from (7.1) to get the error equation

$$\frac{1}{\Delta t}(e^{n+1} - e^n, v_h) + b^*(\overline{u_h^{n+1/2}}^{\hat{h}}, e^{n+1/2}, v_h) + b^*(\overline{e^{n+1/2}}^{\hat{h}}, u^{n+1/2}, v_h) \\ + \nu(\nabla e^{n+1/2}, \nabla v_h) = (p(t^{n+1/2}), \nabla \cdot v_h) + G(u, n, v_h). \quad (7.14)$$

Decompose the velocity error as,

$$e^n = (u(t^n) - P_{V_h}(u(t^n))) + (P_{V_h}(u(t^n)) - u_h^n) =: \eta^n + \phi_h^n.$$

Expanding and choosing $v_h = \phi_h^{n+1/2}$, and reducing by Cauchy-Schwarz and Young's inequalities gives

$$\frac{1}{2\Delta t}(\|\phi_h^{n+1}\|^2 - \|\phi_h^n\|^2) + \frac{\nu}{2}\|\nabla \phi_h^{n+1/2}\|^2 \leq C\nu\|\nabla \eta^{n+1/2}\|^2 + C\nu^{-1} \inf_{q_h \in Q_h} \|p - q_h\|^2 \\ + b^*\left(\overline{\eta^{n+1/2}}^{\hat{h}}, u^{n+1/2}, \phi_h^{n+1/2}\right) + b^*\left(\overline{\phi_h^{n+1/2}}^{\hat{h}}, u^{n+1/2}, \phi_h^{n+1/2}\right) \\ + b^*\left(\overline{u_h^{n+1/2}}^{\hat{h}}, \eta^{n+1/2}, \phi_h^{n+1/2}\right) + G(u, n, \phi_h^{n+1/2}). \quad (7.15)$$

We now bound the three trilinear terms using Lemma 2.0.3 and Young's inequality:

$$b^*\left(\overline{\eta^{n+1/2}}^{\hat{h}}, u^{n+1/2}, \phi_h^{n+1/2}\right) \leq \frac{\nu}{16}\|\nabla \phi_h^{n+1/2}\|^2 + C\nu^{-1}\|\nabla \eta^{n+1/2}\|^2\|\nabla(u(t^{n+1}) + u(t^n))\|^2. \quad (7.16)$$

$$b^*\left(\overline{u_h^{n+1/2}}^{\hat{h}}, \eta^{n+1/2}, \phi_h^{n+1/2}\right) \leq \frac{\nu}{16}\|\nabla \phi_h^{n+1/2}\|^2 + C\nu^{-1}\|\nabla \eta^{n+1/2}\|^2\|\nabla u_h^{n+1/2}\|^2. \quad (7.17)$$

$$
\begin{aligned}
&b^*\left(\overline{\phi_h^{n+1/2}}^{\hat{h}}, u^{n+1/2}, \phi_h^{n+1/2}\right) \\
&\qquad = \frac{1}{2}\left(\overline{\phi_h^{n+1/2}}^{\hat{h}} \cdot u^{n+1/2}, \phi_h^{n+1/2}\right) - \frac{1}{2}\left(\overline{\phi_h^{n+1/2}}^{\hat{h}} \cdot \nabla\phi_h^{n+1/2}, u^{n+1/2}\right) \\
&\qquad \le C\|\overline{\phi_h^{n+1/2}}^{\hat{h}}\|\|\nabla u^{n+1/2}\|_\infty\|\phi_h^{n+1/2}\| + C\|\overline{\phi_h^{n+1/2}}^{\hat{h}}\|\|u^{n+1/2}\|_\infty\|\nabla\phi_h^{n+1/2}\| \\
&\qquad \le C\|\phi_h^{n+1/2}\|(\|\nabla u^{n+1/2}\|_\infty + \|u^{n+1/2}\|_\infty)\|\nabla\phi_h^{n+1/2}\| \\
&\qquad \le \frac{\nu}{16}\|\nabla\phi_h^{n+1/2}\|^2 + C\|\phi_h^{n+1/2}\|^2\|u^{n+1/2}\|_{H^3}^2 \qquad (7.18)
\end{aligned}
$$

Using bounds on the three trilinear terms and the $G(u, n, \phi_h^{n+1/2})$ from [34] and [5], we get

$$
\begin{aligned}
\frac{1}{2\Delta t}(\|\phi_h^{n+1}\|^2 - \|\phi_h^n\|^2) + \nu\|\nabla\phi_h^{n+1/2}\|^2 &\le C\nu\|\nabla\eta^{n+1/2}\|^2 + C\nu^{-1}\inf_{q_h\in Q_h}\|p - q_h\|^2 \\
&+ C\nu^{-1}\|\nabla u^{n+1/2}\|^2\|\nabla\eta^{n+1/2}\|^2 + C\nu^{-1}\|\nabla u_h^{n+1/2}\|^2\|\nabla\eta^{n+1/2}\|^2 \\
&+ C\|u^{n+1/2}\|_{H^3}^2\|\phi_h^{n+1/2}\|^2 + C(\Delta t)^3\int_{t^n}^{t^{n+1}}\|u_{ttt}\|^2 dt \\
&+ C\nu(\Delta t)^3\int_{t^n}^{t^{n+1/2}}\|\nabla u_{tt}\|^2 dt + C\nu^{-1}(\Delta t)^4(\|\nabla u^{n+1/2}\|^4 + \|\nabla u(t^{n+1/2})\|^4) \\
&+ C\nu^{-1}(\Delta t)^3\int_{t^n}^{t^{n+1}}\|\nabla u_{tt}\|^4 dt + C\nu^{-1}\|u^{n+1/2}\|_{H^3}(\alpha^4 + \alpha^2\hat{h}^{2k} + \hat{h}^{2k+2}). \qquad (7.19)
\end{aligned}
$$

Summing over timesteps, multiplying by $2\Delta t$, noting that $\|\phi_h^0\| = 0$, and using regularity assumptions (7.7)-(7.11) yields

$$
\begin{aligned}
\|\phi_h^M\|^2 + \Delta t\sum_{n=0}^{M-1}\nu\|\nabla\phi_h^{n+1/2}\|^2 \le C\Bigg(&\Delta t\sum_{n=1}^{M-1}\|\phi_h^{n+1/2}\|^2 + \Delta t\sum_{n=0}^{M-1}\nu^{-1}\|\nabla\eta^{n+1/2}\|^2 \\
&+ \Delta t^4 + \alpha^4 + \alpha^2\hat{h}^{2k} + \hat{h}^{2k+2} + \Delta t\sum_{n=0}^{M-1}\nu^{-1}\|\nabla u_h^{n+1/2}\|^2\|\nabla\eta^{n+1/2}\|^2\Bigg). \qquad (7.20)
\end{aligned}
$$

Assuming (P_k, P_{k-1}) elements, the last term in (7.20) is bounded by

$$\begin{aligned}
& \Delta t \sum_{n=0}^{M-1} \nu^{-1} \|\nabla u_h^{n+1/2}\|^2 \|\nabla \eta^{n+1/2}\|^2 \\
= \;& \Delta t \sum_{n=0}^{M-1} \nu^{-1} \|\nabla u_h^{n+1/2}\|^2 \inf_{v_h \in V_h} \|\nabla (u(t^{n+1/2}) - v_h)\|^2 \\
\leq \;& \Delta t \sum_{n=0}^{M-1} \nu^{-1} \|\nabla u_h^{n+1/2}\|^2 (C h^{2k} |u|_{k+1}^2) \\
\leq \;& C h^{2k} \Delta t \sum_{n=0}^{M-1} \nu^{-1} \|\nabla u_h^{n+1/2}\|^2 \\
\leq \;& C h^{2k}. \qquad (7.21)
\end{aligned}$$

Combining (7.20) with (7.21) gives

$$\|\phi_h^M\|^2 + \Delta t \sum_{n=0}^{M-1} \nu \|\nabla \phi_h^{n+1/2}\|^2 \leq C \Delta t \sum_{n=1}^{M-1} \|\phi_h^{n+1/2}\|^2 + C(h^{2k} + \Delta t^4 + \alpha^4 + \alpha^2 \hat{h}^{2k} + \hat{h}^{2k+2}). \quad (7.22)$$

For Δt small enough, applying Gronwall's inequality yields

$$\|\phi_h^M\|^2 + \Delta t \sum_{n=0}^{M-1} \nu \|\nabla \phi_h^{n+1/2}\|^2 \leq C(h^{2k} + \Delta t^4 + \alpha^4 + \alpha^2 \hat{h}^{2k} + \hat{h}^{2k+2}). \quad (7.23)$$

Applying the triangle inequality to (7.23) yields

$$\|u(T) - u_h^M\|^2 + \Delta t \sum_{n=0}^{M-1} \nu \|\nabla (u(t^{n+1/2}) - u_h^{n+1/2})\|^2 \leq C(\Delta t^4 + h^{2k} + \alpha^4 + \alpha^2 \hat{h}^{2k} + \hat{h}^{2k+2}). \quad (7.24)$$

□

7.3 Numerical Experiments

In this section, we present several numerical experiments that illustrate the effectiveness of our approach in giving good approximations of incompressible flows. In particular, we show that using fine mesh filtering gives better results than filtering on the same coarse mesh.

7.3.1 Convergence Rate Verification

h	Δt	$\hat{h}$	$\|u - u_h\|_{2,1}$	Rate
1/2	0.001	1/2	1.271e-02	-
1/4	0.001/3	1/6	1.683e-03	2.916
1/8	0.001/9	1/18	2.177e-04	2.951
1/16	0.001/27	1/54	2.816e-05	2.951
1/24	0.001/61	1/122	8.398e-06	2.984

Table 7.1: $L^2(0,T;H^1(\Omega))$ errors and rates found with $(X_{\hat{h}}, Q_{\hat{h}}) = (P_3, P_2)$ for experiment 1, with $\hat{h}$ cut by 3 for each mesh refinement, as predicted by the analysis.

$h = \hat{h}$	Δt	$\|u - u_h\|_{2,1}$	Rate
1/2	0.001	1.271e-02	-
1/4	0.001/3	1.687e-03	2.914
1/8	0.001/9	2.334e-04	2.853
1/16	0.001/27	4.538e-05	2.363
1/24	0.001/61	2.001e-05	2.019

Table 7.2: $L^2(0,T;H^1(\Omega))$ errors and rates found with $(X_{\hat{h}}, Q_{\hat{h}}) = (P_3, P_2)$ for experiment 1, with $h = \hat{h}$ for each mesh refinement. A lower rate of convergence can be observed compared to Table 1.

Our first numerical experiment is to verify the predicted convergence rates in Chapter 4 for Algorithm (7.1.1). The test problem we choose is to compute approximations to the chosen solution

$$u_1(x,y,t) = \sin(2\pi y)(1 + 0.01t)$$

$$u_2(x,y,t) = \cos(2\pi x)(1 + 0.01t)$$

$$p(x,y,t) = x + y$$

on $\Omega = (0,1)^2$ and $t \in [0, 0.001]$. We calculate f from the NSE, the initial condition $u_0 = u(0)$, set $\nu = 1$, and use this data to compute solutions on five mesh refinements.

h	Δt	$\hat{h}$	$\|u - u_h\|_{2,1}$	Rate
1/2	0.001	1/2	1.270e-02	-
1/4	0.001/3	1/6	1.684e-03	2.915
1/8	0.001/9	1/18	2.177e-04	2.951
1/16	0.001/27	1/54	2.816e-05	2.951
1/24	0.001/61	1/122	8.398e-06	2.984

Table 7.3: $L^2(0,T;H^1(\Omega))$ errors and rates found with $(X_{\hat{h}}, Q_{\hat{h}}) = (P_2, P_1)$ for experiment 1, with $\hat{h}$ cut by 3 for each mesh refinement, as predicted by the analysis.

The increased order of convergence for a (P_3, P_2) filter can be seen in Tables 1 and 2. In

$h = \hat{h}$	Δt	$\|u - u_h\|_{2,1}$	Rate
1/2	0.001	1.270e-02	-
1/4	0.001/3	1.686e-03	2.917
1/8	0.001/9	2.333e-04	2.854
1/16	0.001/27	4.539e-05	2.362
1/24	0.001/61	2.001e-05	2.019

Table 7.4: $L^2(0,T;H^1(\Omega))$ errors and rates found with $(X_{\hat{h}}, Q_{\hat{h}}) = (P_2, P_1)$ for experiment 1, with $h = \hat{h}$ for each mesh refinement. A lower rate of convergence can be observed compared to Table 1.

Table 1, where fine mesh filtering is used, we see $O(h^3)$ spatial convergence, whereas when finemesh filtering is not used, (Table 2), the convergence order is decaying away from 3. We found similar results when using a (P_2, P_1) filter space (Tables 3 and 4).

7.3.2 2d Flow Over a Step

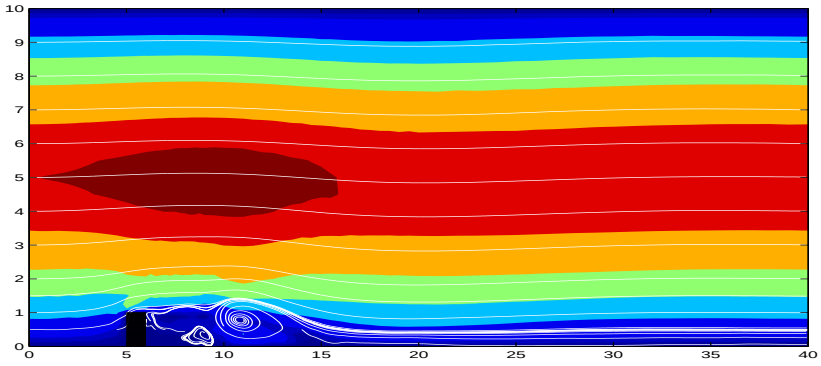

Figure 7.1: Fine mesh filtering with (P_3, P_2) filter.

Our second experiment is for two-dimensional flow over a forward and backward facing step. The domain Ω is a 40 x 10 channel with a 1 x 1 step five units into the channel at the bottom. We assume no-slip boundary conditions on the top and bottom boundaries, and parabolic inflow and outflow profiles, given by $(y(10-y)/25, 0)^T$.

Figure 7.1 shows the $T = 40$ solution using (P_3, P_2) elements on a coarse mesh of 8,023 degrees of freedom, and filtering with (P_3, P_2) elements on a refinement of the coarse mesh, with 31,267 degrees of freedom. Figure 7.2 shows the $T = 40$ solution using (P_3, P_2) elements on the same coarse mesh of 8,023 degrees of freedom, and filtering with (P_2, P_1) elements on a refinement of the coarse mesh, with 12,969 degrees of freedom. In both cases, we see smooth channel flow, with eddies forming and detaching behind the step.

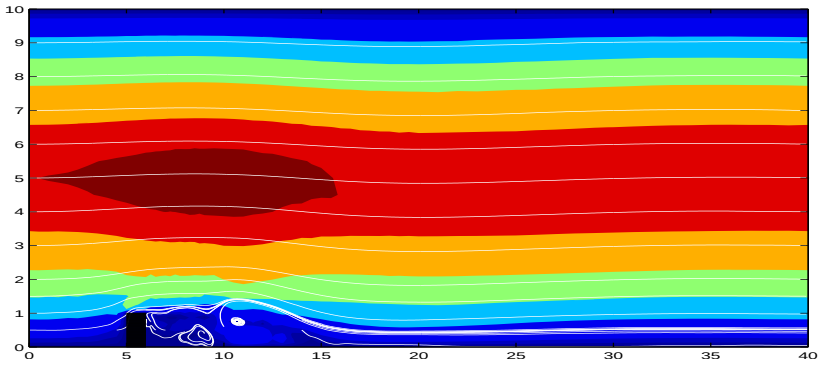

Figure 7.2: Fine mesh filtering with (P_2, P_1) filter.

Chapter 8

Conclusions

Chapter 3 proposed an unconditionally stable and efficient algorithm for computing reduced order approximations to flow problems, by using adaptive nonlinear filtering with the Leray regularization model. We found this method to be very effective, and to give much better solutions on coarse meshes than either direct numerical simulations and the 'usual' regularization model using linear filtering. Of the indicator functions studied, the best choice appears to be a synthesis of the Vreman and Q-criterion based indicator functions.

In Chapter 4, we extended our work with adaptive nonlinear filtering to include a deconvolution-based indicator function. To our knowledge, this is the first indicator function that has been explicitly incorporated into a convergence analysis, where the convergence rate is rigorously shown to be increased due to its use. This was possible because the indicator function was based on mathematical approximation theory, instead of physical phenomenology. We have shown that the proposed method is well-posed, unconditionally stable, efficient, and converges to an NSE solution with optimal rate. We also provided benchmark tests which demonstrated the effectiveness of our approach over the NSE and the regular Leray-α model on coarse meshes.

We further explored use of the deconvolution-based indicator in Chapter 5 by extending our method to the Leray-MHD model. We proved unconditional stability and convergence of our method to the MHD equations, and verified the convergence rate predicted by our analysis.

Our work in Chapter 6 shows that dissipation scale modeling can help in capturing more of the effect of subgrid scales than Leray-α (even when enhanced by deconvolution). A finite element stability and convergence analysis was presented and it is accompanied by computations on

benchmark problems. The regularization the higher order Leray-$\alpha\beta$-deconvolution model gives, has remarkable and positive effects on the results of the computations, giving lower errors over larger time intervals.

In Chapter 7, we developed, analyzed, and tested an efficient algorithm for approximating Navier-Stokes solutions on coarser meshes than a DNS can be performed. We have shown our algorithm to be unconditionally stable, and optimally convergent, using an element choice and filtering radius guided by our analysis. Numerical experiments were provided confirming our analysis and showing our schemes effectiveness.

Bibliography

[1] N. A. Adams and S. Stolz. On the Approximate Deconvolution procedure for LES. *Phys. Fluids*, 2:1699–1701, 1999.

[2] D. Arnold and J. Qin. Quadratic velocity/linear pressure Stokes elements. In R. Vichnevetsky, D. Knight, and G. Richter, editors, *Advances in Computer Methods for Partial Differential Equations VII*, pages 28–34. IMACS, 1992.

[3] A. Bowers. Numerical approximation of a multiscale Leray model for incompressible, viscous flow. In J. Li, E. Macharro, and H. Yang, editors, *Recent Advances in Scientific Computing and Applications: Proceedings of the 8th International Conference on Scientific Computing and Applications*, volume 586. AMS Contemporary Mathematics, 2013.

[4] A. Bowers, T.-Y. Kim, M. Neda, L. Rebholz, and E. Fried. The Leray-$\alpha\beta$-deconvolution model: energy analysis and numerical algorithms. *Applied Mathematical Modelling*, 37(3):1225–1241, 2013.

[5] A. Bowers and L. Rebholz. Increasing accuracy and efficiency in FE computations of the Leray-deconvolution model. *Numerical Methods for Partial Differential Equations*, 28(2):720–736, 2012.

[6] A. Bowers and L. Rebholz. Numerical study of a regularization model for incompressible flow with deconvolution-based adaptive nonlinear filtering. *Computer Methods in Applied Mechanics and Engineering*, 258:1–12, 2013.

[7] A. Bowers, L. Rebholz, A. Takhirov, and C. Trenchea. Improved accuracy in regularization models of incompressible flow via adaptive nonlinear filtering. *International Journal for Numerical Methods in Fluids*, 70:805–828, 2012.

[8] S. Brenner and L. Scott. *The Mathematical Theory of Finite Element Methods*. Springer-Verlag, 1994.

[9] E. Burman and A. Linke. Stabilized finite element schemes for incompressible flow using Scott–Vogelius elements. *Applied Numerical Mathematics*, 58(11):1704–1719, 2008.

[10] M. Case, V. Ervin, A. Linke, and L. Rebholz. Improving mass conservation in FE approximations of the NSE with C^0 velocities: A connection between Scott–Vogelius elements and grad-div stabilization. *SIAM Journal on Numerical Analysis*, 49(4):1461–1481, 2011.

[11] A. Cheskidov, D. Holm, E. Olson, and E. Titi. On a Leray-α Model of Turbulence. *Proceedings of the Royal Society A*, 461:629–649, 2005.

[12] J. Connors. Convergence analysis and computational testing of the finite element discretization of the Navier-Stokes-alpha model. *Numerical Methods for Partial Differential Equations*, 26(6):1328–1350, 2010.

[13] A. Dunca and Y. Epshteyn. On the Stolz-Adams deconvolution model for the Large-Eddy simulation of turbulent flows. *SIAM J. Math. Anal.*, 37(6):1890–1902, 2005.

[14] C. Foias, D.D. Holm, and E.S. Titi. The Navier–Stokes-α model of fluid turbulence. *Physica D*, 152:505–519, 2001.

[15] E. Fried and M. Gurtin. Tractions, balances, and boundary conditions for nonsimple materials with application to liquid flow at small length scales. *Archive for Rational Mechanics and Analysis*, 182:513–554, 2006.

[16] E. Fried and M. Gurtin. A continuum mechanical framework for turbulence giving a generalized Navier–Stokes-α equation with complete boundary conditions. *Theoretical and Computational Fluid Dynamics*, 22:433–470, 2007.

[17] E. Fried and M. Gurtin. Turbulent kinetic energy and a possible hierarchy of length scales in a generalization of the Navier–Stokes-α theory. *Physical Review E*, 75(056306):1–10, 2007.

[18] G. Galdi and W. Layton. Approximating the larger eddies in fluid motion II: A model for space filtered flow. *Math. Methods and Models in Appl. Sci.*, 10(3):1–8, 2000.

[19] V. Girault and P.-A. Raviart. *Finite element methods for Navier-Stokes equations : theory and algorithms*. Springer-Verlag, 1986.

[20] J.L. Guermond, J.T. Oden, and S. Prudhomme. An interpretation of the Navier–Stokes-α model as a frame-indifferent Leray regularization. *Physica D*, 177:23–30, 2003.

[21] M. Gunzburger. *Finite Element Methods for Viscous Incompressible Flow: A Guide to Theory, Practice, and Algorithms*. Academic Press, Boston, 1989.

[22] Y. He and W. Sun. Stability and convergence of the Crank-Nicolson/Adams-Bashforth scheme for the time-dependent Navier-Stokes equations. *SIAM Journal of Numerical Analysis*, 45(2):837–869, 2007.

[23] J. Heywood and R. Rannacher. Finite element approximation of the nonstationary Navier-Stokes problem. Part IV: Error analysis for the second order time discretization. *SIAM J. Numer. Anal.*, 2:353–384, 1990.

[24] J. Heywood, R. Rannacher, and S. Turek. Artificial boundaries and flux and pressure conditions for the incompressible Navier-Stokes equations. *International Journal for Numerical Methods in Fluids*, 22:325–352, 1996.

[25] R. Hill. Benchmark Testing the α-models of Turbulence. Master's thesis, Clemson, 2010.

[26] J. Hunt, A. Wray, and P. Moin. Eddies stream and convergence zones in turbulent flows. *CTR report CTR-S88*, 1988.

[27] V. John. Reference values for drag and lift of a two dimensional time-dependent flow around a cylinder. *International Journal for Numerical Methods in Fluids*, 44:777–788, 2004.

[28] T.-Y. Kim, M. Cassiani, J. Albertson, J. Dolbow, E. Fried, and M. Gurtin. Impact of the inherent separation of scales in the Navier–Stokes-$\alpha\beta$ equations. *Physical Review E*, 79(045307):1–4, 2009.

[29] T.-Y. Kim, M. Neda, L. Rebholz, and E. Fried. A numerical study of the Navier-Stokes-$\alpha\beta$ model. *Computer Methods in Applied Mechanics and Engineering*, 200(41-44):2891–2902, 2011.

[30] T.-Y. Kim, L. Rebholz, and E. Fried. A deconvolution enhancement of the Navier-Stokes-$\alpha\beta$-model. *Journal of Computational Physics*, 231(11):4015–4027, 2012.

[31] A.N. Kolmogorov. The local structure of turbulence in incompressible viscous fluids for very large Reynolds number. *Doklady Akademii Nauk SSR*, 30:9–13, 1941.

[32] P. Kuberry, A. Larios, L. Rebholz, and N. Wilson. Numerical approximation of the Voigt regularization for incompressible Navier-Stokes and magnetohydrodynamic flows. *Computers and Mathematics with Applications*, 64(8):2647–2662, 2012.

[33] W. Layton. *Introduction to the Numerical Analysis of Incompressible Viscous Flows.* SIAM, 2008.

[34] W. Layton, C. Manica, M. Neda, and L. Rebholz. Numerical Analysis and Computational Testing of a High Accuracy Leray-Deconvolution Model of Turbulence. *Numerical Methods for Partial Differential Equations*, 24(2):555–582, 2008.

[35] W. Layton, C. Manica, M. Neda, and L. Rebholz. Numerical analysis and computational comparisons of the NS-omega and NS-alpha regularizations. *Comput. Methods Appl. Mech. Engrg.*, 199:916–931, 2009.

[36] W. Layton, C.C. Manica, M. Neda, M.A. Olshanskii, and L. Rebholz. On the accuracy of the rotation form in simulations of the Navier–Stokes equations. *Journal of Computational Physics*, 228(5):3433–3447, 2009.

[37] W. Layton and L. Rebholz. *Approximate Deconvolution Models of Turbulence: Analysis, Phenomenology and Numerical Analysis, Springer Lecture Notes in Mathematics.* Springer, 2012.

[38] W. Layton, C. Trenchea, and L. Rebholz. Modular nonlinear filter stabilization of methods for higher Reynolds numbers flow. *Journal of Mathematical Fluid Mechanics*, 14(2):325–354, 2012.

[39] J. Leray. Essai sur le mouvement d'un fluide visqueux emplissant l'espace. *Acta. Math.*, 63:193–248, 1934.

[40] A. Linke, G. Matthies, and L. Tobiska. Non-nested multi-grid solvers for mixed divergence free Scott–Vogelius discretizations. *Computing*, 83(2-3):87–107, 2008.

[41] C. Manica, M. Neda, M. Olshanskii, and L. Rebholz. Enabling numerical accuracy of Navier-Stokes-α through deconvolution and enhanced stability. *M2AN: Mathematical Modelling and Numerical Analysis*, 45(2):277–308, 2011.

[42] C. Manica, M. Neda, M. Olshanskii, L. Rebholz, and N. Wilson. On an efficient finite element method for Navier–Stokes-omega with strong mass conservation. *Computational Methods in Applied Mathematics*, 11(1):3–22, 2011.

[43] W. Miles and L. Rebholz. Computing NS-alpha with greater physical accuracy and higher convergence rates. *Numerical Methods for Partial Differential Equations*, 26:1530–1555, 2010.

[44] M.A. Olshanskii, G. Lube, T. Heister, and J. Löwe. Grad-div stabilization and subgrid pressure models for the incompressible Navier-Stokes equations. *Comp. Meth. Appl. Mech. Eng.*, 198:3975–3988, 2009.

[45] J. Qin. *On the convergence of some low order mixed finite elements for incompressible fluids.* PhD thesis, Pennsylvania State University, 1994.

[46] L. Rebholz. Conservation laws of turbulence models. *Journal of Mathematical Analysis and Applications*, 326(1):33–45, 2007.

[47] L. Rebholz and M. Sussman. On the high accuracy NS-α-deconvolution model of turbulence. *Mathematical Models and Methods in Applied Sciences*, 20:611–633, 2010.

[48] M. Schäfer and S. Turek. The benchmark problem 'flow around a cylinder' flow simulation with high performance computers II. *in E.H. Hirschel (Ed.), Notes on Numerical Fluid Mechanics*, 52, Braunschweig, Vieweg:547–566, 1996.

[49] S. Stolz, N. Adams, and L. Kleiser. On the approximate deconvolution model for large-eddy simulations with application to incompressible wall-bounded flows. *Phys. Fluids*, 13, 2001.

[50] M. Vogelius. An analysis of the p-version of the finite element method for nearly incompressible materials. Uniformly valid, optimal error estimates. *Numerische Mathematik*, 41:39–53, 1983.

[51] M. Vogelius. A right-inverse for the divergence operator in spaces of piecewise polynomials. Application to the p-version of the finite element method. *Numerische Mathematik*, 41:19–37, 1983.

[52] A. Vreman. An eddy-viscosity subgrid-scale model for turbulent shear flow: Algebraic theory and applications. *Physics of Fluids*, 16(10):3670–3681, 2004.

[53] Y. Yu and K. Li. Existence of solutions for the mhd-leray-alpha equations and their relations to the mhd equations. *Journal of Mathematical Analysis and Applications*, 329:298–326, 2006.

[54] S. Zhang. A new family of stable mixed finite elements for the 3d Stokes equations. *Math. Comp.*, 74(250):543–554, 2005.

[55] S. Zhang. On the P1 Powell–Sabin divergence-free finite element for the Stokes equations. *Journal of Computational Mathematics*, 26(3):456–470, 2008.

[56] S. Zhang. Divergence-free finite elements on tetrahedral grids for $k \geq 6$. *Mathematics of Computation*, 80(274):669–695, 2011.

[57] S. Zhang. Quadratic divergence-free finite elements on Powell-Sabin tetrahedral grids. *Calcolo*, 48(3):211–244, 2011.